

DESIGN OF LOW COMPLEXITY DETECTION ALGORITHMS FOR UPLINK MASSIVE MIMO SYSTEMS

Ph.D. Thesis

by

ARIJIT DATTA



DEPARTMENT OF ELECTRICAL ENGINEERING
INDIAN INSTITUTE OF TECHNOLOGY
INDORE
FEB, 2022

DESIGN OF LOW COMPLEXITY DETECTION ALGORITHMS FOR UPLINK MASSIVE MIMO SYSTEMS

Ph.D. Thesis

by

ARIJIT DATTA



DEPARTMENT OF ELECTRICAL ENGINEERING
INDIAN INSTITUTE OF TECHNOLOGY
INDORE
FEB, 2021



INDIAN INSTITUTE OF TECHNOLOGY INDORE


CANDIDATE'S DECLARATION

I hereby certify that the work which is being presented in the thesis entitled “**DESIGN OF LOW COMPLEXITY DETECTION ALGORITHMS FOR UPLINK MASSIVE MIMO SYSTEMS**” in the partial fulfillment of the requirements for the award of the degree of **DOCTOR OF PHILOSOPHY** and submitted in the **DEPARTMENT OF ELECTRICAL ENGINEERING, Indian Institute of Technology Indore**, is an authentic record of my own work carried out during the time period from July 2016 to April 2021 under the supervision of Dr. Vimal Bhatia, Professor, Indian Institute of Technology Indore, India.

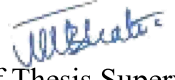
The matter presented in this thesis has not been submitted by me for the award of any other degree of this or any other institute.


Signature of the student with date
(ARIJIT DATTA)

This is to certify that the above statement made by the candidate is correct to the best of my knowledge.


Signature of Thesis Supervisor with date
(Dr. VIMAL BHATIA)

ARIJIT DATTA has successfully given his Ph.D. Oral Examination held on 08/02/2022.


Signature of Thesis Supervisor with date
(Dr. VIMAL BHATIA)

ACKNOWLEDGEMENTS

First and foremost, I would like to praise and thank the merciful and passionate almighty for granting countless blessings, knowledge, and opportunities to me, so that I have finally been able to accomplish the thesis.

I want to extend sincere thank and express my heartfelt gratitude to my supervisor Prof. Vimal Bhatia for his invaluable support, encouragement and guidance over the years. I admire his critical eye on research topics. He always keeps an open mind on every academic discussion. I could hardly complete this thesis without his enthusiasm, encouragement, guidance, support and endless optimism. It has been a great privilege to work under his direction throughout the thesis work. I would also like to thank my PSPC committee members Prof. Abhinav Kranti and Dr. Bhupesh Kumar Lad, for their fruitful discussions and suggestions towards my research.

I want to express my warmest thanks to my labmates Mahendra Singh Thakur, Amit Chatterjee, Shaik Parvez, Sandesh Jain, Krishnendu S, Deepak Kumar, Purva Sharma at Signals and Software group (SaSg). I want to extend my appreciation to my seniors Uday Singh, Anuj Agarwal, Manish Mandloi, Sanjeev Sharma, Abhijeet Bishnu and Nagendra Kumar for giving valuable help whenever I asked for assistance. I am thankful to the Ministry of Electronics and Information technology (MeitY), Government of India, for funding my research work. I am also thankful to all of my co-authors for collaboration over the years. I would also like to show my appreciation to all the academic and nonacademic members of the Indian Institute of Technology Indore to support and help me in various ways.

Special thanks of gratitude are extended to my teachers Mr. Amar Datta (my father), Mr. Gouri Sankar Roy, Mr. Biswajit Dutta, Dr. Premtosh Majumdar and Dr. Atanu Choudhury. I know my life would be drastically different if I were deprived of such outstanding teachers' knowledge, affection and love.

I would also acknowledge my friends Babual Hansda, Soumitra Guin and Arnab Chakraborty for making this journey enjoyable.

Finally, I am forever grateful and indebted to my parents for their endless and unparalleled love, help and support. Their selfless encouragement helps me to explore new directions in life and seek my destiny. I dedicate this milestone to them.

Arijit Datta

Dedicated to my parents

ABSTRACT

Massive multiple-input multiple-output (mMIMO) wireless communication systems play a crucial role in realizing the demand for higher data rates and improved service quality for 5G and beyond communications. The potential benefits of mMIMO are further enhanced by incorporating media-based modulation (MBM). Consequently, reliable detection of transmitted information bits from all the users is one of the challenging tasks for the practical implementation of mMIMO systems. The conventional linear detectors such as zero forcing (ZF) and minimum mean square error (MMSE) achieve near-optimal bit error rate (BER) performance for high system loading factors. However, ZF and MMSE require large dimensional matrix inversion, which induces high computational complexity for symbol detection in such systems. Furthermore, due to the constellation diversity and the consequent sparse nature of symbol vectors in mMIMO with MBM (MBM-mMIMO), those linear detectors' performance drastically degrades. It motivates for devising alternate low-complexity near-optimal detection algorithms for uplink mMIMO systems. In this thesis, with this motivation, different low complexity detection algorithms are studied, and promising solutions are proposed for symbol detection in uplink mMIMO systems. In the first part of the thesis, state-of-the-art detection algorithms for large MIMO systems are investigated. Due to implementation tractability and the requirement of less computational load, evolutionary algorithms are observed to outperform several conventional detection algorithms for large MIMO systems. After investigating the potential drawbacks of existing evolutionary algorithms, a stochastic evolutionary algorithm is proposed for uplink symbol detection in large MIMO systems. However, when the number of antennas scales up in the system, state-of-the-art conventional and evolutionary algorithms are incapable of achieving near-optimal performance in mMIMO systems. Moreover, detection algorithms suitable for large MIMO systems are incapable of benefitting from the hardening nature of mMIMO channel. Hence, in the second part of the thesis, iterative algorithms are investigated for mMIMO systems. As the existing algorithms yield near-optimal performance for a mMIMO system with only high system loading factors, their performance degrades with increased users' numbers. Hence, to improve the drawbacks of existing iterative algorithms, two algorithms based on nonstationary and pseudo stationary iterations are proposed in this thesis. Two mechanisms called quality ordering and reliability feedback are also introduced to improve existing detectors' performance for mMIMO systems. A deep unfolded sparse refinement model is also proposed for low complexity symbol detection in uplink mMIMO systems. Finally, considering the benefits of MBM,

MBM-mMIMO systems are considered. A graph-theoretical approach and minimum support recovery criteria based detection algorithms are proposed for low complexity symbol detection in MBM-mMIMO systems. Simulation results show that the proposed algorithms significantly outperform recently reported large MIMO, mMIMO and MBM-mMIMO detection techniques in terms of BER performance. Convergences of the proposed algorithms are also theoretically analyzed. Computational complexities of the proposed algorithms are substantially lower as compared against existing state-of-the-art algorithms for achieving the same BER performance. It indicates that the proposed algorithms exhibit a desirable trade-off between the complexity and the performance for mMIMO systems and are viable candidates for uplink symbol detection in 5G and beyond wireless communications.

Contents

ABSTRACT	i
LIST OF FIGURES	vii
LIST OF TABLES	xii
LIST OF ALGORITHMS	xiii
LIST OF ABBREVIATIONS/ACRONYMS	xv
LIST OF MATHEMATICAL SYMBOLS	xxii
1 Introduction	1
1.1 Motivation	2
1.2 mMIMO system model	3
1.3 Literature review	5
1.4 Conventional detectors for uplink mMIMO	8
1.4.1 Approximate inverse methods	9
1.4.2 Iterative methods	11
1.5 Contributions	16
1.6 Thesis outline	18
2 Hybrid evolutionary algorithms for large MIMO detection	22
2.1 Introduction	22
2.2 Overview of firefly algorithm	23
2.2.1 Bioluminescence	23
2.2.2 Attractiveness	24
2.2.3 Movement of fireflies	25
2.3 Shortest path problem	25
2.4 Modified firefly algorithm for symbol detection	26
2.5 Analytical expression of BER	30
2.6 Convergence analysis of MFA	31

2.7	Simulation results	34
2.8	Complexity analysis	45
2.9	Summary	45
3	Improved approximate algorithms for massive MIMO detection	48
3.1	Introduction	48
3.2	Hybrid Pseudo-stationary Iterative Detector	50
3.2.1	Initial approximation	50
3.2.2	NSNI for uplink mMIMO detection	51
3.2.3	ISRI for uplink mMIMO detection	53
3.2.4	Pseudo-stationary HA for symbol detection in mMIMO	54
3.2.5	Convergence analysis of HA	55
3.2.6	Simulation results and discussions	56
3.3	Error refinement-based line search for massive MIMO detection	61
3.3.1	ILS for symbol detection in mMIMO systems	61
3.3.2	Convergence analysis of ILS	64
3.3.3	Simulation results	66
3.3.4	Computational analysis	70
3.4	Summary	72
4	Reliability feedback-aided detection in uplink massive MIMO systems	74
4.1	Introduction	74
4.2	Initialization	75
4.3	Quality metric based ordered detection	76
4.4	Reliability feedback mechanism	81
4.5	Convergence analysis	82
4.6	Simulation results	85
4.7	Complexity analysis	90
4.8	Summary	95
5	Deep Unfolded Sparse Refinement Network Based Detection	97
5.1	Introduction	97
5.2	Network Model and Symbol Detection	98
5.2.1	Deep unfolded refinement network	98
5.2.2	Sparsely connected refinement network	99
5.2.3	Symbol detection	101
5.3	Convergence analysis	101
5.4	Complexity analysis	106
5.5	Simulation results	106

CONTENTS

5.5.1	Learning curves	107
5.5.2	BER performance	108
5.6	Summary	109
6	Detection Algorithms for Uplink MBM-mMIMO Systems	113
6.1	Introduction	113
6.2	System Model of MBM-mMIMO	114
6.3	Existing state-of-the-art detectors for MBM-mMIMO	116
6.3.1	MMSE Detection	116
6.3.2	IESP Detection	117
6.4	Graph Traversal Aided Detection in Uplink MBM-mMIMO based on Socio-Cognitive Knowledge of Swarm Optimization	118
6.4.1	Initialization	118
6.4.2	Tree traversal aided symbol detection	119
6.4.3	Theoretical analysis	122
6.4.4	Simulation results	125
6.5	Minimum Error Pursuit Detection Algorithm for MBM-mMIMO	133
6.5.1	Problem Formulation and Symbol Detection	134
6.6	MSRE criteria based detection	135
6.6.1	Simulation results and discussion	139
6.7	Summary	145
7	Conclusion and Future Work	150
7.1	Conclusion	150
7.2	Limitations and Future Work	152
	REFERENCES	157
	LIST OF PUBLICATIONS	168

List of Figures

1.1	massive multiple input multiple output (mMIMO) system. . .	3
2.1	Flow diagram of MFA.	27
2.2	multiple input multiple output (MIMO) detection in MFA. . .	28
2.3	bit error rate (BER) performance comparison of MFA for 8×8 large MIMO system with 4-quadrature amplitude modulation (QAM) modulation.	35
2.4	BER performance comparison of MFA for 16×16 large MIMO system with 4-QAM modulation.	35
2.5	Comparison of BER performances of MFA for 4×4 , 8×8 and 16×16 large MIMO system with 4-QAM modulation.	36
2.6	Comparison of BER performance of MFA with other nature-inspired algorithms for 8×8 large MIMO system with 4-QAM modulation.	36
2.7	Comparison of BER performance of MFA with other nature-inspired algorithms for 16×16 large MIMO system with 4-QAM modulation.	37
2.8	BER performance of MFA under channel state information (CSI) error at the receiver for 8×8 large MIMO system with 4-QAM modulation.	37
2.9	Comparison of BER performance of MFA under CSI error at the receiver for 2×2 , 4×4 and 8×8 MIMO systems with 4-QAM modulation.	42
2.10	Analysis of performance of MFA with variation in absorption coefficient γ for 8×8 large MIMO system with 4-QAM modulation.	42
2.11	Analysis of performance of MFA with variation in k for 8×8 large MIMO system with 4-QAM modulation.	43
2.12	BER vs signal to noise ratio (SNR) plot of MFA with different number of iterations for 8×8 large MIMO system with 4 QAM modulation.	43

LIST OF FIGURES

2.13	Convergence analysis of MFA for 8x8 large MIMO system with 4-QAM modulation.	44
2.14	Comparison of computational complexity versus number of antennas for MFA with 4-QAM modulation	44
3.1	BER performance comparison between non stationary Newton iteration (NSNI) and Newton iteration (NI) for 64-QAM modulation.	57
3.2	BER performance comparison among improved sequential richardson iteration (ISRI) and other iterative mMIMO detection algorithms for 64-QAM modulation.	58
3.3	BER performance comparison among hybrid algorithm (HA) and other mMIMO detection algorithms for 64-QAM modulation.	58
3.4	Comparison of BER performance of HA with other detection algorithms with approximately equal computational complexity.	60
3.5	BER performance of proposed HA for 64-QAM modulation and $L = 2$, under different imperfect CSI at the receiver.	60
3.6	Flowchart of ILS.	65
3.7	Uncoded BER performance of ILS with different number of iterations L	67
3.8	Uncoded BER performance of ILS with different loading factor α	67
3.9	Comparison of uncoded BER performance of ILS for 128×16 mMIMO system.	68
3.10	Comparison of uncoded BER performance of ILS for 144×24 mMIMO system.	68
3.11	Comparison of uncoded BER performance of ILS with zero initial solution for 144×24 mMIMO system.	69
4.1	Flowchart of reliability feedback-aided ordered detection (RFOD).	81
4.2	BER performance comparison for 128×64 mMIMO system with approximately equal real valued multiplications.	86
4.3	BER performance comparison for 128×74 mMIMO system with approximately equal real valued multiplications.	87
4.4	BER performance comparison for 128×64 mMIMO system with increased number of iterations.	88
4.5	BER performance comparison for 128×74 mMIMO system with increased number of iterations.	89

LIST OF FIGURES

4.6	BER performance comparison for 128×64 mMIMO system with approximately equal number of floating point operations (FLOPs).	90
4.7	BER performance comparison for 128×74 mMIMO system with approximately equal number of FLOPs.	92
4.8	Effect of initial solution, reliability feedback and quality ordering on the BER performance of RFOD.	93
4.9	BER performance comparison for 128×64 mMIMO system with different initial solution.	94
5.1	A hidden layer of initial detection network (IDN).	99
5.2	A hidden layer of refinement detection network (RDN).	100
5.3	Differences between sparsely and fully connected networks.	100
5.4	Comparison of BER performances of SRN with other contending algorithms for 128×32 massive MIMO system with 16 QAM modulation.	104
5.5	Comparison of BER performance of SRN with other contending algorithms for 128×32 massive MIMO system with channel estimation error $e = 10\%$ at the BS.	105
5.6	Comparison of computational complexity of SRN with other contending algorithms for different number of hidden layers /iterations with $N_t = 8$	106
5.7	Learning curves of sparse refinement network (SRN).	107
5.8	Comparison of BER performances of SRN with different number of hidden layers.	109
5.9	Comparison of BER performances of SRN with different values of masking ratio.	110
6.1	media based modulation with massive multiple input multiple output (MBM-mMIMO) system model.	115
6.2	MBM-mMIMO symbol detection as a spanning tree.	119
6.3	Flowchart of SID.	122
6.4	Comparison of BER performance of swarm intelligence based detection (SID) with other contending techniques for $N_r = 128$, $N_t = 16$ and $N_{RF} = 2$	126
6.5	Comparison of BER performance of SID with other contending techniques for $N_r = 128$, $N_t = 16$ and $N_{RF} = 3$	127
6.6	Comparison of BER performance of SID with other contending techniques for $N_r = 128$, $N_t = 32$ and $N_{RF} = 3$	128

LIST OF FIGURES

6.7	BER performance comparison of SID with other contending detection techniques under perfect CSI scenarios, $N_r = 128$, $N_t = 16$ and $N_{RF} = 4$	129
6.8	BER performances of SID under different CSI mismatch scenarios for $N_r = 128$, $N_t = 16$ and $N_{RF} = 3$	130
6.9	BER performance comparison of proposed detection technique with other contending detection techniques under imperfect CSI scenario, $N_r = 128$, $N_t = 16$ and $N_{RF} = 3$	131
6.10	Comparison of computational complexity under different number of iterations for $N_r = 128$, $N_t = 16$ and $N_{RF} = 4$	132
6.11	Comparison of computational complexity under different number of base station (BS) antennas for $N_{RF} = 4$, $N_t = 16$ and $L = 4$	133
6.12	Block Diagram of minimum error pursuit detection (MEPD) Technique.	136
6.13	Block Diagram of minimum error pursuit detection with restricted search (MEPDRS) Technique.	139
6.14	BER performance comparison of MEPD with MMSE, inclusion exclusion subspace pursuit (IESP) and iterative interference cancellation (IIC).	141
6.15	BER performance comparison of MEPDRS with MMSE, IESP and IIC.	142
6.16	BER performance comparison of MEPD, IESP and IIC for different number of radio frequency (RF) mirrors.	143
6.17	BER performance comparison of MEPDRS, IESP and IIC for different number of RF mirrors.	144
6.18	BER performance comparison of MEPD, MMSE, IESP and IIC with different number of BS antennas.	145
6.19	Comparison of computational complexity of contending detection techniques for different number of iterations.	146
6.20	Comparison of computational complexity of contending detection techniques for different number of BS antennas.	147
6.21	Computational complexity of contending techniques with number of RF mirrors.	148

List of Tables

2.1	Simulation parameters for the proposed MFA algorithm with 4-QAM modulation.	38
2.2	Comparison of BER performance of MFA with conventional MIMO detection algorithms	38
2.3	Description of different parameters used for simulation of large MIMO detection algorithms.	39
2.4	Abbreviations and simulation parameters of different nature-inspired MIMO detection algorithms.	40
2.5	BER performance of MFA under imperfect CSI at $N_t = N_r = 8$ for 4-QAM modulation.	40
3.1	Comparison of computational complexity of different detection algorithms.	59
3.2	Number of real valued operations	71
4.1	Number of real-valued operations required for detection.	91
4.2	Average number of FLOPs ($\times 10^5$) required for detection.	91
4.3	Real valued operations.	94
6.1	Table of parameters	125
6.2	Computational complexity	140

List of Algorithms

1.1	Neumann series (NS) based detector	10
1.2	NI based detector	11
1.3	Iterative detection	12
1.4	Richardson iteration (RI) based detection	12
1.5	joint steepest descent Jacobi iteration (JSDJI) based detection	13
1.6	Gauss Seidel (GS) iteration based detector	14
1.7	Conjugate gradient based detection	15
1.8	Iterative sequential detection	16
2.1	Firefly algorithm	24
2.2	Proposed MFA algorithm	29
3.1	Proposed NSNI algorithm	53
3.2	Proposed HA algorithm	55
3.3	Proposed ILS algorithm	62
4.1	Proposed RFOD algorithm	80
6.1	Proposed SID algorithm	123
6.2	Proposed MEPD algorithm	137
6.3	Proposed MEPDRS algorithm	138

LIST OF ALGORITHMS

List of Abbreviations

4G fourth generation.

5G fifth generation.

ACO ant colony optimization.

AMI approximate matrix inversion.

AWGN additive white Gaussian noise.

BER bit error rate.

BPSO binary particle swarm optimization.

BS base station.

CCACO congestion control ant colony optimization.

CG conjugate gradient.

CHEMP channel hardening exploiting message passing.

CSI channel state information.

D2D device-to-device communications.

DBNI diagonal band Newton iteration.

DBNIIR diagonal band Newton iteration with iterative refinement.

DetNet detection network.

DL deep learning.

FA firefly algorithm.

FANA firefly algorithm with neighborhood attraction.

FLOPs floating point operations.

FPU floating point unit.

fullyCon fully connected neural network.

GS Gauss Seidel.

HA hybrid algorithm.

HD Hamming distance.

IDN initial detection network.

IESP inclusion exclusion subspace pursuit.

IIC iterative interference cancellation.

ILS iterative line search.

IoT internet of things.

IRS intelligent reflecting surface.

ISD iterative sequential detection.

ISI inter symbol interference.

ISRI improved sequential richardson iteration.

JI Jacobi iteration.

JSDJI joint steepest descent Jacobi iteration.

KS krylov space.

LAS likelihood ascent search.

LCMPD low complexity message passing based detection.

LINPACK linear equations software package.

LM lanxzos method.

LTE long term evolution.

MATLAB matrix Laboratory.

MBER minimum bit error rate.

MBM media based modulation.

MBM-mMIMO media based modulation with massive multiple input multiple output.

MEPD minimum error pursuit detection.

MEPDRS minimum error pursuit detection with restricted search.

MFA modified firefly algorithm.

MGF moment generating function.

MII matrix inversionless iteration.

MIMO multiple input multiple output.

MISO multiple input single output.

ML maximum likelihood.

mMIMO massive multiple input multiple output.

MMSE minimum mean square error.

MPD message passing based detection.

MPSO memetic particle swarm optimization.

MS matrix splitting.

MSD MBM signal detector.

MSE mean square error.

MSRE minimum support recovery error.

MST minimum spanning tree.

NI Newton iteration.

NIIR Newton iteration with iterative refinement.

- NP** nondeterministic polynomial time.
- NS** Neumann series.
- NSI** Newton Schulz iteration.
- NSNI** non stationary Newton iteration.
- OSIC** ordered successive interference cancellation.
- PIC** parallel interference cancellation.
- PL** partial learning.
- PSO** particle swarm optimization.
- QAM** quadrature amplitude modulation.
- QCM** quadrature channel modulation.
- QO** quality ordering.
- RDN** refinement detection network.
- RF** radio frequency.
- RFM** reliability feedback mechanism.
- RFOD** reliability feedback-aided ordered detection.
- RI** Richardson iteration.
- RS** restricted search.
- SD** sphere decoder.
- SDA** steepest descent algorithm.
- SIC** successive interference cancellation.
- SID** swarm intelligence based detection.
- SIMO** single input multiple output.
- SISO** single input single output.
- SNR** signal to noise ratio.

List of Abbreviations

SOR successive over relaxation.

SPSO standard particle swarm optimization.

SR support recovery.

SRE support recovery error.

SRN sparse refinement network.

UCCACO unordered congestion control ant colony optimization.

V-BLAST vertical Bell laboratories layered architecture.

V2X vehicle to everything.

VLC visible light communication.

WiFi wireless fidelity.

WiMAX wireless interoperability for microwave access.

WSN wireless sensor networks.

ZF zero forcing.

List of Mathematical Symbols

\mathbf{x}	Transmit symbol vector
\mathbf{y}	Receive symbol vector
\mathbf{H}	Channel matrix
σ^2	Noise variance
N_t	Number of transmit antenna/users
N_r	Number of BS antenna
N_{RF}	Number of Number of RF mirror
$(.)^\dagger$	Pseudo-inverse operator
$(.)^{-1}$	Matrix inversion
\mathcal{A}	Square QAM constellation set
\mathcal{M}	MBM constellation set
\mathcal{P}	Probability density/mass function
γ	Step size
e	Channel estimation error at the BS
$\ \cdot\ _p$	Lp vector norm
$\#(\cdot)$	Cardinality of a set
$ \cdot $	Absolute value
\mathcal{P}_e	The probability of error
$u \rightsquigarrow^l v$	A path l from vertex u to vertex v
$u.a$	An attribute a for vertex u
$(u, v).a$	An attribute a of an edge (u, v)
$Adj[u]$	The adjacent vertices of vertex u
x_i	The i^{th} element of a vector \mathbf{x}
FES	Functional evaluation of ML-cost
$(.)^T$	Transpose operation
$\langle \cdot, \cdot \rangle$	Inner product
$\langle \cdot, \cdot \rangle_F$	Frobenius inner product
$[\cdot \circ \cdot]$	Hadamard product
$\ \cdot\ $	Matrix norm
$\nabla(\cdot)$	The gradient operator
$\mathbf{x}^{(*)}$	Estimated symbol vector at convergence
$\mathbb{P}_{\mathcal{M}}(\cdot)$	Projection onto a set \mathcal{M}
$\mathcal{D}(\cdot, \cdot)$	Hamming distance operator
\mathbf{H}_j	The matrix corresponding to the j^{th} user
$h_{j,i,k}$	The element in the i^{th} row and the k^{th} column of the sub-matrix \mathbf{H}_j
$\mathbf{h}_{j,k}$	The k^{th} column of \mathbf{H}_j
$x_{j,i}$	The i^{th} element of \mathbf{x}_j
\mathcal{W}	Moment generating function

Chapter 1

Introduction

There is an ever-growing demand for wireless data traffic due to the exponential growth in the usage of smartphones, tablets, laptops and other wireless devices. Hence, to fulfil this demand and improve the wireless throughput, new wireless solutions need to be exploited. As licensed frequency spectrum is an expensive resource, new technologies must be developed to increase the spectral efficiency in wireless communications. Deploying multiple number of antennas at the receiver as well as at the transmitter is a promising solution to improve the spectral efficiency. Furthermore, the involvement of multiple number of antennas at both the transmitter and the receiver sides yields additional benefit of spatial diversity, which in turn gives link reliability. However, wireless links face multipath fading and shadowing due to the involvement of obstacles between the transmitter and the receiver, posing a fundamental challenge in a robust communication scenario. The situation becomes more severe where a massive number of antennas are involved at both the transmitter and the receiver sides in mMIMO wireless communication systems. Hence, viable solutions need to be explored for reliable communication in mMIMO systems.

1.1 Motivation

mMIMO has been a successful technique for achieving improved spectral efficiency in fourth generation (4G) wireless standards such as long term evolution (LTE), LTE-Advanced, wireless interoperability for microwave access (WiMAX) and 802.11 wireless fidelity (WiFi) [1, 2]. MIMO systems' underlying idea is that it facilitates the transmission of multiple data streams simultaneously from source-to-destination, enhancing the diversity and multiplexing gains in wireless systems. Moreover, the introduction of multiple antenna wireless systems has opened up new research dimensions such as space-time block coding, index modulation, and antenna switching for more reliable and efficient communication. With the unprecedented growth in data starving, wireless applications such as internet of things (IoT), wireless sensor networks (WSN), device-to-device communications (D2D) and vehicle to everything (V2X) communications high spectral and energy-efficient wireless techniques are of particular interest [3]. mMIMO is a key enabling technology for realizing the demand for excessive data rate, spectral efficiency and energy efficiency in fifth generation (5G) and beyond wireless communication systems [3, 4]. mMIMO systems have attracted a lot of research attention because such systems, when used in the existing cellular/communication networks, could provide enormous advantages in terms of data rate, quality of service, and the number of users simultaneously [1, 3, 4]. In mMIMO systems, a BS employs hundreds to thousands of antennas to serve a few tens of the users. A large number of BS antennas in mMIMO enhances the diversity and multiplexing gain, which leads to the improvement in both the reliability of service and the rate of information transfer, respectively [4]. The spectral efficiency of mMIMO system further enhances with media based modulation (MBM). Though being limited to low mobility or static communication scenarios, MBM with N_r receiver antennas over a static multipath channel is capable of asymptotically achieving the channel capacity of N_r parallel additive white Gaussian noise (AWGN) channels [5]. However, practically there

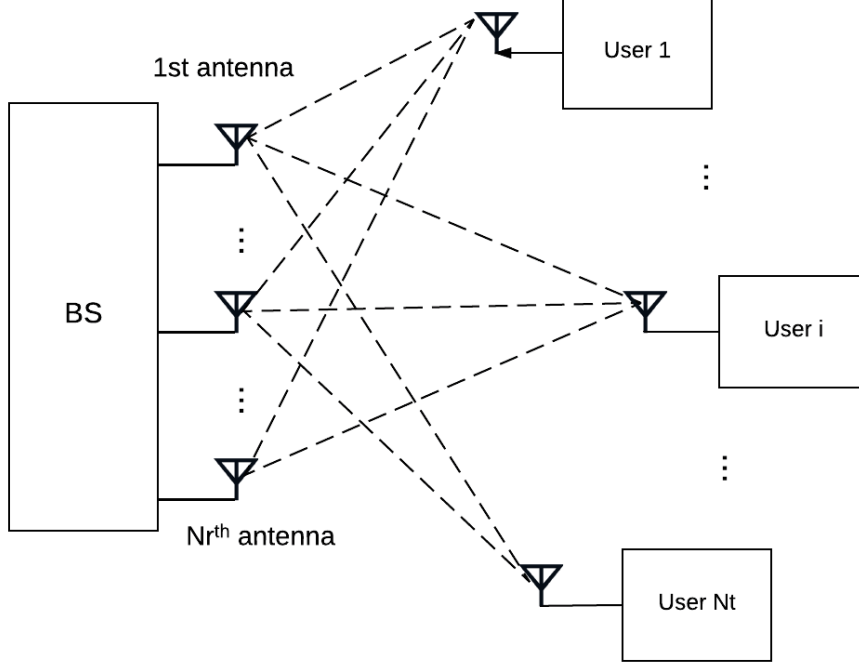


Figure 1.1: mMIMO system.

are several challenging issues such as architectural complexity, power requirements, latency in signal processing, and antenna array [2]. Amongst these challenging issues, the computational complexity for reliable detection of the transmitted information at the receiver side is hugely crucial for robust receiver architectures in 5G and beyond systems [6, 7]. Moreover, the data rate requirement of recent wireless applications such as IoT, WSN, D2D, and V2X necessitates the development of ultra-low latency and highly reliable symbol detection algorithms at the BS.

1.2 mMIMO system model

Consider N_t single antenna users and a BS with N_r antennas ($N_r \gg N_t$ for e.g., $N_r = 128, N_t = 16$) as depicted in Fig. 1.1. Each user transmits its information symbol say x_i , for $i = 1, 2, \dots, N_t$, to the BS simultaneously,

1.2. MMIMO SYSTEM MODEL

which is also known as uplink transmission. Each symbol \tilde{x}_i is assumed to be drawn from a given constellation set say \mathbb{A} , for e.g., 16-QAM, 64-QAM, etc. Without loss of generality, the users are assumed to be synchronised in time during their transmission to the BS. For tractability, a Rayleigh flat fading channel is considered between the i th user and j th receive antenna, denoted as \tilde{h}_{ji} , for $j = 1, 2, \dots, N_r$ and $i = 1, 2, \dots, N_t$. Each element \tilde{h}_{ji} of the channel matrix $\tilde{\mathbf{H}}$ is independent and identically distributed (i.i.d) complex Gaussian with mean zero and variance unity i.e. $\sim \mathcal{CN}(0, 1)$. The received vector $\tilde{\mathbf{y}}$ after demodulation and sampling at the receiver end can be written as¹

$$\tilde{\mathbf{y}} = \tilde{\mathbf{H}}\mathbf{x} + \tilde{\mathbf{n}}, \quad (1.1)$$

where $\tilde{\mathbf{n}}$ is the AWGN vector with each of its elements \tilde{n}_j , for $j = 1, 2, \dots, N_r$. Each element of $\tilde{\mathbf{n}}$ is i.i.d complex normal with mean zero and variance σ^2 i.e. $\sim \mathcal{CN}(0, \sigma^2)$. The average received signal to noise ratio (SNR) at the receiver can be computed as $\frac{N_t E_x}{\sigma^2}$. In equation (1.1), each element \tilde{y}_j of $\tilde{\mathbf{y}}$, for $j = 1, 2, \dots, N_r$, is the received information at the j th receive antenna which consists of combination of symbols from each transmit antenna modified by the channel state \tilde{h}_{ji} and the AWGN noise n_j as

$$\tilde{y}_j = \sum_{i=1}^{N_t} \tilde{h}_{ji} \tilde{x}_i + \tilde{n}_i, \quad \forall \quad j = 1, 2, \dots, N_r. \quad (1.2)$$

Without loss of generality, the complex-valued system model in (1.1) is represented as a real-valued system [8]

$$\mathbf{y} = \mathbf{H}\mathbf{x} + \mathbf{n}, \quad (1.3)$$

¹A MIMO system where tens of antennas are used at both the transmitter and the receiver is known as a large MIMO system. When hundreds of antennas are deployed at the BS to serve few tens of users, it is referred to as mMIMO systems. Consequently, mMIMO has a higher spectral efficiency than large MIMO systems.

where $\mathbf{x} = \left[\Re(\tilde{\mathbf{x}}), \Im(\tilde{\mathbf{x}}) \right]_{2N_t \times 1}^T$, $\mathbf{y} = \left[\Re(\tilde{\mathbf{y}}), \Im(\tilde{\mathbf{y}}) \right]_{2N_r \times 1}^T$, $\mathbf{n} = \left[\Re(\tilde{\mathbf{n}}), \Im(\tilde{\mathbf{n}}) \right]_{2N_r \times 1}^T$ and $\mathbf{H} = \begin{bmatrix} \Re(\tilde{\mathbf{H}}) & -\Im(\tilde{\mathbf{H}}) \\ \Im(\tilde{\mathbf{H}}) & \Re(\tilde{\mathbf{H}}) \end{bmatrix}_{2N_r \times 2N_t}$. Assume corresponding real valued constellation set is \mathcal{A} . However, due to limited time-frequency resources and channel coherence time, mMIMO systems suffer from pilot contamination [9], resulting in imperfect CSI at the BS [1, 10, 11]. Even with the increase in the number of antennas, pilot contamination does not vanish in the mMIMO system. Hence, after considering an imperfect channel estimation at the BS, the MIMO system can be modelled as [12]

$$\mathbf{y} = \hat{\mathbf{H}}\mathbf{x} + \mathbf{n} \quad (1.4)$$

where $\hat{\mathbf{H}} = \mathbf{H} + \mathbf{e}\boldsymbol{\theta}$ with \mathbf{H} as the actual channel gain matrix and $\mathbf{e}\boldsymbol{\theta}$ is the estimation error. Without loss of generality, the elements of $\boldsymbol{\theta}$ are assumed to be i.i.d Gaussian random variables with zero mean and unit variance [13, 14]. The parameter \mathbf{e} refers to the channel estimation accuracy. Due to the interference of symbols from different users at each receive antenna and the presence of additive noise, it becomes challenging to separate and detect the symbol from each user at the receiver. Therefore, reliable symbol detection in the mMIMO system is a demanding research problem.

1.3 Literature review

Maximum likelihood (ML) detection performs optimal symbol detection at the BS in uplink mMIMO system [15]. However, ML conducts an exhaustive search over all the transmit vectors possible from the constellation set. Hence, the ML detection is an NP-hard (non-deterministic polynomial-time hard) problem, and the computational complexity is exponential with the number of users and the modulation order. Due to the low computational complexity ($O(N_t^3)$, where N_t is the number of transmit antennas), linear detectors like zero forcing (ZF) and minimum mean square error (MMSE) are preferable

1.3. LITERATURE REVIEW

in practice. However, these detectors' efficiency degrades with an increase in the number of antennas and/or constellation size. In contrast, nonlinear detectors like vertical Bell laboratories layered architecture (V-BLAST) [16] detector, successive interference cancellation (SIC), and ordered successive interference cancellation (OSIC) based MIMO detection algorithms [15, 16] provide superior performance than linear detectors. Remarkably, they provide inferior performance compared to sphere decoder (SD) [17]. SD is a nonlinear detector which provides near-ML performance; however, its computational complexity increases exponentially with constellation size [15]. Hence, the design of a low complexity efficient detection algorithm is required for reliable detection in large MIMO systems. Several low complexity near-ML performance achieving algorithms have been proposed [18–20] for large scale MIMO systems. The performance of those algorithms [18, 19] degrades with CSI estimation error, and hence, perfect channel estimation is required for reliable detection at the receiver. Likelihood ascent search (LAS) algorithm [20] performs a sequence of likelihood searches, which in turn increases the computational complexity.

The requirement of less number of computational resources in evolutionary algorithms [12, 21, 21–25] make those nature-inspired algorithms promising choices for symbol detection in large scale MIMO systems. Most of the state-of-the-art evolutionary detection algorithms proposed in the literature for MIMO systems focus on ant colony optimization (ACO) [26], particle swarm optimization (PSO) [27] and hybridization of these two algorithms [12]. However, each of these two algorithms and their variants have drawbacks. Consequently, many iterations or populations are required to achieve a near-optimal solution in uplink large MIMO systems while using ACO and PSO for developing detection algorithms. Moreover, the performance of several existing evolutionary algorithms [12, 28–32] suffers from BER degradation due to imperfect CSI estimation at the BS. Few existing algorithms [28, 29] also converge to local optima and their performances [12, 30–32] depend on the choice of the initial solution. Moreover, when the number of

antennas scales up in the system, the existing large MIMO detection algorithms are not suitable for uplink mMIMO systems.

The challenging problem of symbol detection in mMIMO with high reliability is achieved in the literature by using one of the following two techniques, a) low-complexity approximate matrix inversion (AMI) and b) matrix inversionless iteration (MII).

AMI based detectors approximate either the Gram matrix or the MMSE filter matrix and yield near-MMSE BER performance. NS [6] and NI [33] are two primary AMI techniques. NS performs polynomial expansion of the inverse of the Gram matrix for few finite numbers of times. However, NS based detection is computationally acceptable when the number of iterations is less than or equal to two. NS's computational complexity is reduced in MMSE with parallel interference cancellation (PIC) [34] with marginal performance loss. MMSE-PIC is observed to achieve near-MMSE performance with considerably lower computational complexity over NS. NS based detection techniques suffer from significant performance loss when the system loading factor (the ratio between the receive and the transmit antenna) is substantially low. Moreover, the iterations in NS are slow. Slow convergence of NS is improved utilizing Newton Schulz iteration (NSI). However, NSI is not computationally beneficial compared to NS. NI based detection techniques converge faster as compared to NS. NS and NI both have almost equal computational complexity when the number of iterations increases [35].

RI [36, 37], JSDJI [38] and conjugate gradient (CG) [36, 39] based detection techniques are primary MII based techniques. MII techniques based detectors are proposed to improve the performance of primary AMI based detection techniques. Several existing MII techniques based detectors outperform AMI based detectors. However, few hybrid AMI-MII based detectors outperform both AMI and IIM based detectors. Matrix splitting (MS) [40] inspired RI is proposed in the literature to outperform primary AMI based detection techniques. However, RI requires a large number of iterations to achieve near-optimal BER performance. Steepest descent algorithm (SDA)

[41], and CG based detection techniques also require a large number of iterations to provide significant performance gain over primary AMI detection techniques. Krylov space (KS) [42] based Lanczos method (LM) [43–45] is capable of achieving near-MMSE performance even with a small number of iterations. However, LM based detection is not effective in the time-varying channel and consumes high computational load. Successive over relaxation (SOR) iteration based detector is proposed to outperform the NS method in complexity and BER performance [35]. The SOR method becomes the GS [46] method when the relaxation factor has been set at unity. Though GS outperforms NS method, it is practically not suitable for parallel implementation.

When mMIMO systems are used with MBM, conventional detection techniques such as MMSE cannot utilize the transmitted symbol vector's structured sparse nature and shows poor performance compared to the ML detection. To obtain near-ML performance for MBM-mMIMO systems, algorithms such as IIC [47], IESP [48] and channel hardening exploiting message passing (CHEMP)-MBM signal detector (MSD)[49] are proposed in the literature. IIC performs exhaustive search based detection for each user and updates the symbol for one user at a time using the greedy approach. IIC with this search mechanism fails to utilize some key features of MBM-mMIMO like a) the channel hardening phenomenon in mMIMO and b) the structured sparse nature of the transmitted signal. On the other hand, both IESP [48] and CHEMP-MSD achieve inferior BER performance compared to IIC. Hence, further research in this field is crucial for devising novel low-complexity near-optimal detection techniques for achieving potential benefits of mMIMO in 5G and beyond wireless systems.

1.4 Conventional detectors for uplink mMIMO

The symbol detection problem in mMIMO is to find the solution to the expression $\mathbf{Ax} = \mathbf{b}$ without performing the inverse of a matrix \mathbf{A} . $\mathbf{A} =$

$\mathbf{G} + \frac{\sigma^2}{E_x} \mathbf{I}_{N_t}$ is called the MMSE filter matrix. $\mathbf{G} = \mathbf{H}^H \mathbf{H}$ is called the Gram matrix and $\mathbf{b} = \mathbf{H}^T \mathbf{y}$. \mathbf{I}_{2N_t} is an identity matrix.

1.4.1 Approximate inverse methods

In these methods, approximate matrix inverse approaches are discussed wherein an approximation of the regularized Gram matrix \mathbf{A} is computed and used for symbol detection for mMIMO systems.

NS expansion-based detection

This technique is based on the concept of *polynomial expansion* where the inverse of a matrix is expanded as a sum of an infinite number of terms. Each term involves either matrix-matrix multiplication or matrix-vector multiplication or both. The P th order Neumann series approximation (consists of only first P terms of an infinite series) of the inverse of a matrix can be written as

$$\mathbf{A}_P^{-1} = \sum_{k=0}^{P-1} (\mathbf{W} (\mathbf{W}^{-1} - \mathbf{A}))^{(k)} \mathbf{W}, \quad (1.5)$$

where \mathbf{W} denotes an initial low-complexity estimate of the inverse. The series in equation (1.5) converges to the exact inverse with $P \rightarrow \infty$ with \mathbf{W} satisfying the condition

$$\lim_{k \rightarrow \infty} (\mathbf{I} - \mathbf{W}\mathbf{A})^{(m)} = \mathbf{O}. \quad (1.6)$$

The application of NS expansion for mMIMO detection is based on the fact that in mMIMO, due to channel hardening, the regularised Gram matrix \mathbf{A} is a diagonally dominant matrix i.e. the diagonal elements are significantly higher than the off-diagonal elements. Therefore, the matrix \mathbf{A} can be written as $\mathbf{A} = \mathbf{D} + \mathbf{E}$, where \mathbf{D} is the diagonal matrix and \mathbf{E} is the hollow matrix. The matrix \mathbf{D}^{-1} , which is inverse of the diagonal elements of \mathbf{D} is used as a low-complexity initial estimate of the inverse in Neumann series

1.4. CONVENTIONAL DETECTORS FOR UPLINK MMIMO

expansion based detection. The P th order series expansion can be written as

$$\mathbf{A}_P^{-1} = \sum_{k=0}^{P-1} (-\mathbf{D}^{-1}\mathbf{E})^{(k)} \mathbf{D}^{-1}. \quad (1.7)$$

Using \mathbf{A}_P^{-1} , the symbols can be detected as

$$\hat{\mathbf{x}}_{NS} = \mathcal{Q} [\mathbf{A}_P^{-1} \mathbf{b}] = \mathcal{Q} \left[\sum_{k=0}^{P-1} (-\mathbf{D}^{-1}\mathbf{E})^{(k)} \mathbf{D}^{-1} \mathbf{b} \right]. \quad (1.8)$$

Algorithm 1.1 shows the pseudocode of NS expansion-based mMIMO detection.

Algorithm 1.1 NS based detector

- 1: **Input:** \mathbf{y} , \mathbf{H} , N_t , N_r , σ^2
 - 2: Compute matrix $\mathbf{A} = \mathbf{G} + \frac{\sigma^2}{E_x} \mathbf{I}_{N_t}$ where $\mathbf{G} = \mathbf{H}^H \mathbf{H}$
 - 3: Compute the inverse of matrix \mathbf{A} i.e. \mathbf{A}^{-1}
 - 4: Compute the MF output of \mathbf{y} : $\mathbf{b} = \mathbf{H}^H \mathbf{y}$
 - 5: Compute the MMSE estimate $\mathbf{x}_{MMSE} = \mathcal{Q} [\mathbf{A}^{-1} \mathbf{b}]$
 - 6: **Output:** \mathbf{x}_{MMSE}
-

NI based detection

In Newton iteration-based approximate inverse method, an initial estimate of the inverse of a matrix is refined iteratively. The iterative update of the inverse is given by

$$\mathbf{A}^{-1(k+1)} = \mathbf{A}^{-1(k)} \left(2\mathbf{I} - \mathbf{A} \mathbf{A}^{-1(k)} \right). \quad (1.9)$$

The approximate inverse in equation (1.9) converges quadratically to the exact inverse if the initial estimate satisfies

$$\|\mathbf{I} - \mathbf{A} \mathbf{A}^{-1(0)}\|_2 \leq 1. \quad (1.10)$$

Similar to the NS expansion, the initial estimate of the inverse is \mathbf{D}^{-1} , which is refined iteratively. The detected symbols using L iterations can be written as

$$\hat{\mathbf{x}}_{NI} = \mathcal{Q} \left[\mathbf{A}^{-1(L)} \mathbf{b} \right]. \quad (1.11)$$

The pseudocode of the NI based mMIMO detection is shown in Algorithm 1.2.

Algorithm 1.2 NI based detector

- 1: **Input:** $\mathbf{y}, \mathbf{H}, N_t, N_r, \sigma^2$
 - 2: Compute matrix $\mathbf{A} = \mathbf{G} + \frac{\sigma^2}{E_x} \mathbf{I}_K$ where $\mathbf{G} = \mathbf{H}^H \mathbf{H}$
 - 3: Compute the inverse of matrix \mathbf{A} i.e. \mathbf{A}^{-1}
 - 4: Compute the MF output of \mathbf{y} : $\mathbf{b} = \mathbf{H}^H \mathbf{y}$
 - 5: Compute the MMSE estimate $\mathbf{x}_{MMSE} = \mathcal{Q} [\mathbf{A}^{-1} \mathbf{b}]$
 - 6: **Output:** \mathbf{x}_{MMSE}
-

1.4.2 Iterative methods

In this subsection, iterative methods are discussed for symbol detection in mMIMO systems. The key idea behind iterative methods is that a low-complexity initial solution is refined iteratively for a sufficient number of iterations to obtain a better solution. The initial solution is refined in such a way that the final solution achieves superior BER performance without much effort in the computational complexity. There are two main components in the iterative methods, which are

1. Initial solution
2. Iterative update

The pseudocode of each iterative detection technique is more or less similar and is shown as Algorithm 1.3. An excellent initial solution determines how fast the algorithm converges to the final solution. However, the convergence of the algorithm highly depends on the iterative update scheme. Different algorithms in the literature consider different update mechanism and initial solution, which is discussed next.

Algorithm 1.3 Iterative detection

- 1: **Input:** $\mathbf{y}, \mathbf{H}, \mathbf{A}, \mathbf{G}$ N_t, N_r, σ^2
 - 2: Compute initial solution $\mathbf{x}^{(0)}$
 - 3: Update the initial solution iteratively
 - 4: **Output:** Final solution after L iterations $\mathbf{x}^{(L)}$
-

RI based detection

In this technique, the positive semidefiniteness of the regularised Gram matrix is exploited for performing Richardson iterations to detect the symbols efficiently. The Richardson iteration is written as

$$\mathbf{x}^{(k+1)} = \mathbf{x}^{(k)} + \rho (\mathbf{b} - \mathbf{A}\mathbf{x}^{(k)}), \quad (1.12)$$

where ρ is the relaxation parameter in RI. For convergence, the relaxation parameter ρ should be between $0 < \rho < 2/\lambda_{max}$, where λ_{max} is the maximum eigenvalue of the matrix \mathbf{A} . The performance of RI method also depends on the initial solution, and therefore, a low-complexity initial solution is obtained as

$$\mathbf{x}^{(0)} = \mathbf{D}^{-1}\mathbf{b}. \quad (1.13)$$

The refined solution after L iterations is considered as the output of the detector. The pseudocode of the RI is discussed in Algorithm 1.4.

Algorithm 1.4 RI based detection

- 1: **Input:** $\mathbf{y}, \mathbf{H}, \mathbf{A}, \mathbf{G}$ N_t, N_r, σ^2
 - 2: Compute initial solution : $\mathbf{x}^{(0)} = \mathbf{D}^{-1}\mathbf{b}$
 - 3: **for** ($m = 1, m++, m \leq L$) **do**
 - 4: Update the initial solution iteratively as : $\mathbf{x}^{(m+1)} = \mathbf{x}^{(m)} + \rho (\mathbf{b} - \mathbf{A}\mathbf{x}^{(m)})$
 - 5: **end for**
 - 6: **Output:** Final solution after L iterations $\mathcal{Q}[\mathbf{x}^{(L)}]$
-

JSDJI based detection

In this technique, Jacobi iteration (JI) is used for refining the initial solution. The JSDJI can be written as

$$\mathbf{x}^{(m+1)} = \mathbf{x}^{(m)} + \mathbf{D}^{-1} (\mathbf{b} - \mathbf{A}\mathbf{x}^{(m)}) . \quad (1.14)$$

An iteration of the steepest descent is hybridised with JI to accelerate the convergence of the algorithm.

$$\mathbf{x}^{(2)} = \mathbf{x}^{(0)} + v\mathbf{r}^{(0)} + \mathbf{D}^{-1}(\mathbf{r}^{(0)} - v\mathbf{g}^{(0)}), \quad (1.15)$$

where $\mathbf{r}^{(0)} = \mathbf{b} - \mathbf{A}\mathbf{x}^{(0)}$, $v = \frac{\mathbf{r}^{(0)H}\mathbf{r}^{(0)}}{(\mathbf{A}\mathbf{r}^{(0)})^H\mathbf{r}^{(0)}}$ and $\mathbf{g}^{(0)} = \mathbf{A}\mathbf{r}^{(0)}$. The pseudocode of JSDJI is given in Algorithm 1.5.

Algorithm 1.5 JSDJI based detection

- 1: **Input:** $\mathbf{y}, \mathbf{H}, \mathbf{A}, \mathbf{G}, N_r, N_t, \sigma^2$
 - 2: Compute initial solution : $\mathbf{x}^{(0)} = \mathbf{D}^{-1}\mathbf{b}$
 - 3: Perform the first joint iteration as $\mathbf{x}^{(2)} = \mathbf{x}^{(0)} + v\mathbf{r}^{(0)} + \mathbf{D}^{-1}(\mathbf{r}^{(0)} - v\mathbf{g}^{(0)})$
 where $\mathbf{r}^{(0)} = \mathbf{b} - \mathbf{A}\mathbf{x}^{(0)}$, $v = \frac{\mathbf{r}^{(0)H}\mathbf{r}^{(0)}}{(\mathbf{A}\mathbf{r}^{(0)})^H\mathbf{r}^{(0)}}$ and $\mathbf{g}^{(0)} = \mathbf{A}\mathbf{r}^{(0)}$
 - 4: **for** ($m = 3, m++, m \leq L$) **do**
 - 5: Update the initial solution iteratively as : $\mathbf{x}^{(m+1)} = \mathbf{x}^{(m)} + \mathbf{D}^{-1}(\mathbf{b} - \mathbf{A}\mathbf{x}^{(m)})$
 - 6: **end for**
 - 7: **Output:** Final solution after L iterations $\mathcal{Q} [\mathbf{x}^{(L)}]$
-

GS based detection

GS is another iterative technique proposed in the literature for solving the set of linear equations. As discussed earlier in Section 1.2, MMSE detection in mMIMO is nothing but finding a solution to the set of linear equation with noisy measurements. However, due to channel hardening, the MMSE solution turns out to be a near-optimal one. Therefore, the techniques which can find the solution without explicitly computing the matrix inverse are of high interest. GS method is one such technique that computes the solution

1.4. CONVENTIONAL DETECTORS FOR UPLINK MMIMO

iteratively. Similar to other iterative techniques such as Richardson and Jacobi methods, this technique also exploits the positive semi-definite property of the regularised Gram matrix \mathbf{A} . The key idea behind the GS technique is to represent the matrix \mathbf{A} as

$$\mathbf{A} = \mathbf{D} + \mathbf{L} + \mathbf{L}^H, \quad (1.16)$$

where \mathbf{D} , \mathbf{L} and \mathbf{L}^H denote the diagonal matrix, strictly lower triangular matrix, and strictly upper triangular matrix of \mathbf{A} , respectively. The Gauss-Seidel iterations are then used for refining the initial solution as

$$\mathbf{x}^{(m+1)} = (\mathbf{D} + \mathbf{L})^{-1} (\mathbf{b} - \mathbf{L}^H \mathbf{x}^{(m)}). \quad (1.17)$$

The pseudocode of GS based detection is shown in Algorithm 1.6

Algorithm 1.6 GS iteration based detector

- 1: **Input:** \mathbf{y} , \mathbf{H} , \mathbf{A} , \mathbf{G} N_t, N_r, σ^2
 - 2: Compute initial solution : $\mathbf{x}^{(0)} = \mathbf{D}^{-1} \mathbf{b}$
 - 3: **for** ($m = 1, m++$, $m \leq L$) **do**
 - 4: Update the initial solution iteratively as : $\mathbf{x}^{(m+1)} = (\mathbf{D} + \mathbf{L})^{-1} (\mathbf{b} - \mathbf{L}^H \mathbf{x}^{(m)})$
 - 5: **end for**
 - 6: **Output:** Final solution after L iterations $\mathcal{Q} [\mathbf{x}^{(L)}]$
-

CG based detection

CG is another way of solving a set of linear equations [50] where the search for the solution is performed in the conjugate direction with a stepsize moving towards the better solution iteratively. In CG based mMIMO detection [39], the search direction and the step size for the movement are determined first, and the solution is updated by moving a step in the search direction next. The detailed steps involved in the CG method are shown in Algorithm 1.7.

Algorithm 1.7 Conjugate gradient based detection

```

1: Input:  $\mathbf{y}, \mathbf{H}, \mathbf{A}, \mathbf{G}$   $N_t, N_r, \sigma^2$ 
2: Initialization:  $\mathbf{b} = \mathbf{H}^H \mathbf{y}$ ,  $\mathbf{v}^{(0)} = \mathbf{O}$ ,  $\mathbf{r}^{(0)} = \mathbf{b}$ ,  $\mathbf{p}^{(0)} = \mathbf{r}^{(0)}$ 
3: for ( $m = 1, m++, m \leq L$ ) do
4:    $\mathbf{e}^{(m-1)} = \mathbf{A} \mathbf{p}^{(m-1)}$ 
5:    $\alpha^{(m)} = \|\mathbf{r}^{(m-1)} / \mathbf{p}^{(m-1)H} \mathbf{e}^{(m-1)}\|$ 
6:    $\mathbf{v}^{(m)} = \mathbf{v}^{(m-1)} + \alpha^{(m)} \mathbf{p}^{(m-1)}$ 
7:    $\mathbf{r}^{(m)} = \mathbf{r}^{(m-1)} - \alpha^{(m)} \mathbf{e}^{(m-1)}$ 
8:    $\beta^m = \|\mathbf{r}^m\|^2 / \|\mathbf{r}^{(m-1)}\|^2$ 
9:    $\mathbf{p}^m = \mathbf{r}^m + \beta^m \mathbf{p}^{(m-1)}$ 
10: end for
11: Output: Final solution after  $L$  iterations  $\mathbf{x}^{(L)} = \mathcal{Q}[\mathbf{v}^{(L)}]$ 

```

Iterative sequential detection

The iterative detection techniques discussed so far are based on the conventional iterative methods that solve linear equations without computing matrix inversion. On the other hand, iterative sequential detection (ISD) is inspired from the SIC based MIMO detection where symbol transmitted from each user is detected successively. The key idea in ISD is to detect the symbol corresponding to each user while nulling all users' interference. The ISD algorithm starts with an initial solution $\mathbf{x}^{(0)} = \mathbf{D}^{-1} \mathbf{b}$. Let $x_i^{(m)}$ denote the symbol detected corresponding to the i th user in the m th iteration. Now, let us consider the case of detecting the symbol corresponding to the j th user in the $(m+1)$ th iteration, which can be written as

$$\mathbf{r}_j^{(m+1)} = \mathbf{y} - \mathbf{H} \phi^{(m)} + \mathbf{h}_j x_j^{(m)} \quad (1.18)$$

where $\phi^{(m+1)} = (x_1^{(m+1)}, x_2^{(m+1)}, \dots, x_{j-1}^{(m+1)}, x_j^{(m)}, x_{j+1}^{(m)}, \dots, x_{N_t}^{(m+1)})$ is the symbol update vector and \mathbf{h}_j is the j th column of channel matrix \mathbf{H} . To detect the symbol for the j th user, matched filtering of equation (1.18) is performed followed by quantization operation as

$$\mathbf{x}_j^{(m+1)} = \mathcal{Q} \left[\frac{\mathbf{h}_j^H \mathbf{r}_j^{(m+1)}}{\|\mathbf{h}_j\|} \right]. \quad (1.19)$$

1.5. CONTRIBUTIONS

The detected symbol is then updated in the symbol update vector $\phi^{(m+1)}$. These operations are performed iteratively for each user till the maximum number of iterations is not completed. Algorithm 1.8 describes the pseudocode of the ISD algorithm.

Algorithm 1.8 Iterative sequential detection

```

1: Input:  $\mathbf{y}, \mathbf{H}, \mathbf{A}, \mathbf{G}, N_t, N_r, \sigma^2$ 
2: Compute initial solution :  $\mathbf{x}^{(0)} = \mathbf{D}^{-1}\mathbf{b}$ 
3: for ( $m = 1, m++ , m \leq L$ ) do
4:   for  $j = 1, j++ , j \leq N_t$  do
5:     Perform interference nulling :  $\mathbf{r}_j^{(m+1)} = \mathbf{y} - \mathbf{H}\phi^{(m)} + \mathbf{h}_j x_j^{(m)}$ 
6:     Detect symbol :  $\mathbf{x}_j^{(m+1)} = \mathcal{Q} \left[ \frac{\mathbf{h}_j^H \mathbf{r}_j^{(m+1)}}{\|\mathbf{h}_j\|} \right]$ 
7:     Update symbol vector :  $\phi^{(m+1)} =$ 
        $(x_1^{(m+1)}, x_2^{(m+1)}, \dots, x_{j-1}^{(m+1)}, x_j^{(m)}, x_{j+1}^{(m)}, \dots, x_{N_t}^{(m+1)})$ 
8:   end for
9: end for
10: Output: Final solution after  $L$  iterations  $\mathbf{x}^L = \phi^L$ 

```

1.5 Contributions

The thesis's objective is to design and analyze low complexity detection algorithms for uplink symbol detection at the BS in wireless mMIMO systems.

In Chapter 2, a stochastic bio-inspired meta-heuristic algorithm is proposed for large MIMO detection. The proposed modified firefly algorithm (MFA) is motivated by the bioluminescence of fireflies and uses a probabilistic metric to update solutions in the search space. Robustness of MFA is verified under channel estimation errors at the receiver.

In Chapter 3, the drawbacks of NI and RI are eliminated by a novel and robust hybrid pseudo-stationary algorithm for symbol detection in mMIMO systems with a large number of users. At first, non-stationary iteration-based NSNI is proposed to find the MMSE filter matrix approximate. NSNI overcomes the limitations of NI and yields superior BER performance than NI

with the same computational complexity. Next, stationary iteration-based ISRI is introduced, where symbol-index based optimal step size is computed for updating each element of the estimated symbol vector at each iteration. RI and ISRI have the same computational complexity. However, ISRI outperforms RI. Finally, NSNI and ISRI are combined to design a HA. Proposed HA yields superior performance over NI, RI, JSDJI and CG in terms of BER and computational complexity, under both perfect and imperfect CSI at the receiver. The superiority and robustness of the proposed HA are validated through simulations. Furthermore, an iterative symbol detection algorithm is proposed based on nonstationary iterations. The residual error is computed based on a low complexity initial symbol vector in the proposed nonstationary iteration-based work. Next, iterative refinement is performed on both the estimated error and the symbol estimate using a line search technique. Finally, in the nonstationary iteration-based detection, the output solution is obtained by refining the estimated symbol with the estimated error. Through simulations, it is observed that the proposed algorithms perform superior to several symbol detection algorithms with comparable complexity and achieves excellent BER performance for scenarios when the number of users scales up in the system.

In Chapter 4, a novel low-complexity ordered sequential detection algorithm is devised for an uplink mMIMO system with a massive number of users. In this proposed RFOD algorithm, the concept of reliability feedback mechanism (RFM) is introduced while deciding the symbol corresponding to each user. First, a low-complexity initial solution is used to compute the quality metric for ordering the detection sequence. Next, for detecting the symbol corresponding to each user, the interference from all other users is cancelled, followed by RFM. Ordering of the detection sequence along with the reliability feedback reduces the effect of error propagation. Through multiple iterations of RFOD, an enhanced BER performance is achieved. Furthermore, RFOD outperforms MMSE with quadratic computational complexity for large user mMIMO systems. Simulation results corroborate RFOD's su-

periority over the recently introduced mMIMO detection algorithms in terms of computational complexity and the BER performance.

In Chapter 5, a sparsely connected deep unfolded network is developed to outperform state-of-the-art mMIMO detection algorithms measured against BER performance and computational complexity. The proposed SRN prunes insignificant parameters while training and provides a low complexity detection model. Simulation results corroborate viability of the proposed detection network compared to several existing mMIMO detection techniques.

In Chapter 6, a low-complexity tree-traversal aided detection technique with social and cognitive knowledge of swarm optimization is proposed for uplink symbol detection in MBM-mMIMO. Residual error-based ordering technique is utilized for ordered detection of users in MBM-mMIMO systems. A convergence of the proposed SID technique is analyzed. Simulations are carried out to compare the BER performance of SID technique with state-of-the-art detection techniques under both perfect and imperfect CSI at the BS.

In Chapter 7, minimum support recovery error (MSRE) criteria based two low-complexity sequential symbol detection technique is proposed for the uplink of MBM-mMIMO system. After that, another improved detection technique is devised by enhancing the previous technique's exploration capability to a limited message space. Comparisons of proposed methods are drawn with other state-of-art methods for the uplink MBM-mMIMO systems. Simulation is drawn that supports the viability of the proposed detection techniques in terms of error rate performance and computational complexity.

1.6 Thesis outline

The rest of the thesis is organized as follows.

In Chapter 2, the symbol detection problem in an uplink large MIMO systems is considered, and MFA is proposed for low complexity symbol de-

tection at the BS. MFA maintains a balance between exploring and exploiting the search space compared to conventional evolutionary and other state-of-the-art detectors for large MIMO systems.

In Chapter 3, approximate iterative detectors for uplink mMIMO systems are explored. Considering the drawbacks of conventional AMI based and MII detectors, two detectors based on pseudo stationary and nonstationary iterations are proposed for low complexity symbol detection in uplink mMIMO systems.

In Chapter 4, symbol detection in mMIMO systems with a large number of users is considered. Two techniques, namely RFM and quality ordering (QO), are proposed to improve the performance of conventional iterative detectors. Finally, in this Chapter, reliability feedback aided ordered detection algorithm is proposed for low complexity symbol detection in uplink mMIMO systems. The algorithm outperforms state-of-the-art detectors for large user mMIMO systems in terms of both BER and computational complexity.

In Chapter 5, deep learning (DL) algorithms are explored for symbol detection in uplink mMIMO systems. A sparsely connected deep unfolded network is proposed for uplink mMIMO systems. The proposed model utilizes a masking technique that prunes the insignificant parameters while training and results in a low-complexity detection network. The proposed technique is found to outperform both computational complexity and BER compared to iterative detectors for mMIMO systems.

In Chapter 6, mMIMO systems with MBM are investigated, and the conventional MBM-mMIMO detectors are studied. The symbol detection problem in the uplink MBM-mMIMO system is investigated from a graph-theoretical perspective. A low complexity detection algorithm is proposed based on graph theory and socio-cognitive knowledge of swarm intelligence. The proposed algorithm outperforms several convention detectors for uplink MBM-mMIMO systems.

In Chapter 7, considering the transmit MBM-mMIMO symbol vector's sparse nature, MSRE criteria is derived. Low complexity detectors with

1.6. THESIS OUTLINE

projected gradient descent based update rule formed from MSRE constraint are proposed. The proposed algorithm is computationally and in terms of performance more efficient than state-of-the-art MBM-mMIMO detectors.

In Chapter 8, the contributions of this thesis are summarized, and conclusions are drawn. Suggestions are also made for future works based on this thesis.

Chapter 2

Hybrid evolutionary algorithms for large MIMO detection

2.1 Introduction

The system model (1.1) described in Chapter 1 shows that the received symbol vector at the BS in uplink MIMO system experiences interuser interference and noise. Hence, the robust detection of the transmit MIMO symbol vector is of utmost importance to practically acquire the benefits of diversity and multiplexing gains in MIMO systems. Thus, in this Chapter, the problem of low complexity symbol detection in a large MIMO system is considered.

In this Chapter, a stochastic bio-inspired meta-heuristic algorithm is proposed for large MIMO detection. The proposed algorithm is motivated by fireflies' bioluminescence and uses a probabilistic metric to update solutions in the search space.

There are several evolutionary algorithms in the literature [12, 21–25] which have gained prominence with communication and signal processing researchers for providing improved performance at low computational complexity [21]. Among the existing evolutionary algorithms, ACO and PSO are two promising evolutionary algorithms that are applied in the literature for symbol detection in uplink small and large scale MIMO systems. Both of

these algorithms can be seen as exceptional cases of firefly algorithm (FA) [51–54].

FA is a fast converging algorithm capable of achieving a better solution compared against ACO and PSO. Unlike PSO and ACO, FA involves a randomization parameter which forces the estimated solution to wandering around the optima for the symbol detection problem in large MIMO systems. Consequently, the conventional FA sometimes converges to local optima and needs to be modified for symbol detection in uplink mMIMO systems. In this Chapter, the proposed MFA maintains a balance between exploration and exploitation of the search space.

The following terminology is used in this Chapter. Boldface lowercase and uppercase alphabets represent vectors and matrices respectively. $u \rightsquigarrow^l v$ denotes that there is a path l from vertex u to vertex v . An attribute a for vertex u is represented by $u.a$. Similarly, an attribute a for an edge (u, v) is denoted by $(u, v).a$ and $Adj[u]$ denotes the adjacent vertices of vertex u . $\| \cdot \|_p$ denotes the Lp-norm. x_i refers to the i^{th} element of a vector \mathbf{x} . **FEs** implies the ML-cost evaluations. $(.)^T$ denotes the matrix transpose.

The Chapter is organized as follows. Section 2.2 gives a brief overview of FA followed by the description of the shortest path problem in Section 2.3. MFA is presented in Section 2.4. Section 2.6 analyzes the convergence of MFA. Simulation results of MFA are discussed in Section 2.7. Complexity analysis of MFA is presented in Section 2.8. Section 2.9 summarizes the Chapter.

2.2 Overview of firefly algorithm

This section briefly describes the conventional FA.

2.2.1 Bioluminescence

Bioluminescence refers to the flashing of light from a firefly’s abdomen to attract its mating partner [55]. Three rules govern the flashing character-

2.2. OVERVIEW OF FIREFLY ALGORITHM

istics of fireflies in FA [56]: (a) all fireflies are assumed to be unisex, (b) attractiveness is directly proportional to the brightness of flashing, and both attractiveness and flashing decrease with the distance d between the fireflies, and (c) the brightness of a firefly is determined by the landscape of the objective function.

Algorithm 2.1 Firefly algorithm

```
1: Objective function  $f(x)$ .
2: Generate initial population  $P$ .
3: Evaluate attractiveness  $\beta$  and light intensity  $I$  for each firefly  $x_i \in x$  in
   population  $P$ .
4: while  $N < \text{Max-function-evaluations}$  do
5:   for  $i=1:\text{Population-size}$  do
6:     for  $j=1:i$  do
7:       if  $I_j > I_i$  then
8:         Move firefly  $i$  to  $j$ 
9:       end if
10:      Update  $\beta$  using (2.2)
11:      Evaluate new solution using (2.3)
12:    end for
13:  end for
14:  Arrange the fireflies in ascending order of objective function value and
    update global best solution
15:   $N = N + 1$ 
16: end while
```

2.2.2 Attractiveness

Attractiveness is one of the important parameters involved in FA for efficient exploration of the search space. It is computed by the intensity I of flashing light. The intensity I in a medium with a fixed absorption coefficient γ is expressed as [54]

$$I = I_o e^{-\gamma d^k}, \quad (2.1)$$

where I_o refers to the light intensity at $d = 0$. Hence, attractiveness, β , of a firefly is defined as

$$\beta = \beta_o e^{-\gamma d^k} \quad (k \geq 1), \quad (2.2)$$

where β_o is a firefly's attractiveness at $d = 0$.

2.2.3 Movement of fireflies

In conventional FA, a firefly always tries to move towards an attractive firefly using the following update equation [54]

$$x_i = x_i + \beta_o e^{-\gamma d_{ij}^k} (x_j - x_i) + \alpha [r_1 - 0.5] \quad (2.3)$$

The distance d_{ij} denotes the Cartesian distance between i^{th} and j^{th} fireflies at positions x_i and x_j respectively. α refers to the randomization parameter and $r_1 \in [0, 1]$. The pseudo code [54] of FA is given in Algorithm 2.1.

2.3 Shortest path problem

The problem of finding the shortest path in a directed acyclic graph is discussed in this section. Consider a weighted, directed graph $G(V, E)$, where V denotes the set of vertices, and E refers to the set of edges. The shortest path l from vertex u to v is defined by the following equality [57] .

$$w(l) = \delta(u, v), \quad (2.4)$$

where $w(.)$ is the path-weight function. $\delta(u, v)$ is the shortest path-weight function between u and v . $u, v \in V$ and $(u, v) \in E$. The weight function w on the path $l = \langle v_0, v_1, \dots, v_n \rangle$ is computed as

$$w(l) = \sum_{i=1}^n w(v_{i-1}, v_i), \quad (2.5)$$

where n denotes the number of vertices. The shortest path-weight function $\delta(u, v)$ is defined as

$$\delta(u, v) = \begin{cases} \min \{w(l) : u \rightsquigarrow^l v\} \\ \infty \end{cases}, \quad (2.6)$$

where $u \rightsquigarrow^l v$ implies the existence of a path l from u to v .

2.4 Modified firefly algorithm for symbol detection

In this section, MFA is presented for symbol detection in the uplink mMIMO system. To apply, firefly algorithm for symbol detection in mMIMO systems, the large MIMO system model is simplified as [58]

$$\hat{\mathbf{y}} = \mathbf{R}\mathbf{x} + \hat{\mathbf{n}}, \quad (2.7)$$

where $\hat{\mathbf{y}} = \mathbf{Q}^T \mathbf{y}$, $\hat{\mathbf{n}} = \mathbf{Q}^T \mathbf{n}$. \mathbf{Q} and \mathbf{R} are respectively the unitary matrix and the upper triangular matrix obtained from the CSI matrix $\mathbf{H} = \mathbf{Q}\mathbf{R}$. Hence, in terms of Euclidean distance, the ML cost function is simplified as

$$E(\mathbf{x}) = \sum_{i=1}^{2N_r} u_i \cdot d_i, \quad (2.8)$$

where

$$u_i \cdot d_i = \|\hat{y}_i - \sum_{j=i}^{2N_t} r_{ij} x_j\|_2^2 \quad (2.9)$$

$$u_i \cdot d_i = \|\hat{y}_i - \sum_{j=i+1}^{2N_t} r_{ij} x_j - r_{ii} x_i\|_2^2, \quad (2.10)$$

where $r_{ij} \in \mathbf{R}$ and $x_i \in \mathbf{x}$ refers to the symbols to be detected. Each transmit antenna is assumed as a firefly nest having two fireflies inside. Each firefly inside a nest corresponds to a 4-QAM modulated symbol (after considering a real-valued system model of large MIMO). As a consequence, the symbol

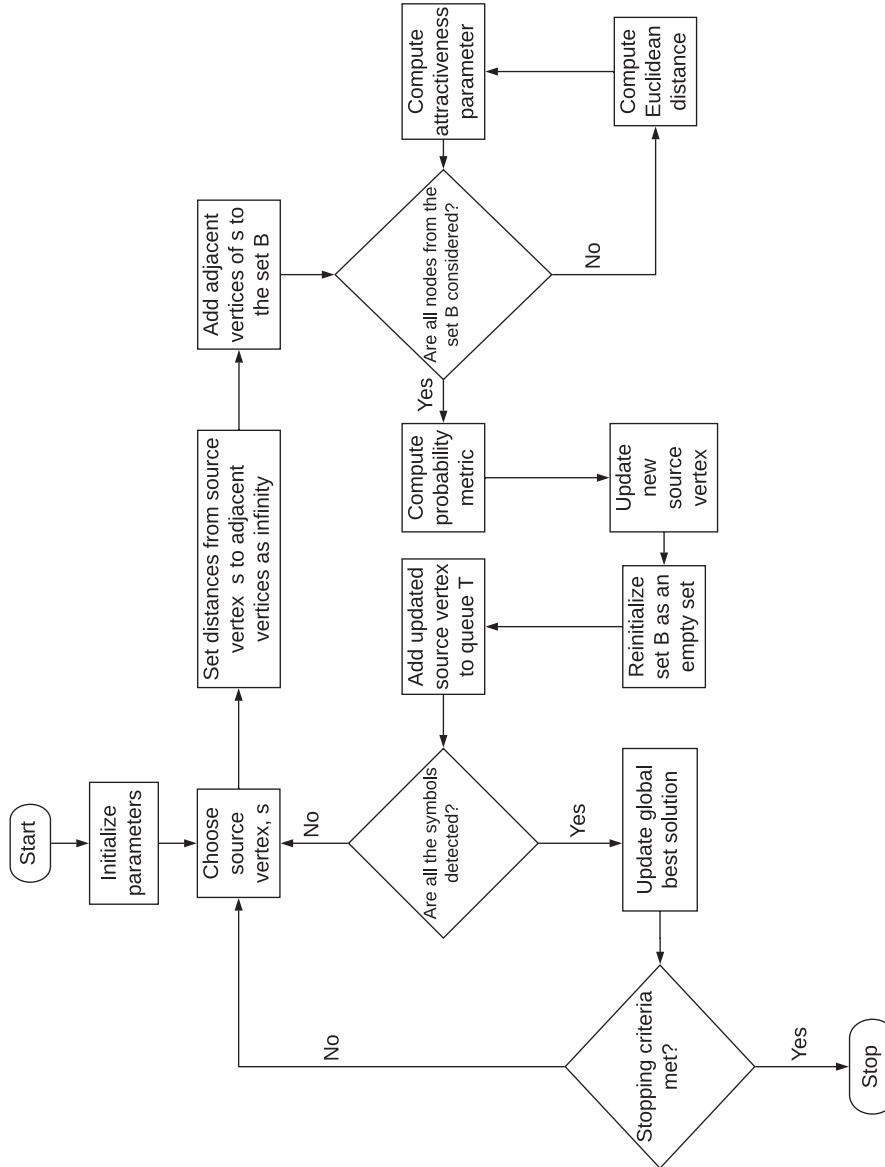


Figure 2.1: Flow diagram of MFA.

2.4. MODIFIED FIREFLY ALGORITHM FOR SYMBOL DETECTION

detection problem is modelled as a shortest path problem. A firefly from one nest searches for its best mating partner in near nests. Two dummy nests are considered as source and the destination vertices. The traversing starts from the source and ends at the destination vertex, which maintains a queue T of fireflies chosen from the nests. The detected symbols are the fireflies dequeued from T in reverse order. The detection scheme is depicted as a directed acyclic graph in Fig. 2.2.

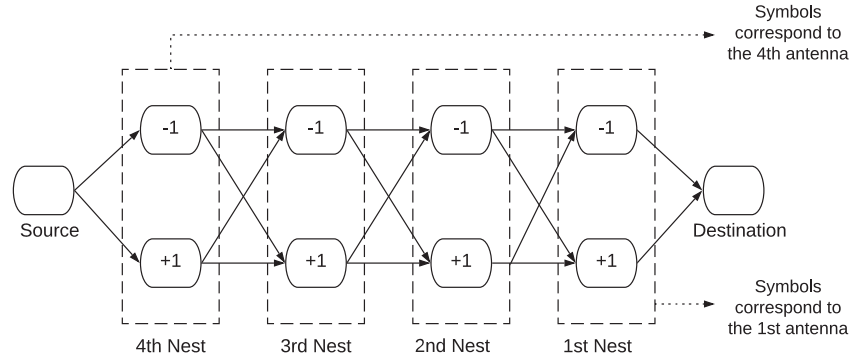


Figure 2.2: MIMO detection in MFA.

The flow chart and pseudocode of the proposed algorithm are given in Fig 2.1 and Algorithm 2.2. MFA works as follows. A firefly starts its journey from the source vertex s and calculates the distance $u.d$ to its nearby fireflies/symbols at vertex u and selects the firefly/symbol based on the attractiveness of the firefly/symbol. The following equation is used for converting the distance metric to attractiveness value at the i^{th} nest.

$$\beta_{u_{i-1}, u_i} = e^{-\gamma u_i \cdot d_i^k} \quad (2.11)$$

The probability of selecting i^{th} firefly by the $(i-1)^{th}$ firefly from i^{th} nest is

$$p_{u_{i-1}, u_i} = \frac{\beta_{u_{i-1}, u_i}}{\sum_{u_{i-1} \in B, (u_{i-1}, u_i) \in E} \beta_{u_{i-1}, u_i}} \quad (2.12)$$

Algorithm 2.2 Proposed MFA algorithm

```

1:  $T = \{\}$ 
2: for iterations  $\leq iT$  do
3:   for  $i = 2N_t : 1$  do
4:     Choose  $s_{i-1}$  as source
5:     for each  $u_i \in G.Adj[s_{i-1}]$  do
6:        $u_i.d_i = \infty$ 
7:     end for
8:     while  $G.Adj[s_{i-1}] \neq \{\}$  do
9:        $B = G.Adj[s_{i-1}]$ 
10:    end while
11:    for each  $u_i \in B$  do
12:      Compute Euclidean distance  $(u_i.d_i)$  using (2.10)
13:      Compute attractiveness  $\beta_{u_i} = e^{-\gamma u_i.d_i^k}$ 
14:    end for
15:     $p_{s_{i-1},u_i} = \frac{\beta_{s_{i-1},u_i}}{\sum_{s_{i-1} \in B, (s_{i-1},u_i) \in E} \beta_{s_{i-1},u_i}}$ 
16:    Select  $s_i$  based on  $p_{s_{i-1},u_i}$ 
17:     $B = \{\}$ 
18:     $T = T \cup \{s_i\}$ 
19:  end for
20:  Update the best solution.
21: end for

```

In line 1 of Algorithm-2.2 , an empty queue T is initialised. At each iteration, i , the symbol transmitted by the i^{th} antenna is estimated in lines 3-19. The previously chosen symbol is updated as the new source vertex in line 4. In lines 5-7, the distance to the adjacent vertices from the source is set as infinity. Each adjacent vertex of the source is stored in the queue B in lines 8-10. Euclidean distance using equation (2.10) is calculated in line 12 for each element of B . The attractiveness parameter of symbols from the source is computed in line 13. In line 16, the symbol is chosen based on the probability metric, p computed in line 15. The set B is reinitialized in line 17 as an empty set. Line 18 stores the detected symbols in T . The best solution achieved so far is selected in line 20. The proposed algorithm stores the detected symbols in T , starting from the last nest. The correct sequence of the symbols corresponding to different antennas is obtained by dequeuing the symbols in reverse order from queue T . The solution with the minimum value of $E(\mathbf{x})$ is considered the best solution.

2.5 Analytical expression of BER

Considering $\hat{\mathbf{x}}$ as the estimated symbol vector, the term $\|\tilde{\mathbf{H}}(\tilde{\mathbf{x}} - \hat{\mathbf{x}})\|_2^2$ can be rewritten as $\|\tilde{\mathbf{H}}(\tilde{\mathbf{x}} - \hat{\mathbf{x}})\|_2^2 = \sum_{i=1}^{N_r} \tilde{\mathbf{h}}_i(\tilde{\mathbf{x}} - \hat{\mathbf{x}})(\tilde{\mathbf{x}} - \hat{\mathbf{x}})^\dagger \tilde{\mathbf{h}}_i^\dagger$, where $\tilde{\mathbf{h}}_i$ is the i^{th} row of the matrix $\tilde{\mathbf{H}}$. Each element of $\tilde{\mathbf{H}}$ is independent and identically distributed. Moreover, the rank of the matrix $(\tilde{\mathbf{x}} - \hat{\mathbf{x}})(\tilde{\mathbf{x}} - \hat{\mathbf{x}})^\dagger$ is unity. Hence, MGF corresponding to average instantaneous received SNR $\tilde{\gamma}$ is [59] $\mathcal{Y}_\gamma(s) = (1 - s\tilde{\gamma})^{-N_r}$. Thus, probability of error is computed as [60]

$$\begin{aligned} \mathcal{P}_e &\leq \frac{1}{\pi} \int_0^{\pi/2} \mathcal{Y}_\gamma\left(-\frac{\kappa^2}{2\sin^2\theta}\right) d\theta \\ &\leq c {}_2F_1\left(1, N_r + \frac{1}{2}; N_r + 1; \frac{N_r}{N_r + \kappa^2\tilde{\gamma}}\right), \end{aligned}$$

where $c = \frac{\sqrt{\kappa}\Gamma(N_r + \frac{1}{2})}{2\sqrt{\pi}(1+\kappa)^{m+\frac{1}{2}}\Gamma(N_r+1)}$. ${}_2F_1(\cdot, \cdot; \cdot; \cdot)$ refers to hypergeometric function, N_r is the number of receive antennas and κ is a modulation dependent pa-

parameter.

2.6 Convergence analysis of MFA

In this section, the theoretical convergence of MFA is analyzed. The upper bound on the probability of reaching the optimal solution at least once, for a fixed iteration, iT gives crucial information on the convergence characteristic of MFA. Necessary definitions are stated below before analyzing the convergence of MFA.

Definition 1 Let \mathcal{S} be a finite region where $n = 2^{2N_t+1}$ nodes are distributed in a directed acyclic graph $G = (V, E)$ where V is the set of nodes and E is the set of edges. $V = \{v_1, v_2, \dots, v_n\}$

Definition 2 Let D be a dynamic set of already visited nodes and $I = V \cap D^c$ denotes the set of nodes to be visited. If a node belongs to set D , it can not be visited again. Let Z be the set of neighborhood nodes directly linked to the present node.

Remark 1 It is obvious that all the nodes in I are the nodes that can be visited in future, however, all the nodes in set V or I will not be visited for searching. The actual set of nodes to be visited is $(V \cap D^c) \cap Z$.

Definition 3 Let $L = \{l_1, l_2, \dots, l_m\}$ be the set of $m = 2^{2N_t}$ feasible unidirectional paths from the source node v_1 to the destination node v_n in the directed acyclic graph $G = (V, E)$ where $v_1, v_n \in V$, $|L| = 2^{2N_t}$. A feasible path from source to destination contains a node at most once.

Definition 4 Let $l^* \in L$ be the unique optimal path to be determined. The attractiveness value is assumed to satisfy $\beta_{v_i, v_j}(w) > 0$ along the optimal path l^* for $(v_i, v_j) \in E$ and partial path $w \subset V$. The term partial path denotes the path traversed so far in search of the optimal path. As optimal path l^* is a collection of nodes, partial path can be understood as a subset of l^* . When the optimal path is achieved, partial path merges with the optimal path.

2.6. CONVERGENCE ANALYSIS OF MFA

Definition 5 Let $(\Omega, \mathcal{F}, \mathbb{P})$ be the probability space associated with the search process of the proposed algorithm. Ω be the sample space, \mathcal{F} be the set of events and \mathbb{P} be the probability measure defined over the probability space.

Definition 6 Let F_t , B_t and H be the subsets of \mathcal{F} . E_t denotes the event that the optimal path l^* is found in t^{th} iteration. B_t is the event that the optimal path l^* is not found in t^{th} iteration. Hence, $B_t = E_t^c$. If H denotes the event that the optimal path is found atleast once in t iterations. Hence, $H = (\bigcap_{i=1}^{i=t} B_i)^c$

Definition 7 Two variables K and R are considered such that

$$K = \min\{\beta_{v_i, v_j}(w) \in l^*, w \subset l^*\} > 0 \quad (2.13)$$

and

$$R = \max\{\beta_{v_i, v_j}(w) \in l^*, w \subset l^*\} < 1 \quad (2.14)$$

Proposition 1 The probability $\mathbb{P}(B_t)$ that the optimal solution l^* is not found in t^{th} iteration is lesser or equal to $(1 - K^{2N_t})^t$.

Proof Since, $\beta_{v_i, v_j}(w) > 0$ for $(v_i, v_j) \in E$ and $w \subset l^*$, the following equality can be established for conditional transition probabilities

$$p_{v_i, v_j}(t, w_{v_i} | w_{v_{i-1}}) = \frac{\beta_{v_i, v_j}(w_{v_i})}{\sum_{v_k \notin w_{v_i}, (v_i, v_j) \in E} \beta_{v_i, v_k}(w_{v_i})} \quad (2.15)$$

where w_{v_i} denotes the partial path from the source node v_1 to the current node v_i and $i \in R = \{1, 2, 3, \dots, n\}$.

By equation (2.13), the inequality can be written as

$$\prod_{v_i=1, v_j \in (V \cap D^c) \cap Z}^{v_i=2N_t} p_{v_i, v_j}(t, w_{v_i} | w_{v_{i-1}}) \geq \prod_{v_i=1, v_j \in (V \cap D^c) \cap Z}^{v_i=2N_t} K \quad (2.16)$$

$$\mathbb{P}(E_t) \geq \prod_{v_i=1, v_j \in (V \cap D^c) \cap Z}^{v_i=2N_t} K \quad (2.17)$$

$$\mathbb{P}(E_t) \geq K^{2N_t} \quad (2.18)$$

$$\mathbb{P}(B_t) \leq 1 - K^{2N_t} \quad (2.19)$$

Proposition 2 $\mathbb{P}(B_t|B_1 \cap B_2 \cap B_3 \cap \dots \cap B_{t-1}) \leq (1 - K^{2N_t})^t$

Proof This proposition is obvious because the inequality (2.16) holds independent of previous conditions and $B_1 \cap B_2 \cap B_3 \cap \dots \cap B_{t-1}$. Hence, $\mathbb{P}(B_t|B_1 \cap B_2 \cap B_3 \cap \dots \cap B_{t-1}) \leq (1 - K^{2N_t})^t$

Theorem 1 *The proposed algorithm achieves the optimal path (solution) l^* at least once in a fixed iteration $t = iT$ with a probability $\mathbb{P} = 1$.*

Proof From definition (6), $H = (B_1 \cap B_2 \cap \dots \cap B_t)^c$.

$$\mathbb{P}(H) = \mathbb{P}(B_1 \cap B_2 \cap \dots \cap B_t)^c. \quad (2.20)$$

$$\mathbb{P}(H) = 1 - \mathbb{P}(B_1 \cap B_2 \cap \dots \cap B_t). \quad (2.21)$$

By using proposition (1) and (2),

$$\mathbb{P}(H) \geq 1 - (1 - K^{2N_t})^t. \quad (2.22)$$

$$\mathbb{P}(H) \geq 1 - f(t, N_t). \quad (2.23)$$

where $f(t, N_t) = (1 - K^{2N_t})^t$. From the above expression, it concludes that $f(t, N_t)$ tends to zero for a sufficient large value of $t = iT$ when N_t is fixed. Hence, when $t = iT$ is a relatively large value,

$$\mathbb{P}(H) \geq 1 - \epsilon \approx 1. \quad (2.24)$$

Remark An upper bound on iT can be found from equation (2.23) and (2.24),

$$\log \epsilon = iT \log(1 - K^{2N_t}). \quad (2.25)$$

Using inequality $\log x \leq x - 1$ for $x > 0$,

$$iT \leq \frac{\log(1/\epsilon)}{K^{2N_t}}. \quad (2.26)$$

The number of iterations is upper bounded by the number of transmit antennas N_t , and the minimum value of attractiveness parameter K . The parameter K has an inverse relation with the modulation order. Consequently, keeping N_t fixed, the number of iterations required for convergence to near-ML performance increases with the modulation order.

2.7 Simulation results

In this section, the simulation results for BER performance comparison and convergence of MFA are presented. MFA is simulated in matrix Laboratory (MATLAB) for 4x4, 8x8 and 16x16 MIMO systems with 4-QAM and up to 10^3 errors are counted for averaging during simulations. The simulation parameters for MFA are listed in Table 2.1.

In Figs. 2.3 and 2.4, performances of MFA are compared with MMSE, MMSE-OSIC and SD techniques. As observed in Figs. 2.3 and 2.4, MFA outperforms MMSE and MMSE-OSIC in terms of BER performance, and provides near-ML performance. An SNR gain of 2.73 dB for a target BER of 10^{-2} is achieved in MFA over MMSE-OSIC as illustrated in Fig. 2.4.

Fig. 2.5 illustrates the performance of MFA with an increase in the number of antennas. Improvement in BER performance with an increase in the number of transmit and receive antennas makes MFA an ideal candidate for large MIMO detection. A comparison of BER performance of MFA with several conventional detection techniques is shown in Table 2.2.

In Fig. 2.6 and 2.7, MFA is also compared with nature-inspired BPSO, SPSO, MPSO, UCCACO, CCACO, FA and FANA algorithms for symbol

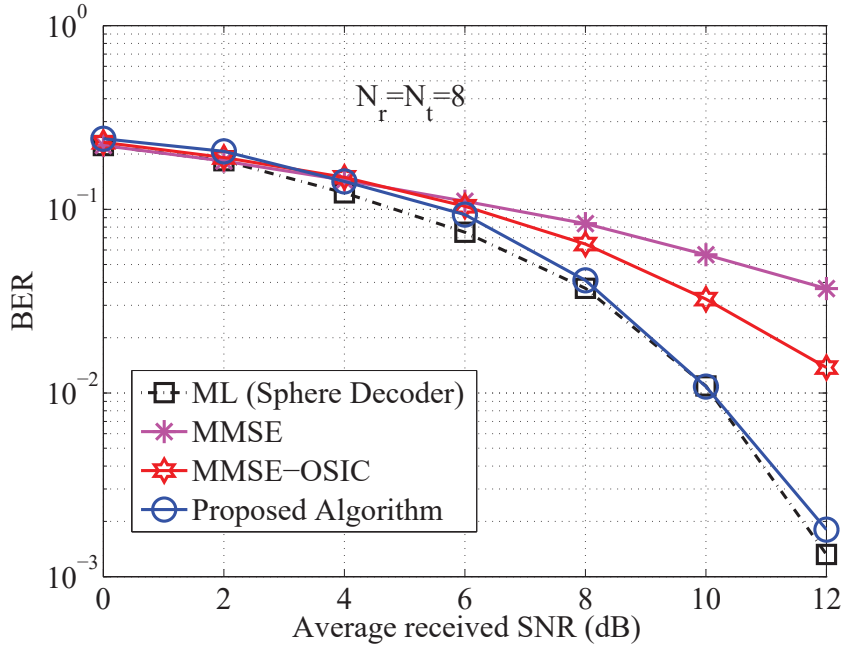


Figure 2.3: BER performance comparison of MFA for 8×8 large MIMO system with 4-QAM modulation.

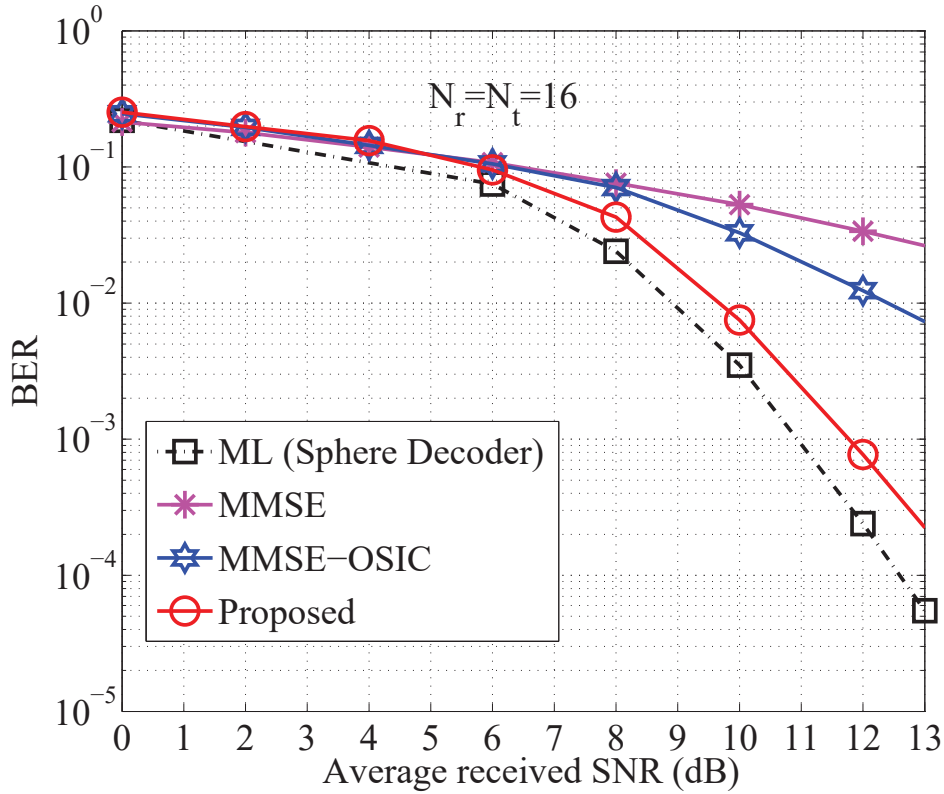


Figure 2.4: BER performance comparison of MFA for 16×16 large MIMO system with 4-QAM modulation.

2.7. SIMULATION RESULTS

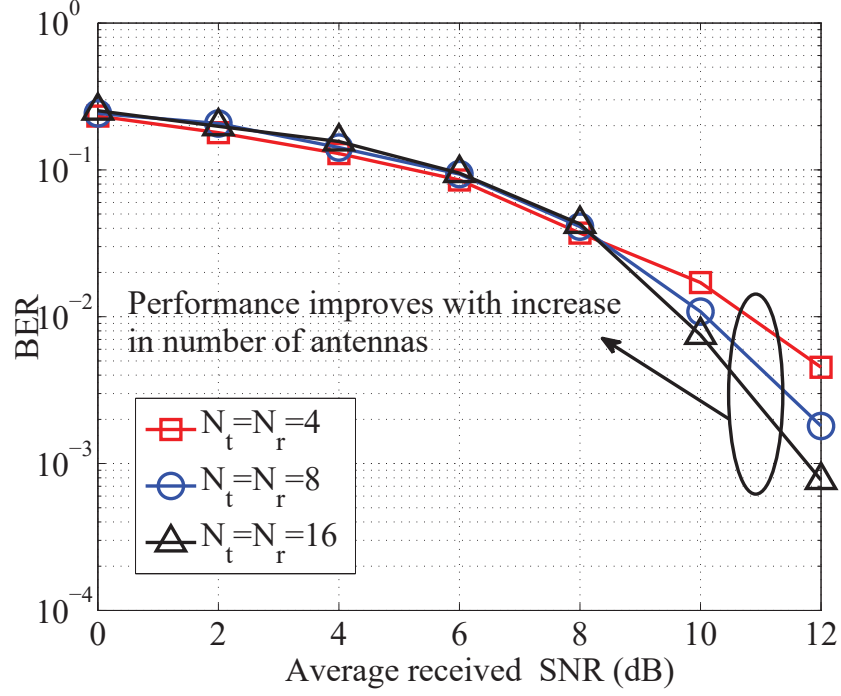


Figure 2.5: Comparison of BER performances of MFA for 4×4 , 8×8 and 16×16 large MIMO system with 4-QAM modulation.

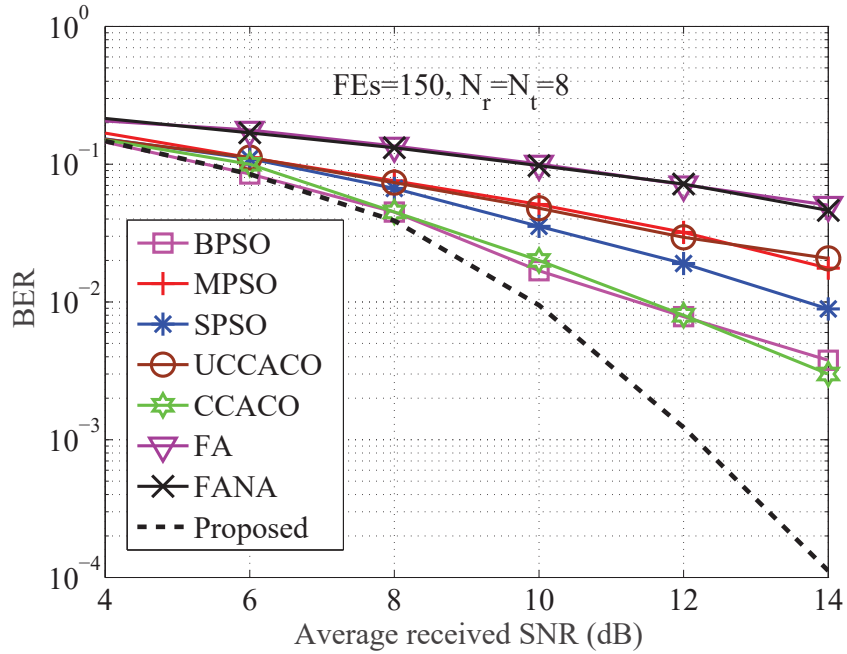


Figure 2.6: Comparison of BER performance of MFA with other nature-inspired algorithms for 8×8 large MIMO system with 4-QAM modulation.

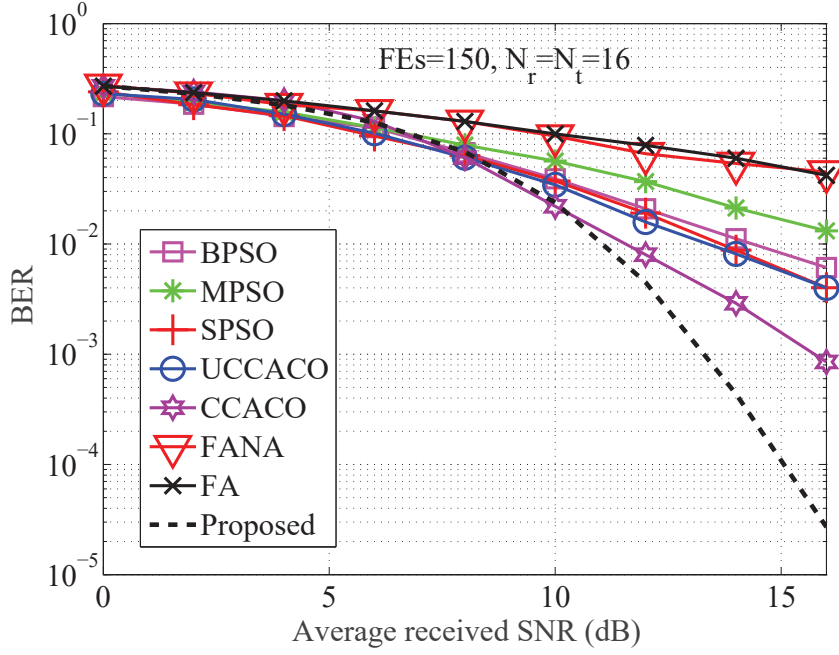


Figure 2.7: Comparison of BER performance of MFA with other nature-inspired algorithms for 16×16 large MIMO system with 4-QAM modulation.

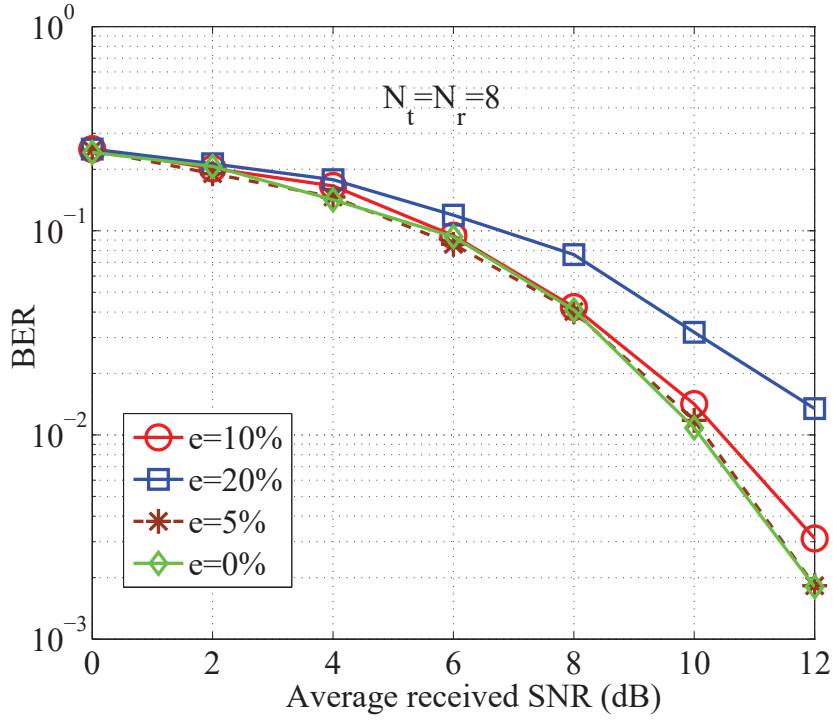


Figure 2.8: BER performance of MFA under CSI error at the receiver for 8×8 large MIMO system with 4-QAM modulation.

2.7. SIMULATION RESULTS

Table 2.1: Simulation parameters for the proposed MFA algorithm with 4-QAM modulation.

Algorithm parameters	Value
Absorption coefficient (γ)	0.5
k	1
No of feasible paths (N_l)	2^{2N_t}

Table 2.2: Comparison of BER performance of MFA with conventional MIMO detection algorithms

No of Antennas	MIMO Detector	BER (SNR=12 dB)	Approximate SNR gain over MMSE for a targeted BER of 10^{-2}
$N_t = N_r = 16$	MMSE	3.366×10^{-2}	0 dB
	MMSE-OSIC	1.173×10^{-2}	4.2 dB
	ML	2.4×10^{-4}	7.69 dB
	Proposed	7.719×10^{-4}	6.93 dB
$N_t = N_r = 8$	MMSE	3.7×10^{-2}	0 dB
	MMSE-OSIC	1.375×10^{-2}	4.4 dB
	ML	1.32×10^{-3}	7 dB
	Proposed	1.803×10^{-3}	7 dB

Table 2.3: Description of different parameters used for simulation of large MIMO detection algorithms.

Parameter	Description
γ	Absorption coefficient.
β_o	Attractiveness at the source.
α	Mutation coefficient.
α_{damp}	Mutation coefficient damping ratio.
β_{min}	Minimum value of attractiveness.
k_{best}	Number of neighborhood fireflies.
c_1	Cognitive parameter of the swarm.
c_2	Social parameter of the swarm.
ω	Inertia weight.
ω_1	Pheromone evaporation coefficient.
α_1	Pheromone weight controlling parameter.
ρ	Multiplicative constant for congestion control.

2.7. SIMULATION RESULTS

Table 2.4: Abbreviations and simulation parameters of different nature-inspired MIMO detection algorithms.

Abbreviation	Parameters
Binary particle swarm optimization (BPSO) [32]	$c_1 = 2, c_2 = 2, \omega = 2$
Standard particle swarm optimization (SPSO) [61]	$c_1 = 2, c_2 = 2, \omega = 2$
Memetic particle swarm optimization (MPSO) [62]	$c_1 = 2, c_2 = 2, \omega = 2$
Congestion control ant colony optimization (CCACO) [12]	$\alpha_1 = 0.8, \rho = 0.3, \omega_1 = 0.5$
Unordered congestion control ant colony optimization (UCCACO) [12]	$\alpha_1 = 0.8, \rho = 0.3, \omega_1 = 0.5$
FA [54]	$\gamma = 1, \beta_0 = 2, \alpha = 0.2, \alpha_{damp} = 0.98, m = 2$
Firefly algorithm with neighborhood attraction (FANA) [63]	$\gamma = 1, \beta_0 = 2, \beta_{min} = 0.2, \alpha = 0.2, k_{best} = 2, m = 2$

Table 2.5: BER performance of MFA under imperfect CSI at $N_t = N_r = 8$ for 4-QAM modulation.

Error	Approximate SNR gain over MMSE for targeted BER of 10^{-1}
e=0%	1.4 dB
e=5%	1.2 dB
e=10%	1 dB
e=20%	0 dB

detection in large MIMO systems. The simulation parameters required for implementing those nature-inspired algorithms for large MIMO detection are listed in Tables 2.3 and 2.4.

As depicted in Fig. 2.6 for 8×8 large MIMO system, SNR gains of 1.36 dB, 1.3 dB and 3.69 dB are achieved in MFA over BPSO, CCACO and SPSO respectively for a targeted BER of 10^{-2} . Moreover, Fig. 2.7 shows that MFA outperforms BPSO and SPSO with SNR gains of 2.5 dB and 2.3 dB respectively of target BER of 10^{-2} , and achieves 2.3 dB gain over CCACO for targeted BER of 10^{-3} . However, the BER performances of FA and FANA are far inferior compared to MFA. Hence, Figs. 2.6 and 2.7 prove that MFA is an appropriate choice for large MIMO detection.

Robustness of MFA is observed from Figs. 2.8 and 2.9. Fig. 2.8 shows that MFA is capable of providing near-ML performance even at 5% CSI mismatch. As illustrated in Fig. 2.9, by increasing the number of antennas even under CSI mismatch conditions, MFA provides improved performance. For $N_t = N_r = 2$ and $e = 10\%$, the BER degrades to 1.77×10^{-2} for SNR= 12 dB. However, the BER improves to 7.94×10^{-3} and 3.1×10^{-3} when N_t and N_r are increased to $N_t = N_r = 4$ and $N_t = N_r = 8$ respectively for SNR= 12 dB. A comparative analysis of SNR gains in MFA for targeted BER of 10^{-1} under different imperfect CSI scenarios is summarized in Table 2.5. This highlights the robustness of MFA under practical consideration.

The performance of MFA depends on two important parameters: the absorption coefficient γ and the variable k . The absorption coefficient γ plays a vital role in the convergence and performance of MFA. A comparative analysis of various values of γ on the performance of MFA is illustrated in Fig. 2.10. High values of γ lead to rapid convergence to a suboptimal solution. Based on simulations, the value of γ is found to be 0.5.

Another crucial parameter that affects the convergence and performance of MFA is the variable k . Analysis on the effect of the above parameter on the performance of MFA is shown in Fig. 2.11. The value of the constant k must be kept as unity to get a rapid convergence of MFA to a near-optimal

2.7. SIMULATION RESULTS

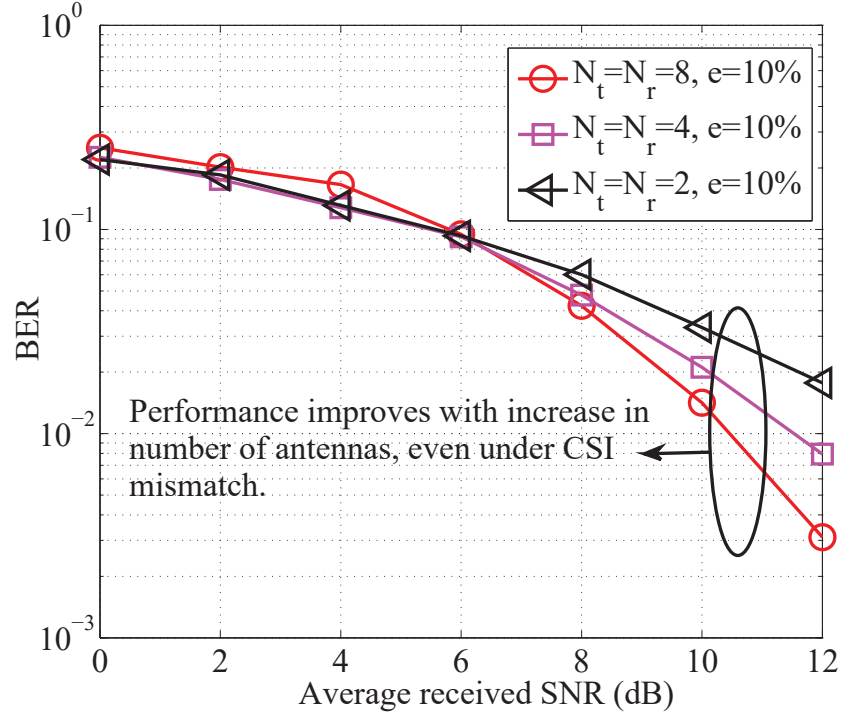


Figure 2.9: Comparison of BER performance of MFA under CSI error at the receiver for 2×2 , 4×4 and 8×8 MIMO systems with 4-QAM modulation.

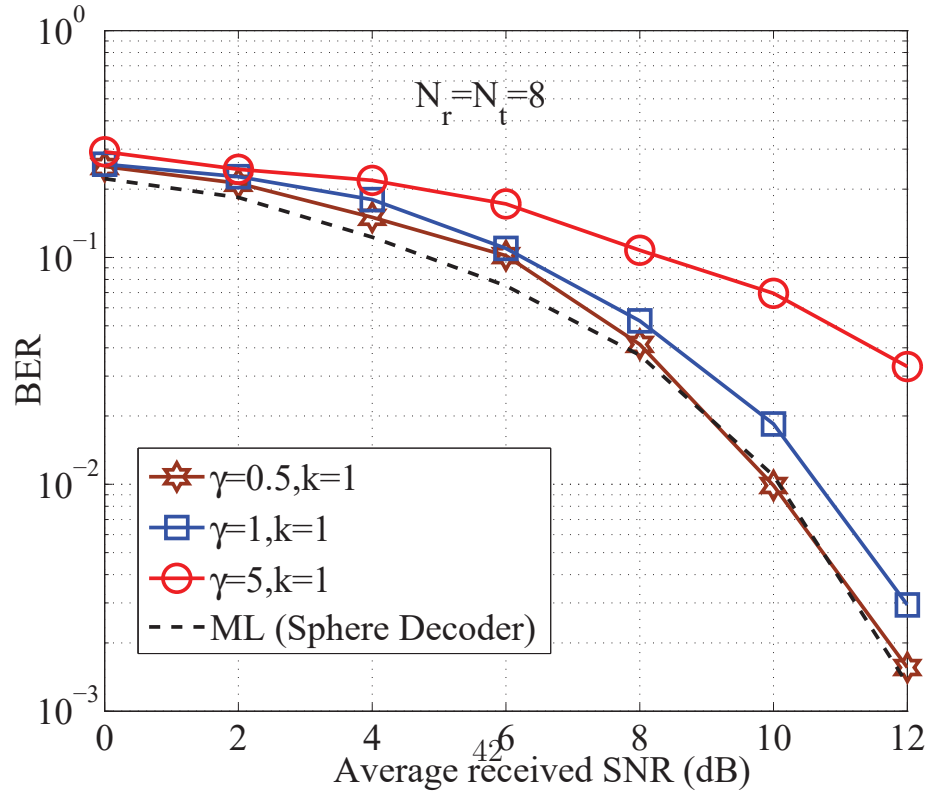


Figure 2.10: Analysis of performance of MFA with variation in absorption coefficient γ for 8×8 large MIMO system with 4-QAM modulation.

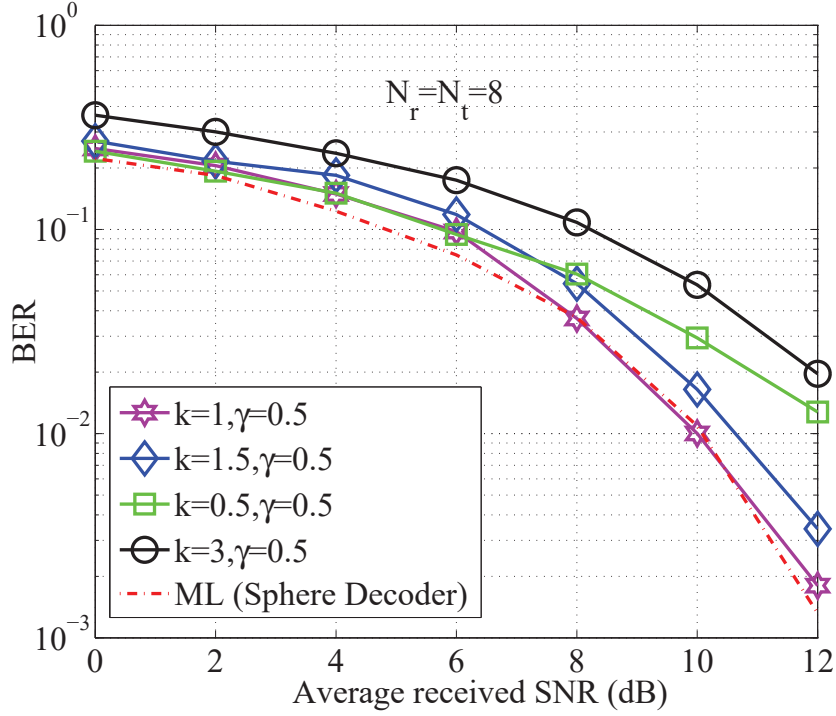


Figure 2.11: Analysis of performance of MFA with variation in k for 8×8 large MIMO system with 4-QAM modulation.

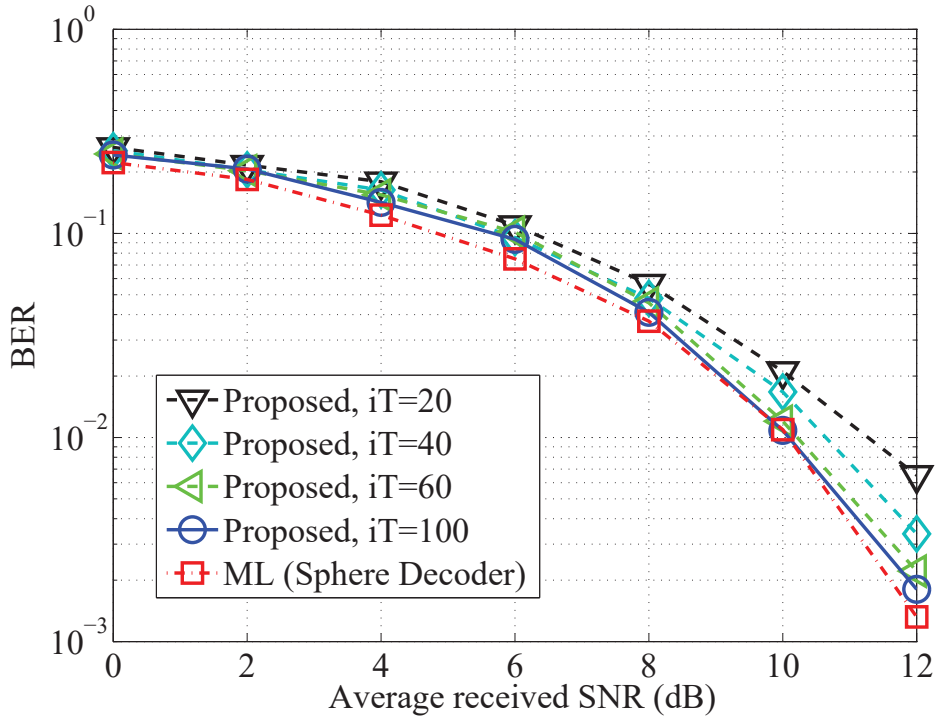


Figure 2.12: BER vs SNR plot of MFA with different number of iterations for 8×8 large MIMO system with 4 QAM modulation.

2.7. SIMULATION RESULTS

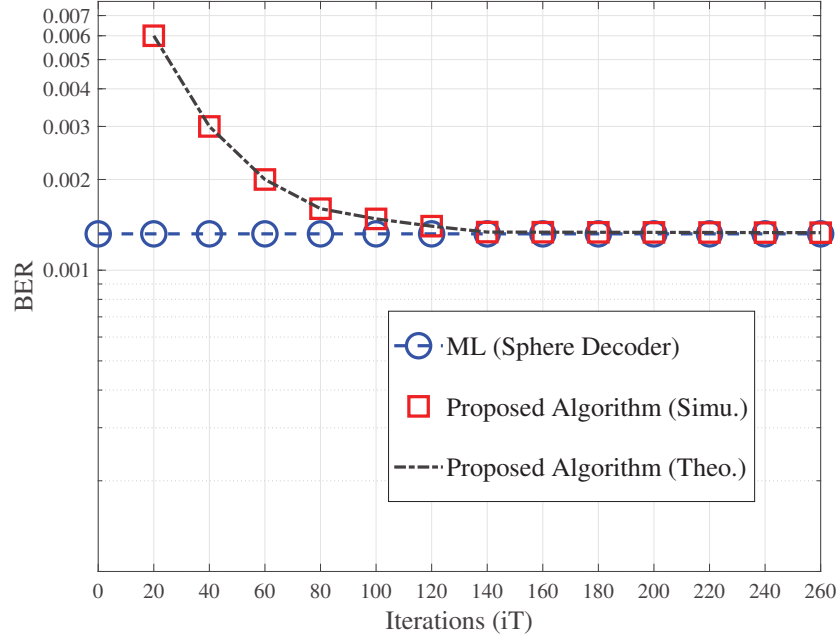


Figure 2.13: Convergence analysis of MFA for 8x8 large MIMO system with 4-QAM modulation.

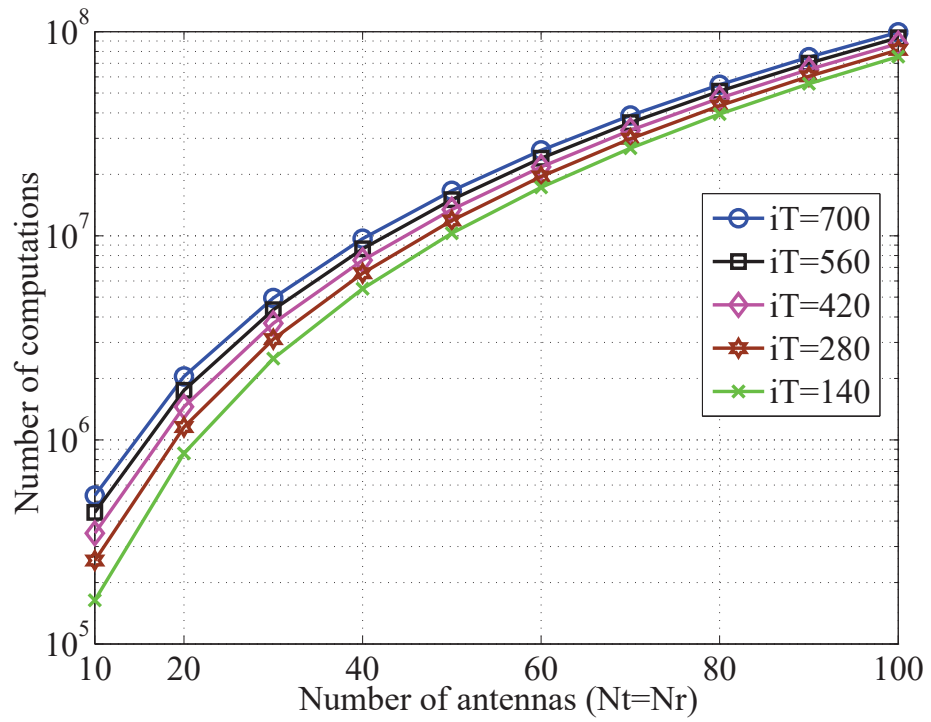


Figure 2.14: Comparison of computational complexity versus number of antennas for MFA with 4-QAM modulation.

result.

Figs. 2.12 and 2.13 show the convergence behaviour of MFA. As observed from Figs. 2.12 and 2.13, MFA converges to near-ML solution as the number of iterations increases. It is also observed that as the number of antennas increases, the number of iterations required for convergence of MFA also increases.

2.8 Complexity analysis

In this section, the computational complexities of contending detection algorithms are compared. The computational complexity of MFA is computed in terms of the number of real-valued multiplications required while estimating the transmitted symbols. In Fig.2.14, the computational complexity of the proposed algorithm is plotted against different numbers of antennas $N_t = N_r$ and iterations iT . As observed from Fig. 2.14, the computational complexity of MFA increases as the number of antennas increases. However, in Fig. 2.14, it is observed that as the number of antennas increases, the difference in computations decreases and becomes nearly equal for various values of iT . Additionally, MFA uses a significantly fewer number of computations than ML detection because the complexity of ML detection exponentially increases with the constellation size \mathcal{A} . Consequently, Fig. 2.14 concludes that the proposed detection algorithm is computationally more efficient than the ML. Hence, the MFA is suitable for deployments where a large number of antennas are deployed in the MIMO systems.

2.9 Summary

This Chapter is devoted to the symbol detection problem in large MIMO systems. In this Chapter, a novel and robust symbol detection algorithm MFA motivated by the concept of bioluminescence of fireflies are proposed. A new path selection strategy based on probability metric has been proposed

2.9. SUMMARY

for FA. Randomness in FA is reduced by devising an effective value of the absorption coefficient, which improves quality of the solution, and avoids early convergence to a local minimum. Simulation results support the improved performance of MFA over MMSE, MMSE-OSIC, UCCACO, CCACO, BPSO, MPSO, SPSO, FA and FANA based MIMO detection techniques. The BER performance of MFA is near-ML which makes the algorithm a suitable candidate for large MIMO detection. Moreover, to validate the robustness of MFA, BER performance is also analyzed under different CSI estimation errors. It is observed that MFA is capable of yielding near-ML solutions under considerable CSI mismatch, and the performance of the algorithm improves with an increase in the number of antennas even under CSI estimation error scenarios at the BS.

A significant improvement in spectral efficiency is achieved in mMIMO and MBM-mMIMO systems compared to large MIMO systems. However, due to high computational complexity and degraded performance, the algorithms proposed for large MIMO are not suitable for mMIMO systems. Hence, in the subsequent chapters, symbol detection in uplink mMIMO and MBM-mMIMO systems are explored, and viable low complexity detection algorithms are proposed.

Chapter 3

Improved approximate algorithms for massive MIMO detection

3.1 Introduction

In mMIMO systems, hundreds of BS antennas are deployed to serve few tens of users, resulting in high spectral efficiency and high link reliability in mMIMO compared to large MIMO systems. Consequently, as a massive number of antennas are involved in mMIMO systems, the existing evolutionary algorithms discussed and the MFA algorithm proposed in Chapter 2 are not computationally efficient for symbol detection in uplink mMIMO systems.

This Chapter is devoted to designing and studying low complexity iterative detection algorithms for uplink mMIMO systems. In this Chapter, the drawbacks of existing low-complexity iterative detection techniques are explored, and improved approximate iterative algorithms are proposed for uplink mMIMO systems. Existing detection algorithms for mMIMO systems are based on AMI [6, 33, 64] and MII [39, 65] and approximates high dimensional matrix inversion to avoid cubic order computational complexity

in terms of the number of transmit antennas. Among AMI techniques, NI is a promising but simplest technique for finding approximate matrix inversion in mMIMO systems. However, the computational complexity of NI intractably increases with the number of iterations. Alternatively, RI is the simplest MII based technique [65] for symbol detection in mMIMO; however, RI requires a large number of iterations to yield a near-MMSE solution. Besides, most of the existing iterative detection techniques [6, 33, 39, 65] perform iterations over an initial estimate of the transmitted symbol vector, which may lead to error propagation if the initial approximation of the transmitted symbol vector is erroneous.

In this Chapter, at first, a low-complexity hybrid pseudo-stationary iterative detection algorithm, HA, is developed by removing the limitations of NI and RI for mMIMO systems. The proposed HA overcomes the drawbacks of NI and RI, and exploits their advantages by integrating two novel techniques, NSNI and ISRI, which are proposed in this Chapter. Major contributions in HA are : a) a nonstationary iteration based NSNI is proposed to improve the performance and overcome the drawbacks of NI for approximate matrix inversion in mMIMO, b) the optimal step size for each symbol-index is computed to boost BER performance of RI with a small number of iterations, and a novel iterative sequential method, ISRI is proposed c) a novel and robust algorithm HA, based on NSNI and ISRI is proposed to further boost BER performance for symbol detection in mMIMO systems, d) BER superiority, robustness and low complexity of proposed HA compared to NI, RI, JSDJI and CG is validated through simulations. Next, in this Chapter, the iterative line search (ILS) algorithm is proposed to achieve near-optimal BER performance in uplink mMIMO systems. In ILS, at first, the residual error is computed based on a low complexity initial symbol vector. Iterative refinement is performed on both the estimated error and the symbol estimate using a line search technique. Finally, the output solution is obtained by refining the estimated symbol with the estimated error. Through simulations, it is observed that the proposed HA and ILS algorithms perform superior to

several symbol detection algorithms with comparable complexity and achieve superior BER performance.

The following notations are used in this Chapter. $|\cdot|$ denotes absolute value. $\langle \cdot, \cdot \rangle$ and $\langle \cdot, \cdot \rangle_F$ denotes inner product, and Frobenius inner product respectively. $[\cdot \circ \cdot]$ implies Hadamard product. $\|\cdot\|$ refers to the matrix norm. $\nabla(\cdot)$ denotes the gradient operator. $\mathbf{x}^{(*)}$ refers to the estimated symbol vector at convergence. $(\cdot)^{-1}$ denotes matrix inverse.

The Chapter is organized as follows. Proposed HA is presented in Section 3.2. Error refinement based ILS algorithm is discussed in Section 3.3. Finally, Section 3.4 summarizes the Chapter.

3.2 Hybrid Pseudo-stationary Iterative Detector

In this section, NSNI and ISRI algorithms are discussed, followed by the promising HA. NI performs stationary iterations and yields suboptimal solution for less number of iterations. NSNI enhances NI by introducing non-stationary iterations where the step size at each iteration changes with the search direction. The performance of RI is improved in ISRI by computing the step sizes from the eigen values of the approximate inverse of the MMSE filter matrix, instead of exploiting a fixed step size for each iteration. Finally, to further boost BER performance, NSNI and ISRI are integrated into a low complexity pseudo-stationary HA.

3.2.1 Initial approximation

One of the interesting properties of mMIMO is the channel hardening phenomenon [66], which implies that the off-diagonal elements of gram matrix \mathbf{G} become weaker compared to diagonal elements when the number of antennas increases ($N_r \geq N_t$). Mathematically,

$$\lim_{N_r \rightarrow \infty} \frac{\mathbf{H}^H \mathbf{H}}{N_r} \rightarrow \mathbf{I}, \quad \frac{N_r}{N_t} = \alpha \quad (3.1)$$

As a consequence, the MMSE filter matrix \mathbf{A} is also diagonally dominant. Hence, \mathbf{A}^{-1} is approximated exploiting the diagonal dominant nature of \mathbf{A} . Hence,

$$\mathbf{W}^{(0)} \approx \mathbf{D}^{-1} \quad (3.2)$$

where \mathbf{D} is the diagonal matrix of \mathbf{A} , $\mathbf{W}^{(0)}$ is an approximation of \mathbf{A}^{-1} and $\mathbf{W}^{(*)} = \mathbf{A}^{-1}$.

3.2.2 NSNI for uplink mMIMO detection

This subsection introduces proposed NSNI for matrix inversion in mMIMO systems. NI for the mMIMO system is derived from 1st order Taylor series expansion, and gives an approximate inverse of MMSE filter matrix \mathbf{A} . The $(k+1)^{th}$ iteration of NI is

$$\begin{aligned} \mathbf{W}^{(k+1)} &= \mathbf{W}^{(k)}(2\mathbf{I} - \mathbf{W}^{(k)}\mathbf{A}) \\ &= \mathbf{W}^{(k)} + \mathbf{W}^{(k)}\mathbf{T}^{(k)}, \end{aligned} \quad (3.3)$$

where $\mathbf{T}^{(k)} = (\mathbf{I} - \mathbf{W}^{(k)}\mathbf{A})$ is the iteration matrix and $\mathbf{W}^{(k+1)}$ denotes the inverse of matrix \mathbf{A} after $(k+1)^{th}$ iterations. The iteration matrix $\mathbf{T}^{(k)} = \mathbf{I} - \mathbf{W}^{(k)}\mathbf{A}$ eventually must vanish to assure convergence of $\mathbf{W}^{(k+1)}$ to $\mathbf{W}^{(*)} = \mathbf{A}^{-1}$. Hence, each column vector $\mathbf{T}_i^{(k)}$ can be considered as a search direction which leads $\mathbf{W}_i^{(k)}$ to the optimal vector $\mathbf{W}_i^{(*)}$. Hence, the update rule (3.3) can be formulated as stationary iterative process.

$$\mathbf{W}_i^{(k+1)} = \mathbf{W}_i^{(k)} + \mathbf{W}^{(k)}\mathbf{T}_i^{(k)} \quad (3.4)$$

3.2. HYBRID PSEUDO-STATIONARY ITERATIVE DETECTOR

In the above iterative process (3.4), iteration matrix $\mathbf{W}^{(k)}$ does not depend on search direction $\mathbf{T}_i^{(k)}$ at iteration k , which results in the early convergence of NI to suboptimal solutions with small number of iterations. Hence, to improve the convergence speed and performance of NI, NSNI is proposed as

$$\mathbf{W}^{(k+1)} = \mathbf{W}^{(k)} + \gamma_o^{(k)}(\mathbf{I} - \mathbf{A}\mathbf{W}^{(k)}) \quad (3.5)$$

In equation (3.5), nonstationary step size $\gamma_o^{(k)}$ adapts itself with search direction $(\mathbf{I} - \mathbf{A}\mathbf{W}^{(k)})$ and hence, yields superior performance than NI with same computational complexity. Inspecting the columns of equation (3.5),

$$\mathbf{W}_i^{(k+1)} = \mathbf{W}_i^{(k)} + \gamma_{oi}^{(k)}(\mathbf{I}_i - \mathbf{A}\mathbf{W}_i^{(k)}), \quad (3.6)$$

where \mathbf{I}_i denotes the i^{th} column of \mathbf{I} . $\mathbf{T}_i^{(k)} = (\mathbf{I}_i - \mathbf{A}\mathbf{W}_i^{(k)})$ is defined as a search direction for the nonstationary iterative process (3.6) and $\gamma_{oi}^{(k)}$ as the nonstationary step size. From equations (3.5) and (3.6), assuring convergence of $\mathbf{W}^{(k+1)}$ to $\mathbf{W}^{(*)}$, it is obvious that $\langle \mathbf{T}^{(k)}, \mathbf{T}^{(k+1)} \rangle_F = 0$. Since \mathbf{T} is real, $[\mathbf{T}^{(k)} \circ \mathbf{T}^{(k+1)}]_{i,j} = 0$. Hence,

$$\langle \mathbf{T}_i^{(k)}, \mathbf{T}_i^{(k+1)} \rangle = 0 \quad (3.7)$$

Hence, from (3.6) and (3.7), $\gamma_{oi}^{(k)}$ is computed as follows

$$\gamma_{oi}^{(k)} = \frac{\mathbf{T}_i^{(k)} (\mathbf{T}_i^{(k)})^T}{(\mathbf{A}\mathbf{T}_i^{(k)})^T \mathbf{T}_i^{(k)}} \quad (3.8)$$

If equation (3.2) is considered as initial approximation of \mathbf{W} , it can be shown from MMSE filter matrix \mathbf{A} that the smallest diagonal element of \mathbf{D} corresponds to the minimum value of error and hence, it yields the smallest step size [40]. Hence, to reduce the computational load in each iteration k without compromising with exploitation capability of the algorithm, a constant

CHAPTER 3. IMPROVED APPROXIMATE ALGORITHMS FOR
MASSIVE MIMO DETECTION

value of $\gamma_o^{(k)} = \gamma_{oj}^{(k)}$ is considered (where j denotes the index corresponding to the minimum diagonal element of \mathbf{D}) for all indices of \mathbf{x} at an iteration k , instead of computing $\gamma_{oi}^{(k)}$ for each index i . However, the value of $\gamma_o^{(k)} = \gamma_{oj}^{(k)}$ must change with iteration k . The pseudocode of proposed NSNI is given in Algorithm 3.1.

Algorithm 3.1 Proposed NSNI algorithm

```

1: Inputs:  $\mathbf{A}, \mathbf{D}, \mathbf{b}$ 
2: Outputs:  $\mathbf{W}^{(*)}$ 
3: Initialization:  $\mathbf{G} = \mathbf{H}^T \mathbf{H}$ ,  $\mathbf{b} = \mathbf{H}^T \mathbf{y}$ ,  $\mathbf{W}^{(0)} = \mathbf{D}^{-1}$ 
4: for  $k = 1, k \leq L$  do
5:   Choose index ' $i$ ' corresponds to minimum diagonal element of  $\mathbf{W}^{(k-1)}$ 
6:    $\mathbf{T}_i^{(k)} = \mathbf{I}_i - \mathbf{A} \mathbf{W}_i^{(k-1)}$ 
7:    $\gamma_{0i}^{(k)} = \frac{\left( \mathbf{T}_i^{(k)} \right)^T \mathbf{T}_i^{(k)}}{\left( \mathbf{A} \mathbf{T}_i^{(k)} \right)^T \mathbf{T}_i^{(k)}}$ 
8:   Set  $\gamma_0^{(k)} = \gamma_{0i}^{(k)}$ 
9:    $\mathbf{W}^{(k)} = \mathbf{W}^{(k-1)} + \gamma_o^{(k)} \mathbf{T}^{(k)}$ 
10: end for
11:  $\mathbf{W}^{(L)} \approx \mathbf{W}^{(*)}$ 

```

3.2.3 ISRI for uplink mMIMO detection

In this subsection, ISRI for symbol detection in the uplink mMIMO system is presented. RI [65] for mMIMO uses the fixed step size $\omega = 0.00645$. However, choosing a fixed step size for all indices results in low convergence speed or convergence to suboptimal points. Hence, it is proposed to use different step sizes for different indexes. From Banach lemma [40], the iterative process (3.3) converges if $\|\mathbf{T}\| < 1$. Consequently, the spectral radius $\rho(\mathbf{T}) \leq \|\mathbf{T}\| < 1$ [40]. Suppose, $0 < \lambda_1 \leq \lambda_2 \leq \dots \leq \lambda_i \leq \dots \leq \lambda_n$ are the eigen values of \mathbf{A} . Hence, to assure convergence of (3.3),

$$\lim_{k \rightarrow \infty} \mathbf{T}^{(k)} = 0 \quad (3.9)$$

3.2. HYBRID PSEUDO-STATIONARY ITERATIVE DETECTOR

or,

$$\lim_{k \rightarrow \infty} (1 - \omega_i \lambda_i)^{(k)} = 0 \quad (3.10)$$

From the equation (3.10), it is concluded that $|1 - \omega_i \lambda_i| < 1$. Hence, to improve the performance of RI, ISRI with step size $\omega_i = \frac{1}{\lambda_i}$ is proposed as,

$$x_i^{(k+1)} = x_i^{(k)} + \omega_i \left(b_i - \sum_{j=1}^{2Nt} a_{i,j} x_j^{(k)} \right) \quad (3.11)$$

3.2.4 Pseudo-stationary HA for symbol detection in mMIMO

In this subsection, the hybrid pseudo-stationary iterative algorithm, HA based on NSNI and ISRI is proposed. Since NSNI utilizes nonstationary iterations, it can achieve superior performance compared to NI with the same computational complexity. Hence, proposed HA utilizes a single iteration of the proposed NSNI method to generate an initial solution.

$$\mathbf{x}^{(1)} = \mathbf{W}^{(1)} \mathbf{b}, \quad (3.12)$$

where $\mathbf{W}^{(1)}$ which is obtained by single iteration of NSNI, is an approximate inverse of MMSE filter matrix \mathbf{A} . Next, $k \leq (L - 1)$ iteration of ISRI is performed on initial solution $\mathbf{x}^{(1)}$ to enhance the performance. It is worth mentioning that NSNI requires more matrix-vector multiplications than ISRI. Hence, only a single iteration of NSNI and multiple $(L - 2)$ iterations of ISRI are performed to reduce computational load of HA. The pseudocode of the proposed HA is given in Algorithm 3.2.

Algorithm 3.2 Proposed HA algorithm

```

1: Inputs:  $\mathbf{A}, \mathbf{D}, \mathbf{b}$ 
2: Output:  $\mathbf{x}^{(*)}$ 
3: Initialization:  $\mathbf{G} = \mathbf{H}^T \mathbf{H}$ ,  $\mathbf{b} = \mathbf{H}^T \mathbf{y}$ ,  $\mathbf{W}^{(0)} = \mathbf{D}^{-1}$ 
4: Compute  $\mathbf{W}$  using NSNI (Single-iteration)
5:  $\mathbf{x}^{(1)} = \mathbf{W}^{(1)} \mathbf{b}$ 
6: for  $k = 2, k \leq L$  do
7:   for  $i = 1, i \leq 2N_t$  do
8:     Choose relaxation parameter  $\omega_i = \frac{1}{\lambda_i}$ 
9:      $x_i^{(k)} = x_i^{(k-1)} + \omega_i \left( b_i - \sum_{j=1}^{2N_t} a_{i,j} x_j^{(k-1)} \right)$ 
10:   end for
11: end for
12:  $k = k + 1$ 
13:  $\mathbf{x}^{(*)} = \mathbf{x}^{(L)}$ 

```

3.2.5 Convergence analysis of HA

In this subsection, the convergence of HA is theoretically analysed. To prove convergence of the proposed hybrid detection algorithm, consider the errors \mathbf{e}_1 and \mathbf{e}_2 associated with (3.6) and (3.11) respectively as

$$\mathbf{e}_1^{(k+1)} = \mathbf{I}_i - \mathbf{A} \mathbf{W}_i^{(k)} \quad (3.13)$$

$$\mathbf{e}_2^{(k+1)} = \mathbf{x}^{(k+1)} - \mathbf{x}^{(k)} \quad (3.14)$$

From equations (3.11) and (3.14),

$$\begin{aligned} \mathbf{e}_{2_i}^{(k+1)} &= (1 - \omega_i a_{i,i}) \mathbf{e}_{2_i}^{(k)} \\ &= (1 - \omega_i a_{i,i})^k \mathbf{e}_{2_i}^{(1)} \end{aligned} \quad (3.15)$$

From equations (3.6) and (3.13),

3.2. HYBRID PSEUDO-STATIONARY ITERATIVE DETECTOR

$$\mathbf{e}_1^{(k+1)} = (1 - \gamma_0^{(k)} \mathbf{A}) \mathbf{e}_1^{(k)} \quad (3.16)$$

Hence, from equations (3.15) and (3.16),

$$\lim_{k \rightarrow \infty} \mathbf{e}_{2i}^{(k+1)} = \lim_{k \rightarrow \infty} (1 - \omega_i a_{i,i})^k \mathbf{e}_1^{(1)} \quad (3.17)$$

$$= \lim_{k \rightarrow \infty} (1 - \omega_i a_{i,i})^k (\mathbf{I}_i - \gamma_o^{(0)} \mathbf{A}) \mathbf{e}_1^{(0)} \quad (3.18)$$

Since \mathbf{A} is positive semi definite for mMIMO systems, $\mathbf{D} = \mathbf{A}^{-1}$ and $\omega_i = \frac{1}{\lambda_i}$. Hence, it can be shown that

$$\lim_{k \rightarrow \infty} \mathbf{e}_2^{(k+1)} \approx \mathbf{0} \quad (3.19)$$

Consequently, the error \mathbf{e} vanishes in the proposed HA with the number of iterations. As a result, the proposed HA eventually converges to $\mathbf{x}^{(*)}$. In addition, proposed NSNI and ISRI methods improve the convergence rate of HA.

3.2.6 Simulation results and discussions

This subsection compares and analyzes the simulation results for the proposed NSNI, ISRI and HA detection algorithms with NI, RI, JSDJI and CG detection algorithm to justify superiority and robustness of the proposed detection algorithms. For all simulations, 64-QAM modulation scheme, rate-1/2 convolution code with [133₀, 171₀] polynomial, and hard decision Viterbi decoder [67] are considered .

Comparison between NSNI and NI: Fig. 3.1 analyzes BER performances of proposed NSNI and conventional NI methods. It is observed from Fig. 3.1 that a single iteration of NSNI outperforms two iterations of NI with

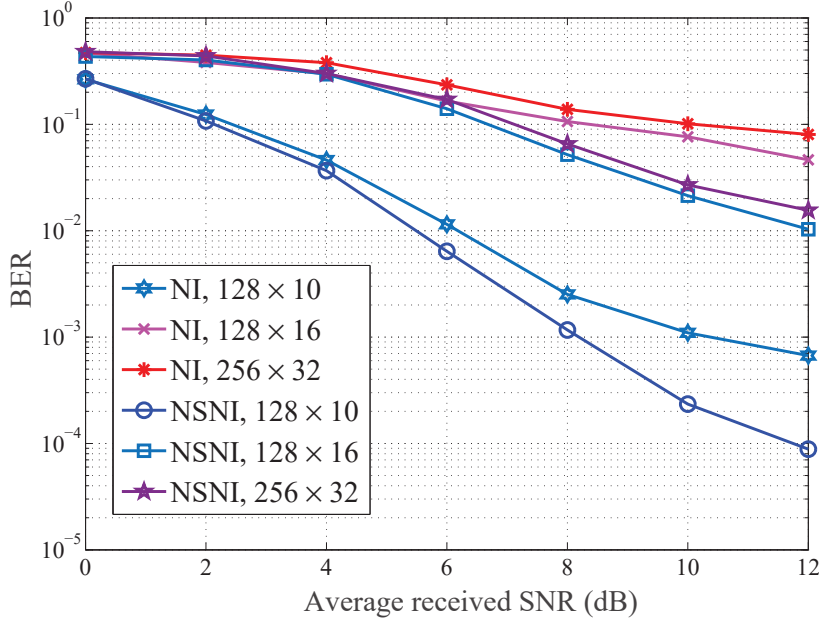


Figure 3.1: BER performance comparison between NSNI and NI for 64-QAM modulation.

86.8%, 77.7% and 80.6% improvement in BER performance at SNR=12 dB, respectively for 128×10 , 128×16 and 128×32 , mMIMO systems.

Comparison among ISRI, RI, JSDJI and CG: BER performance of proposed ISRI method is compared with RI, JSDJI and CG in Fig. 3.2 for 128×16 and 128×32 mMIMO systems. As depicted in Fig. 3.2(a), SNR gains of 2.5 dB, 3.2 dB and 4.1 dB are achieved in ISRI over RI, JSDJI and CG respectively at a targeted BER of 10^{-3} for 128×16 mMIMO system. Similarly, in Fig. 3.2(b), ISRI outperforms other contending detection algorithms for 128×32 mMIMO systems.

Comparison of BER performance of HA with other detection algorithms: Fig. 3.3(a) depicts that the proposed HA with $L = 2$ outperforms state-of-art mMIMO detection algorithms with $L = 4$ for 128×16 mMIMO system. Fig. 3.3(a) also depicts that an SNR gain of 2.45 dB is achieved in the proposed HA with $L = 2$ as compared to CG with $L = 4$ for a target BER of 10^{-2} . Moreover, at SNR=16 dB, proposed HA shows BER improvements of 79%

3.2. HYBRID PSEUDO-STATIONARY ITERATIVE DETECTOR

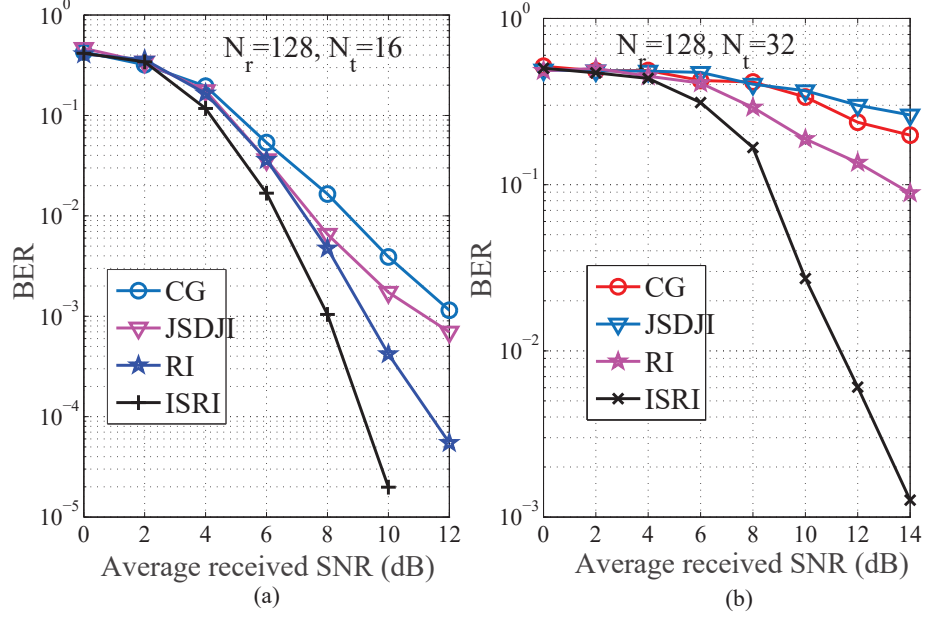


Figure 3.2: BER performance comparison among ISRI and other iterative mMIMO detection algorithms for 64-QAM modulation.

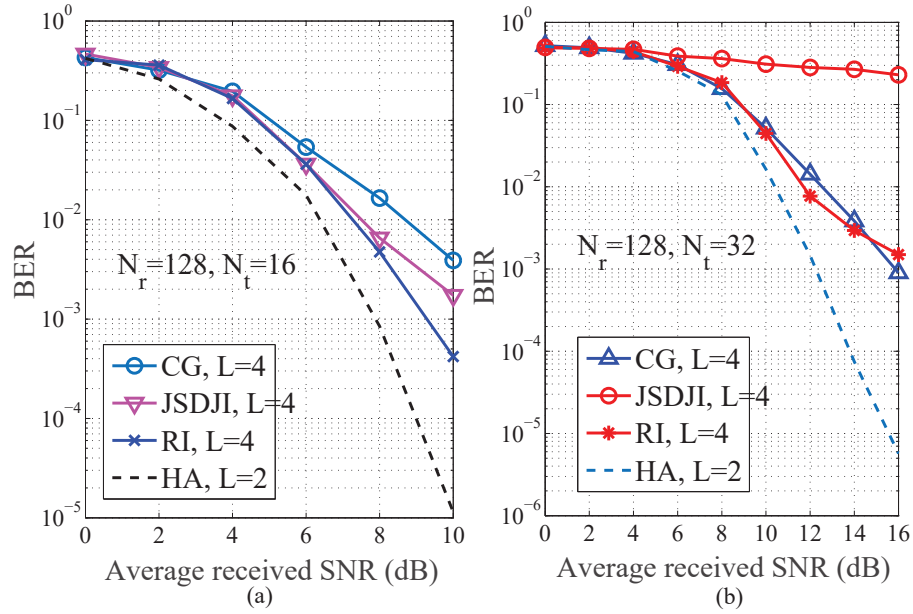


Figure 3.3: BER performance comparison among HA and other mMIMO detection algorithms for 64-QAM modulation.

compared to RI for 128×16 mMIMO system.

BER performance of HA when users scale up: To demonstrate the effect of increasing the number of users N_t , the BER performance of the proposed HA for 128×32 mMIMO system is investigated. Fig. 3.3(b) reveals that the proposed HA achieves superior BER performance than JSDJI, RI and CG, even if the number of users increases in mMIMO systems. An SNR gain of approx 3.8 dB is observed in the proposed HA with $L = 2$ as compared to CG with $L = 4$ for a target BER of 10^{-3} .

Complexity analysis: The computational complexities of the proposed NSNI, ISRI and HA are compared with NI, RI, CG and JSDJI based on the number of real valued multiplications. The computational complexities in calculating the initial parameters and the values \mathbf{G} , \mathbf{A} , \mathbf{D} , and \mathbf{D}^{-1} are ignored in comparing computational complexities as these initial parameters require equal amount of computational loads for all mMIMO detection algorithms mentioned above. Table 3.1 compares the number of real valued multiplications involved in different mMIMO detection algorithms.

Table 3.1: Comparison of computational complexity of different detection algorithms.

Detection algo- rithm	Real valued multi- plications
NI [33] ($L = 2$)	$12N_t^2 + 2N_t$
RI [65]	$4LN_t^2 + 2LN_t$
CG [39]	$4LN_t^2 + 8LN_t$
JSDJI[40]	$(4N_t^2 - 2N_t)L + 6N_t$
NSNI (Proposed) ($L = 1$)	$12N_t^2 + 2N_t$
ISRI (Proposed)	$4LN_t^2 + 2LN_t$
HA (Proposed)	$2(2L + 3)N_t^2 + 2(L + 1)N_t$

As shown in Table 3.1, it is observed that NSNI and NI have equal computational complexities for mMIMO systems. However, it is depicted in Fig. 3.4 that a single iteration of NSNI yields superior BER performance over NI. This corroborates computational efficiency of NSNI. On the other hand, as

3.2. HYBRID PSEUDO-STATIONARY ITERATIVE DETECTOR

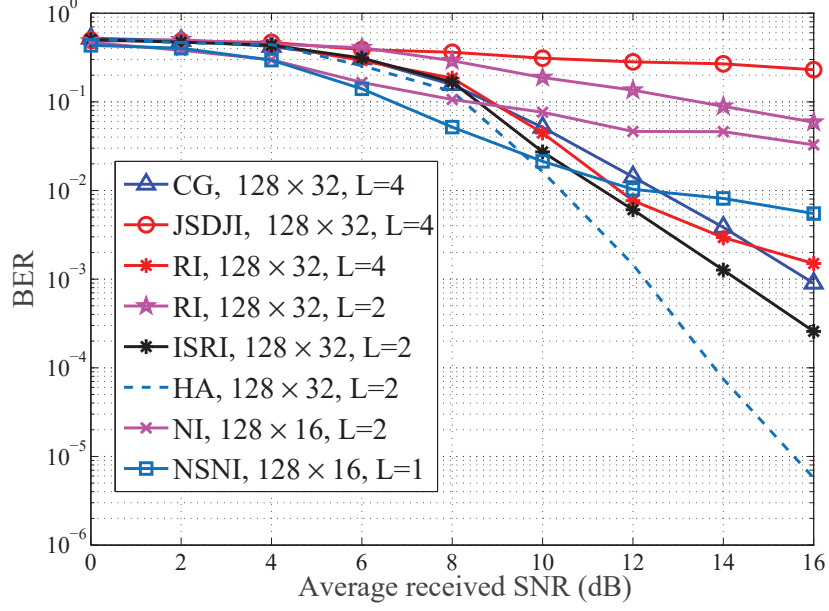


Figure 3.4: Comparison of BER performance of HA with other detection algorithms with approximately equal computational complexity.

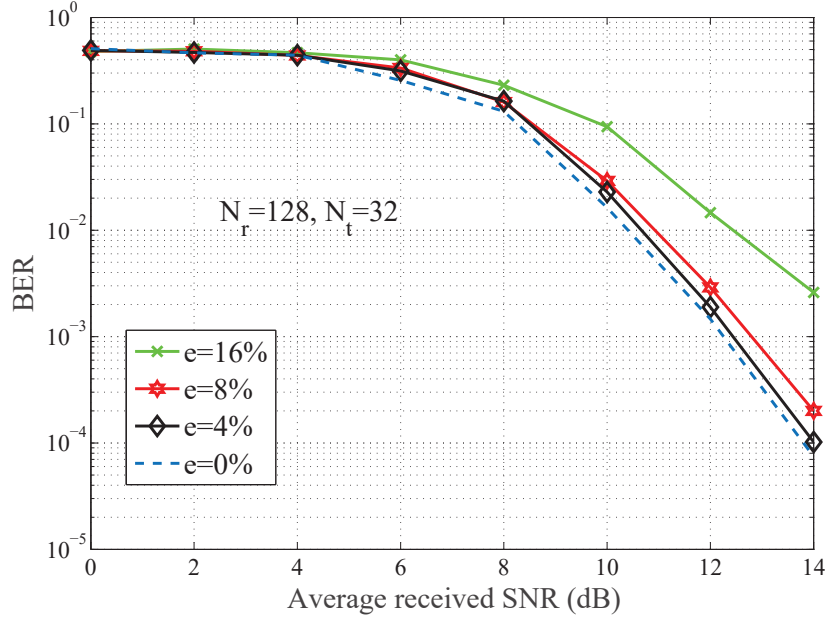


Figure 3.5: BER performance of proposed HA for 64-QAM modulation and $L=2$, under different imperfect CSI at the receiver.

shown in Table 3.1, ISRI and RI require approximately the same number of multiplications, however, Fig. 3.4 shows that ISRI outperforms RI for same number of iterations, $L = 2$.

As shown in Fig 3.4, HA with $L = 2$ takes approximately $14N_t^2$ multiplications to achieve $\text{BER} = 5.72 \times 10^{-6}$ at $\text{SNR} = 16$ dB. However, CG, JSDJI and RI with approximately $16N_t^2$ multiplications produce inferior BER performances as compared to HA with approximately $14N_t^2$ multiplications.

Robustness Analysis: Fig. 3.5 validates the robustness of HA under imperfect CSI at the receiver. As depicted in Fig. 3.5, HA shows promising BER performance even under CSI mismatch of $e = 4\%$ with $N_t = 32$ and $N_r = 128$. Negligible SNR losses of approximately 0.1 dB, 0.5 dB and 2.3 dB are observed from Fig. 3.5 at $e = 4\%$, $e = 8\%$ and $e = 16\%$ respectively for a targeted BER of 3×10^{-3} as compared to perfect CSI at the receiver. It proves the robustness of HA.

3.3 Error refinement-based line search for massive MIMO detection

The proposed ILS algorithm is presented in this section.

3.3.1 ILS for symbol detection in mMIMO systems

ILS starts with an initial estimate of the transmitted symbols. Utilizing the channel hardening phenomenon, a suboptimal initial estimate of the transmitted symbol vector is found as [38]

$$\hat{\mathbf{x}}^{(0)} = \mathbf{D}^{-1}\mathbf{b}, \quad (3.20)$$

If $\mathbf{x}^{(*)} = \mathbf{A}^{-1}\mathbf{b}$ is the desired symbol vector to be detected, the error $\mathbf{e}^{(*)}$ of initial estimate symbol vector $\hat{\mathbf{x}}^{(0)}$ is

$$\mathbf{e}^{(*)} = \mathbf{x}^{(*)} - \hat{\mathbf{x}}^{(0)} \quad (3.21)$$

3.3. ERROR REFINEMENT-BASED LINE SEARCH FOR MASSIVE MIMO DETECTION

Now, the accuracy of the initial solution $\mathbf{x}^{(0)}$ can be improved if an approximate estimate $\hat{\mathbf{e}}^{(1)}$ of error vector $\mathbf{e}^{(*)}$ is iteratively refined by solving the system of linear equations given by

$$\mathbf{A}\hat{\mathbf{e}}^{(1)} = \mathbf{r}^{(1)}, \quad (3.22)$$

where $\mathbf{r}^{(1)}$ is the residual vector given by

$$\mathbf{r}^{(1)} = \mathbf{b} - \mathbf{A}\hat{\mathbf{x}}^{(0)} \quad (3.23)$$

Algorithm 3.3 Proposed ILS algorithm

```

1: Input:  $\mathbf{A}, \mathbf{D}, \mathbf{G}, \hat{\mathbf{x}}^{(0)}, \mathbf{b}$ 
2: Outputs:  $\mathbf{x}^{(*)}$ 
3: for  $k = 1, k \leq L$  do
4:    $\mathbf{r}^{(k)} = \mathbf{b} - \mathbf{A}\hat{\mathbf{x}}^{(k-1)}$ 
5:    $\hat{\mathbf{e}}^{(k)} = \mathbf{D}^{-1}\mathbf{r}^{(k)}$ 
6:    $\mathbf{t}_0^{(k)} = \mathbf{r}^{(k)} - \mathbf{A}\hat{\mathbf{e}}^{(k)}$ 
7:    $\gamma_0^{(k)} = \frac{\left(\mathbf{t}_0^{(k)}\right)^T \mathbf{t}_0^{(k)}}{\left(\mathbf{A}\mathbf{t}_0^{(k)}\right)^T \mathbf{t}_0^{(k)}}$ 
8:    $\hat{\mathbf{e}}^{(k+1)} = \hat{\mathbf{e}}^{(k)} + \gamma_0^{(k)}\mathbf{t}_0^{(k)}$ 
9:    $\hat{\mathbf{x}}^{(k+1)} = \hat{\mathbf{x}}^{(k)} + \hat{\mathbf{e}}^{(k+1)}$ 
10:   $k = k + 1$ 
11: end for
12:  $\mathbf{x}^{(*)} = \hat{\mathbf{x}}^{(L)}$ 

```

Furthermore, in the case of CSI mismatch, computing the direct inverse of \mathbf{A} is not only computationally expensive but also leads to large errors in calculating $\mathbf{x}^{(*)}$. This comes from the fact that since the entries of \mathbf{H} are i.i.d Gaussian, the Gram matrix $\mathbf{G} = \mathbf{H}^T\mathbf{H}$ is a Wishart Matrix [68] and hence, based on the random matrix theory [68], the condition number $\eta(\mathbf{A})$ can be expressed as

$$\eta(\mathbf{A}) = \frac{\lambda'_{max}}{\lambda'_{min}} = \frac{(\sqrt{\alpha} + 1)^2\lambda_c + \alpha\lambda}{(\sqrt{\alpha} - 1)^2\lambda_c + \alpha\lambda} \quad (3.24)$$

where λ_c is a constant and λ is proportional to the eigen value of $\frac{\sigma^2}{E_x}\mathbf{I}_{2N_t}$.

Therefore, with increase in N_t , the matrix \mathbf{A} becomes more ill-conditioned. Hence, computing the direct inverse of \mathbf{A} to get $\hat{\mathbf{e}}$ is not an intelligent choice. By considering the diagonal dominance of \mathbf{A} , error $\hat{\mathbf{e}}^{(1)}$ is approximated as $\hat{\mathbf{e}}^{(1)} = \mathbf{D}^{-1}\mathbf{r}^{(1)}$ and the error refinement problem in equation (3.22) can be rewritten as

$$\begin{aligned}\hat{\mathbf{e}} &= \underset{\hat{\mathbf{e}} \in \mathbb{Q}}{\operatorname{argmin}} \{(\mathbf{r} - \mathbf{A}\mathbf{e})^T(\mathbf{r} - \mathbf{A}\mathbf{e})\} \\ &= \underset{\hat{\mathbf{e}} \in \mathbb{Q}}{\operatorname{argmin}} \{\mathbf{e}^T \mathbf{A}^T \mathbf{A} \mathbf{e} - 2\mathbf{r}^T \mathbf{A} \mathbf{e} + \mathbf{r}^T \mathbf{r}\}\end{aligned}\quad (3.25)$$

Since \mathbf{A} is symmetric positive definite, the gradient of the function will be $\psi(\mathbf{e}) = \mathbf{e}^T \mathbf{A}^T \mathbf{A} \mathbf{e} - 2\mathbf{r}^T \mathbf{A} \mathbf{e} + \mathbf{r}^T \mathbf{r}$ is $\nabla \psi(\mathbf{e}) = \mathbf{A} \mathbf{e} - \mathbf{r}$. Thus, the above quadratic function has a critical point when $\mathbf{A} \mathbf{e} = \mathbf{r}$ and solving equation $\mathbf{A} \mathbf{e} = \mathbf{r}$ is equivalent to minimizing the quadratic error function $\psi(\mathbf{e})$ with initial condition $\hat{\mathbf{e}}^{(1)} = \mathbf{D}^{-1}\mathbf{r}$. Therefore, $\hat{\mathbf{e}}$ is iteratively refined through nonstationary iterations with step size γ_o and search direction \mathbf{t}_o .

$$\hat{\mathbf{e}}^{(2)} = \hat{\mathbf{e}}^{(1)} + \gamma_o^{(1)} \mathbf{t}_o^{(1)} \quad (3.26)$$

It is proven that iteration towards negative gradient direction results in rapid convergence; hence, the search direction is chosen as

$$\mathbf{t}_o^{(1)} = -\nabla \psi(\hat{\mathbf{e}}) = -(\mathbf{A}\hat{\mathbf{e}}^{(1)} - \mathbf{r}^{(1)}) \quad (3.27)$$

The convergence rate of ILS is improved by performing a line search on γ_o such that

$$\langle \nabla \psi(\hat{\mathbf{e}}^{(1)}), \mathbf{t}_o^{(1)} \rangle = 0 \quad (3.28)$$

It can be shown from equations (3.22) and (3.28) that

$$\gamma_o = \frac{\|\mathbf{t}_o\|_2^2}{(\mathbf{A}\mathbf{t}_o)^T \mathbf{t}_o} \quad (3.29)$$

Note that \mathbf{t}_o indicates how far the approximated value $\hat{\mathbf{e}}$ is from the optimum

3.3. ERROR REFINEMENT-BASED LINE SEARCH FOR MASSIVE MIMO DETECTION

value $\hat{\mathbf{e}}^{(*)}$.

$$\mathbf{t}_0^{(1)} = \mathbf{r}^{(1)} - \mathbf{A}\hat{\mathbf{e}}^{(1)} \quad (3.30)$$

Hence, at each iteration $k \leq L$, the approximated value of $\hat{\mathbf{e}}^{(k)}$ is iteratively refined and the refined value of $\hat{\mathbf{e}}^{(k)}$ is added to the solution $\hat{\mathbf{x}}^{(k)}$. Hence, the accuracy of the initial solution $\hat{\mathbf{x}}^{(0)}$ is improved at each iteration k . The flowchart and pseudocode of ILS are given in Fig. 3.6 and Algorithm 3.3 respectively.

3.3.2 Convergence analysis of ILS

The convergence of ILS is analysed in this subsection. Based on the linear convergence theorem, it can be shown from equations (3.25), (3.26) and (3.29) that

$$\begin{aligned} \psi(\hat{\mathbf{e}}^{(k+1)}) - \psi(\mathbf{e}^{(*)}) &\leq \left(\frac{\left(\frac{\lambda'_{max}}{\lambda_{min}} \right) - 1}{\left(\frac{\lambda'_{max}}{\lambda_{min}} \right) + 1} \right)^2 \left(\psi(\hat{\mathbf{e}}^{(k)}) - \psi(\mathbf{e}^{(*)}) \right) \\ f(\hat{\mathbf{e}}^{(k)}) - \psi(\mathbf{e}^{(*)}) &\leq \left(1 - \frac{2}{\frac{\lambda'_{max}}{\lambda_{min}}} \right)^{k-1} \left(\psi(\hat{\mathbf{e}}^{(1)}) - \psi(\mathbf{e}^{(*)}) \right) \end{aligned} \quad (3.31)$$

Since, $\frac{\lambda'_{max}}{\lambda_{min}} > 0$, it is obvious that

$$\lim_{k \rightarrow \infty} \left(1 - \frac{2}{\frac{\lambda'_{max}}{\lambda_{min}}} \right)^{k-1} \approx 0 \quad (3.32)$$

As a consequence, having promising initial conditions, $f(\hat{\mathbf{e}}^{(k)}) - f(\mathbf{e}^{(*)})$ converges to zero with increasing k . In other words, the approximate error $\hat{\mathbf{e}}$ converges to the exact error $\mathbf{e}^{(*)}$. Moreover,

$$\lim_{k \rightarrow \infty} \hat{\mathbf{x}}^{(k+1)} = \lim_{k \rightarrow \infty} (\hat{\mathbf{x}}^{(k)} + \hat{\mathbf{e}}^{(k)}) = \lim_{k \rightarrow \infty} \hat{\mathbf{x}}^{(k)} + \mathbf{e}^{(*)}$$

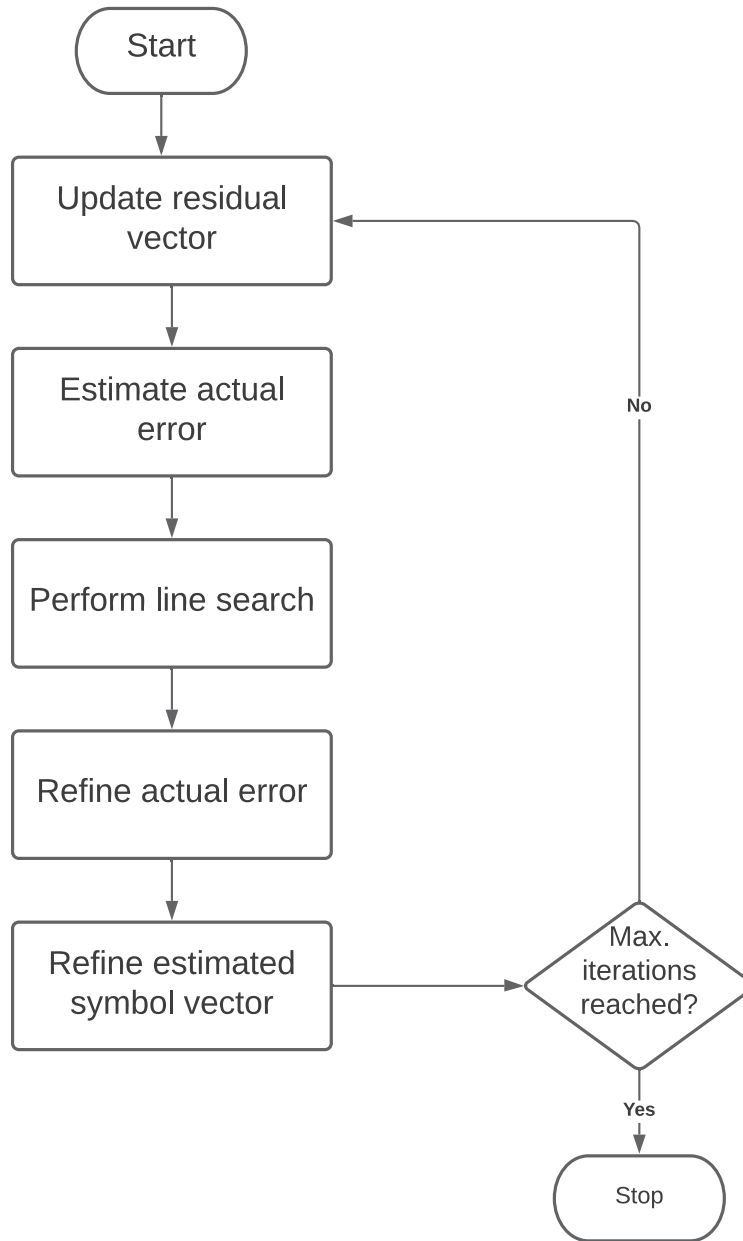


Figure 3.6: Flowchart of ILS.

3.3. ERROR REFINEMENT-BASED LINE SEARCH FOR MASSIVE MIMO DETECTION

and thus,

$$\begin{aligned} \lim_{k \rightarrow \infty} (\hat{\mathbf{x}}^{(k+1)} - \hat{\mathbf{x}}^{(k)}) &= \mathbf{e}^{(*)} = \mathbf{A}^{-1} \mathbf{r}^{(*)} \\ &= \mathbf{A}^{-1} (\mathbf{b} - \mathbf{A} \mathbf{x}^{(*)}) \approx 0 \end{aligned} \quad (3.33)$$

Therefore, ILS converges to the exact solution $\mathbf{x}^{(*)}$ after a sufficient number of iterations.

3.3.3 Simulation results

This subsection depicts the simulation results wherein performance of ILS is compared with several existing mMIMO detection algorithms which include NS, DBNI, Newton iteration with iterative refinement (NIIR), diagonal band Newton iteration with iterative refinement (DBNIIR) and JSDJI methods. For simulations, 128×16 and 144×24 mMIMO systems with 64-QAM modulation in MATLAB are considered. An ensemble of 10^3 errors are considered for averaging the BER performance over random channel and noise conditions.

BER performance of ILS: In Fig. 3.7, the BER performance of ILS is investigated for 128×16 mMIMO system with 64-QAM modulation for different number of iterations L . In Fig. 3.8, the BER performance of ILS is compared for different values of loading factor α with $L = 2$. It is observed that ILS shows improvement in BER performance with an increase in L and achieves within 0.05 dB of the MMSE performance at a target BER of 10^{-4} with $L = 3$ as shown in Fig. 3.7. Furthermore, it is also observed from Fig. 3.8 that the BER performance of ILS improves with the increase in α which is the direct consequence of the channel hardening. As depicted in Fig. 3.8, at $\text{SNR} = 20$ dB, the BER performance of ILS changes from $\text{BER} = 4.2 \times 10^{-3}$ with 128×32 system to $\text{BER} = 1.47 \times 10^{-7}$ with 128×16 system, when the loading factor is increased from $\alpha = 4$ to $\alpha = 8$.

BER performance comparison with other detection algorithms: In Fig. 3.9, performance of ILS is compared with other recently reported detection

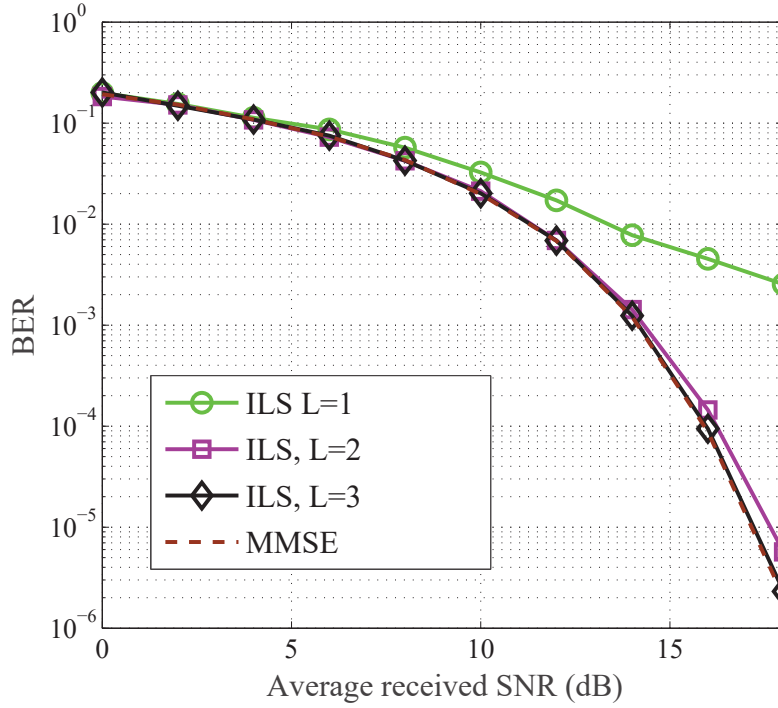


Figure 3.7: Uncoded BER performance of ILS with different number of iterations L .

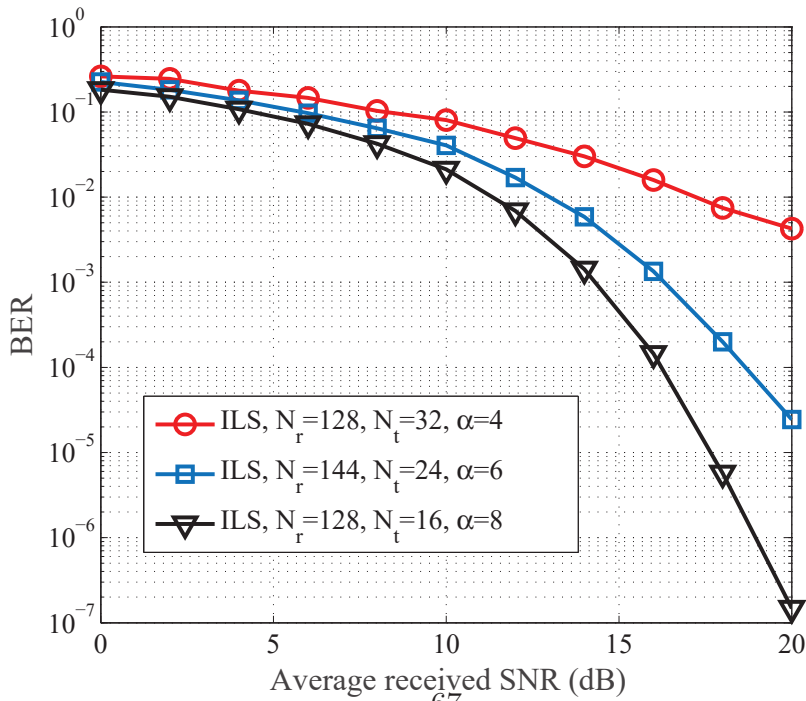


Figure 3.8: Uncoded BER performance of ILS with different loading factor α .

3.3. ERROR REFINEMENT-BASED LINE SEARCH FOR MASSIVE MIMO DETECTION

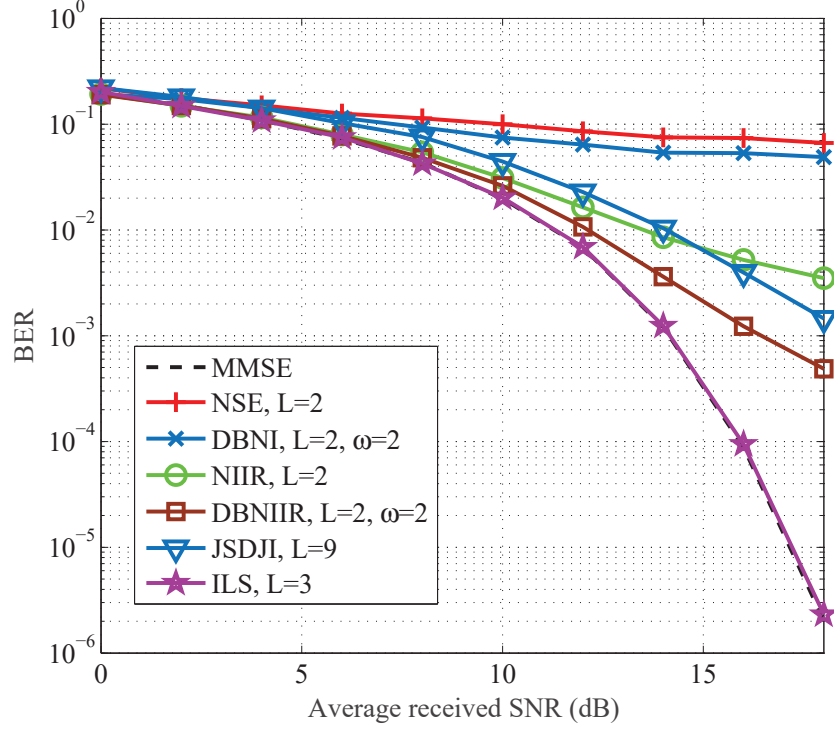


Figure 3.9: Comparison of uncoded BER performance of ILS for 128×16 mMIMO system.

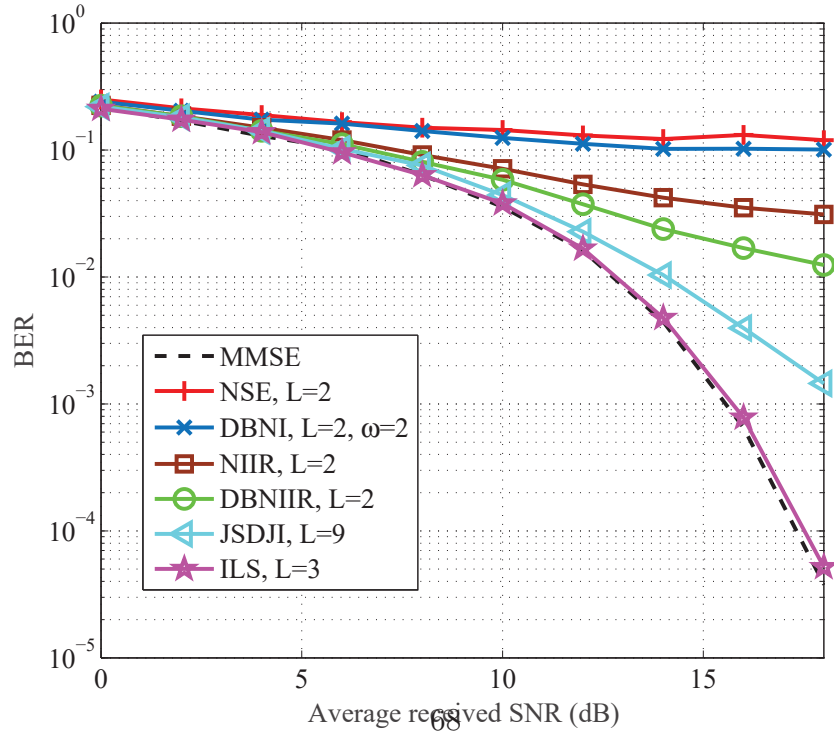


Figure 3.10: Comparison of uncoded BER performance of ILS for 144×24 mMIMO system.

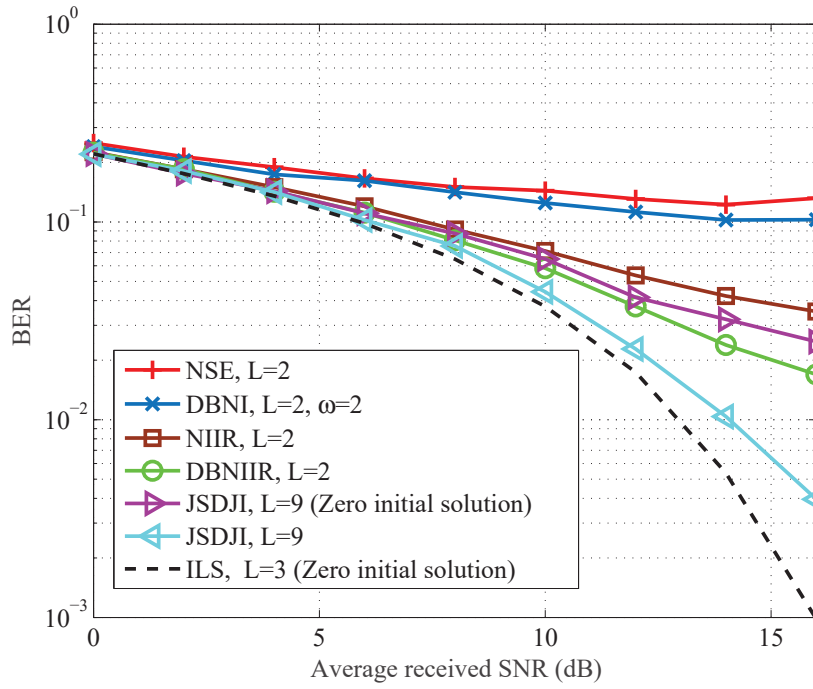


Figure 3.11: Comparison of uncoded BER performance of ILS with zero initial solution for 144×24 mMIMO system.

3.3. ERROR REFINEMENT-BASED LINE SEARCH FOR MASSIVE MIMO DETECTION

algorithms. It is observed that ILS with $L = 3$ performs superior in terms of BER when compared with the existing mMIMO detection algorithms for 128×16 mMIMO system and achieves near MMSE performance. An SNR gain of 1.7 dB is achieved in ILS over DBNIIR for a target BER of 10^{-3} as depicted in Fig. 3.9. Since a single iteration of JSDJI requires less number of computations compared to ILS, ILS is compared with $L = 3$ (approximately $36N_t^2$ multiplications) and JSDJI with $L = 9$ (approximately $40N_t^2$ multiplications). As shown in Figs. 3.9 and 3.10, JSDJI even with $L = 9$ yields far inferior BER performance compared to ILS for both 128×16 and 144×24 mMIMO systems. A BER improvement of approximately 96% at SNR=20dB is achieved in ILS compared to JSDJI as observed from Fig. 3.10.

The BER performance ILS with zero initial solution is also compared in Fig. 3.11 with other contending detection algorithms. In Fig. 3.11, ILS, even with zero initial solution, outperforms other algorithms initialized with the diagonal dominance property of MMSE filter matrix. Moreover, as depicted in Fig.3.11, SNR gain of approximately 1.8 dB is achieved in ILS as compared to JSDJI for a targeted BER of 4×10^{-3} .

3.3.4 Computational analysis

In this subsection, the computational complexity of ILS is compared with several contending detection algorithms for uplink mMIMO systems. Table 3.2 analyzes and compares the computational complexity of ILS with different state-of-the-art mMIMO detection algorithms in terms of the number of real valued multiplications. The computational complexity of ILS is computed as follows. The computation of residual error in line 2 of Algorithm 3.3 requires $4N_t^2$ real valued multiplications. Since \mathbf{D} is a diagonal matrix, $2N_t$ multiplications are sufficient to get the actual error vector \mathbf{e} in line 3. Line 4 involves matrix-vector multiplications, and hence requires $4N_t^2$ multiplications. The computation of γ_o requires $4N_t^2 + 4N_t$ real-valued multiplications. Lines 6 and 7 respectively, require $2N_t$ and 0 multiplications. Hence, for L iterations,

ILS requires total $(12N_t^2 + 8N_t)L$ real-valued multiplications. For fair comparison, the computational complexity in calculating the initial parameters \mathbf{G} , \mathbf{A} , \mathbf{b} , \mathbf{D} , \mathbf{D}^{-1} and $\mathbf{D}^{-1}\mathbf{b}$ are ignored, as these parameters are required to be calculated in all detection algorithms. However, the number of terms ω and iterations in NS, diagonal band Newton iteration (DBNI), NIIR and DBNIIR methods are restricted to 2 only to avoid matrix-matrix multiplications, which increases their computations to $\mathcal{O}(N_t^3)$. As the computations of JSDJI requires approximately $4(L+1)N_t^2$ real valued multiplications, $L = 3$ is set for the proposed algorithm while $L = 9$ for JSDJI, so that JSDJI approximately requires more real valued multiplications compared to ILS for fair comparison. However, the simulation results in subsection 3.3.3 corroborate that ILS outperforms JSDJI for both 128×16 and 144×24 mMIMO systems.

Table 3.2: Number of real valued operations

Detection algo- rithm	No of real val- ued multiplica- tions
NS ($L = 2$) [6]	$12N_t^2 + 2N_t$
DBNI ($L = 2, \omega = 2$) [33]	$20N_t^2 + 8N_t$
NIIR ($L = 2$) [69]	$20N_t^2 + 10N_t$
DBNIIR ($L = 2, \omega = 2$) [69]	$28N_t^2 + 16N_t$
JSDJI [38]	$4(L+1)N_t^2 + 2(L+4)N_t$
ILS	$(12N_t^2 + 16N_t)L$

Therefore, from Figs. 3.7-3.11 and Table 3.2, it is well-explained that ILS yields a superior performance-complexity trade-off compared to several existing detection algorithms.

3.4 Summary

In this Chapter, two detection algorithms called HA and ILS are proposed for uplink mMIMO systems. In the proposed HA, nonstationary iteration based NSNI and stationary iteration based ISRI are combined to circumvent the drawbacks of existing iterative detection techniques. NSNI overcomes the limitations of NI and yields superior BER performance than NI with the same computational complexity. Similarly, RI and ISRI have the same computational complexity; however, ISRI outperforms RI. Accordingly, the proposed HA yields superior performance over NI, RI, JSDJI and CG in terms of BER and computational complexity, under both perfect and imperfect CSI at the BS. The proposed ILS iteratively refines both the actual error and symbol estimate by using a line search and combines the estimated error with the estimated symbol vector. Simulation results reveal the viability and robustness of the proposed detection algorithms compared to several existing stationary and nonstationary symbol detection algorithms for uplink mMIMO systems.

This Chapter's focus is to achieve near-MMSE performance, which is near-optimal for the mMIMO system with small system loading factors. However, MMSE yields near-optimal performance when $\frac{N_r}{N_t} \geq 10$ and achieves suboptimal results when users scale up in the mMIMO system. Hence, in the next Chapter, a low complexity detection algorithm is devised for large user mMIMO systems.

Chapter 4

Reliability feedback–aided detection in uplink massive MIMO systems

4.1 Introduction

In the preceding Chapter, it is seen that pseudo-stationary iterations based HA and nonstationary error refinement based ILS provides near-MMSE performance. Both HA and ILS exhibit comparatively low computational complexity to achieve better BER results than conventional iterative detectors for mMIMO systems. However, MMSE yields near-optimal performance for mMIMO systems for high system loading factors. The uplink symbol detection in mMIMO systems becomes a more challenging task when users scale up in the system. In this Chapter, the signal detection problem in mMIMO systems is explored when there are a large number of users in the system.

In this Chapter, RFOD is proposed for large user uplink mMIMO systems. First, a low-complexity initial solution is used to compute the quality metric for finding the detection sequence. Next, for detecting the symbol corresponding to each user, the interference from all other users is cancelled, followed by RFM. Ordering of the users along with the reliability feedback re-

duces the effect of error propagation. Through multiple iterations of RFOD, an enhanced BER performance is achieved. Furthermore, RFOD outperforms several existing detection algorithms (including MMSE) with quadratic computational complexity for symbol detection in large user mMIMO systems. Simulation results corroborate the superiority of RFOD over the recently introduced mMIMO detection algorithms in terms of both the computational complexity and the BER performance.

The Chapter is structured as follows: Initialization is described in Section 4.2. In Section 4.3, the quality metric-based ordered detection is presented, and RFM is described in Section 4.4. Convergence analysis of RFOD is provided in Section 4.5. The simulation results on BER performance are drawn in Section 4.6. The computational complexity analysis is done in Section 4.7. Finally, Section 4.8 summarizes the Chapter.

4.2 Initialization

A low-complexity initial solution is expressed using the diagonal dominance of MMSE filter matrix [44, 46], as discussed in Chapter 3.

$$\mathbf{x}^{(0)} \approx \mathbf{W}^{-1}\mathbf{b}. \quad (4.1)$$

It is worth mentioning that RFOD can be initialized with zero initial solution. However, for a fair comparison with existing detection algorithms, the above initial solution is chosen for RFOD.

4.3 Quality metric based ordered detection

In this section, quality metric-based detection is proposed. The mMIMO detection problem is written as

$$\hat{\mathbf{x}} = Q \left(\arg \min_{\mathbf{x} \in \mathcal{A}^{2N_t}} \{ \|\mathbf{y} - \mathbf{H}\mathbf{x}\|_2^2 \} \right), \quad (4.2)$$

where $Q(\cdot)$ is the quantization function. Each component of the gradient of the cost function $\phi(\mathbf{x}) = \|\mathbf{y} - \mathbf{H}\mathbf{x}\|_2^2$ is nullified at the global minima/optimal point. The gradient of the cost function $\phi(\mathbf{x})$ is

$$\nabla \psi(\mathbf{x}) = -2\mathbf{H}^T(\mathbf{y} - \mathbf{H}\mathbf{x}) \quad (4.3)$$

Similarly, the i^{th} component of the gradient of the cost function $\phi(\mathbf{x})$ is

$$\nabla_i \psi(\mathbf{x}) = -2\mathbf{h}_i^T(\mathbf{y} - \mathbf{H}\mathbf{x}) \quad (4.4)$$

At the global optimal point, the following conditions must hold

$$\begin{aligned} \nabla \psi(\mathbf{x}^*) &= 0 \\ \text{or, } -2\mathbf{H}^T(\mathbf{y} - \mathbf{H}\mathbf{x}^*) &= 0 \end{aligned} \quad (4.5)$$

$$\begin{aligned} \nabla_i \psi(\mathbf{x}^*) &= 0 \\ \text{or, } -2\mathbf{h}_i^T(\mathbf{y} - \mathbf{H}\mathbf{x}^*) &= 0 \end{aligned} \quad (4.6)$$

If $\hat{\mathbf{x}}$ is assumed to be the estimate of \mathbf{x} , the term $(\mathbf{y} - \mathbf{H}\hat{\mathbf{x}})$ is called the residual error (as discussed in Chapter 3). Residual error gives vital information about the deviation of the estimate $\mathbf{H}\hat{\mathbf{x}}$ from the received symbol vector \mathbf{y} . The residual error at iteration $(k + 1)$ after the $(i - 1)^{th}$ symbol update is

represented as

$$\mathbf{r}_{\mathbf{e}(i-1)}^{(k+1)} = \mathbf{y} - \sum_{j=1, j < i}^{2Nt} \mathbf{h}_j \hat{x}_j^{(k+1)} - \sum_{j=1, j \geq i}^{2Nt} \mathbf{h}_j \hat{x}_j^{(k)} \quad (4.7)$$

The quality metric is the projection of the residual error onto the column space of \mathbf{H} . Hence, the quality metric for the i^{th} symbol is computed as [70, 71]

$$q_i^{(k+1)} = \frac{\mathbf{h}_i^T}{\|\mathbf{h}_i\|_2^2} \mathbf{r}_{\mathbf{e}(i-1)}^{(k+1)} \quad (4.8)$$

Hence, the quality metric for the i^{th} symbol denotes the error associated with the estimated i^{th} symbol. Consequently, an estimated symbol with a greater value of the quality metric will contribute more to the interuser interference. As a result, before detecting the symbols, the symbols are ordered in descending order (quality ordering, \mathcal{O}) of the quality metric, which leads to the improved BER performance.

Suppose the detection algorithm converges at $(k+1)^{th}$ iteration. Further suppose, at $(k+1)^{th}$ iteration, the i^{th} symbol is to be updated. Since the symbols are being sequentially detected based on the quality order \mathcal{O} , the symbols for which $j < i$ hold updated values from iteration $(k+1)$. On the other hand, the symbols for which $j \geq i$ are yet to be updated. Hence, from (4.6),

$$\mathbf{h}_i^T (\mathbf{y} - \sum_{j < i} \mathbf{h}_j \hat{x}_j^{(k+1)} - \sum_{j > i} \mathbf{h}_j \hat{x}_j^{(k)} - \mathbf{h}_i \hat{x}_i^{(k)} - \mathbf{h}_i d_i^{(k+1)}) = 0, \quad i \in \mathcal{O}, \quad (4.9)$$

where \mathcal{O} contains indices of the elements, $x_i \in \mathbf{x}$ in descending order of quality metric, and $d_i^{(k+1)}$ is the deviation of the symbol $\hat{x}_i^{(k)}$ from $\hat{x}_i^{(k+1)}$. $d_i^{(k+1)}$ is defined as

$$d_i^{(k+1)} = \hat{x}_i^{(k+1)} - \hat{x}_i^{(k)}, \quad i \in \mathcal{O} \quad (4.10)$$

4.3. QUALITY METRIC BASED ORDERED DETECTION

Hence, from equation (4.9),

$$\mathbf{h}_i^T (\mathbf{y} - \sum_{j < i} \mathbf{h}_j \hat{x}_j^{(k+1)} - \sum_{j > i} \mathbf{h}_j \hat{x}_j^{(k)} - \mathbf{h}_i x_i^{(k)} + \mathbf{h}_i \hat{x}_i^{(k)}) = \mathbf{h}_i^T \mathbf{h}_i \hat{x}_i^{(k+1)}, \quad i \in \mathcal{O} \quad (4.11)$$

$$\hat{x}_i^{(k+1)} = \hat{x}_i^{(k)} + \frac{(b_i - \mathbf{h}_i^T \sum_{j < i} \mathbf{h}_j \hat{x}_j^{(k+1)} - \mathbf{h}_i^T \sum_{j \geq i} \mathbf{h}_j \hat{x}_j^{(k)})}{\|\mathbf{h}_i\|_2^2}, \quad i \in \mathcal{O} \quad (4.12)$$

Analysis of residual error: Residual error denotes the lack of agreement between the estimate $\mathbf{H}\hat{\mathbf{x}}$ and the received vector \mathbf{y} . A continuously decreasing residual error confirms the substantial mitigation of noise during detection. At iteration $(k+1)$, the residual error vector after the update of $(i+1)^{th}$ symbol $\hat{x}_{i+1}^{(k+1)}$ is

$$\mathbf{r}_{\mathbf{e}(i+1)}^{(k+1)} = \mathbf{y} - \sum_{j=1, j \leq i+1}^{2Nt} \mathbf{h}_j \hat{x}_j^{(k+1)} - \sum_{j=1, j > i+1}^{2Nt} \mathbf{h}_j \hat{x}_j^{(k)}. \quad (4.13)$$

Since $q_{i+1}^{(k+1)} = \hat{x}_{i+1}^{(k+1)} - \hat{x}_{i+1}^{(k)}$, the residual error $\mathbf{r}_{\mathbf{e}(i+1)}^{(k+1)}$ from equation (4.13) is further simplified as

$$\begin{aligned} \mathbf{r}_{\mathbf{e}(i+1)}^{(k+1)} &= \mathbf{r}_{\mathbf{e}(i)}^{(k+1)} - \mathbf{h}_{i+1} (\hat{x}_{i+1}^{(k+1)} - \hat{x}_{i+1}^{(k)}) \\ &= \mathbf{r}_{\mathbf{e}(i)}^{(k+1)} - \mathbf{h}_{i+1} q_{i+1}^{(k+1)}. \end{aligned} \quad (4.14)$$

The detection algorithm arranges the symbols in descending order of q_i and hence, the largest amount of residual error is minimized even in the first symbol update compared to ISD[8]. Mathematically,

$$\begin{aligned} q_1^{(k+1), Proposed} &> q_1^{(k+1), ISD}, \\ \mathbf{r}_{\mathbf{e}(1)}^{(k+1), Proposed} &< \mathbf{r}_{\mathbf{e}(1)}^{(k+1), ISD}. \end{aligned} \quad (4.15)$$

Since $\mathbf{h}_{i+1}^T \mathbf{r}_{\mathbf{e}(i+1)}^{(k+1)} = 0$, using the expression of $\mathbf{r}_{\mathbf{e}(i)}^{(k+1)}$ from (4.14),

$$\begin{aligned} \|\mathbf{r}_{\mathbf{e}(i+1)}^{(k+1)}\|_2^2 &= \|\mathbf{r}_{\mathbf{e}(i)}^{(k+1)}\|_2^2 - \|\mathbf{h}_{i+1} q_{i+1}^{(k+1)}\|_2^2 \\ &= \|\mathbf{r}_{\mathbf{e}(i)}^{(k+1)}\|_2^2 - \left(q_{i+1}^{(k+1)}\right)^2 \|\mathbf{h}_{i+1}\|_2^2. \end{aligned} \quad (4.16)$$

Since $\left(q_{i+1}^{(k+1)}\right)^2 \|\mathbf{h}_{i+1}\|_2^2 > 0$, it is obvious from (4.16) that

$$\|\mathbf{r}_{\mathbf{e}(i+1)}^{(k+1)}\|_2^2 < \|\mathbf{r}_{\mathbf{e}(i)}^{(k+1)}\|_2^2. \quad (4.17)$$

It concludes that the L2-norm of residual error or ML cost reduces after each symbol update in the QO based detection algorithm. Hence, QO significantly mitigates the effect of interference and noise during symbol detection.

Analysis of actual error: Actual error gives the deviation of the detected value from the true value. The actual error $e_i^{(k+1)} = x_i^{(k+1)} - x_i^{(*)}$ associated with symbol $x_i^{(k+1)}$ after each iteration $(k+1)$ is defined as

$$e_i^{(k+1)} = e_i^{(k)} - \frac{\mathbf{h}_i^T \sum_{j=1, j \geq i}^{2U} \mathbf{h}_j e_j^{(k)} + \mathbf{h}_i^T \sum_{j=1, j < i}^{2U} \mathbf{h}_j e_j^{(k+1)}}{\|\mathbf{h}_i\|^2}, \quad (4.18)$$

where $x^{(*)}$ is the optimal detected symbol from the i^{th} user. Since $e_i^{(k)} > 0$, it is obvious from (4.18) that

$$e_i^{(k+1)} < e_i^{(k)}. \quad (4.19)$$

Thus, it concludes from the above analysis that the actual error associated with each symbol reduces after each iteration in the QO based detection algorithm. Hence, as the number of iteration increase, the actual errors related to the symbols decrease, and the QO based detection algorithm gradually reaches the optimal solution.

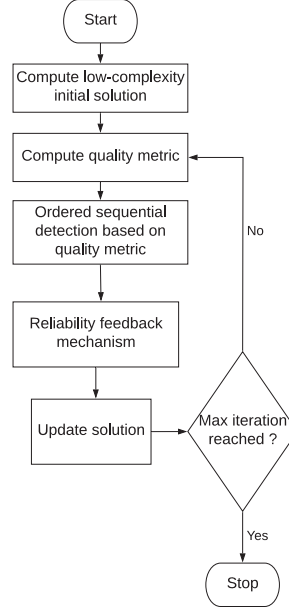
4.3. QUALITY METRIC BASED ORDERED DETECTION

Algorithm 4.1 Proposed RFOD algorithm

```

1: Inputs:  $\mathbf{y}, \mathbf{H}, \sigma^2, E_x, Nr, Nt$  and  $l_{th}$ 
2: Outputs:  $\mathbf{x}^{(*)}$ 
3: Initialization:  $\mathbf{G} = \mathbf{H}^T \mathbf{H}, \mathbf{A} = \mathbf{G} + \frac{\sigma^2}{E_x} \mathbf{I}_{2Nt}, \mathbf{W} = \text{diag}(\mathbf{A}), \mathbf{b} = \mathbf{H}^T \mathbf{y}, \mathbf{x}^{(1)} = \mathbf{W}^{-1} \mathbf{b}$ 
4: Preprocessing:  $t_i = (\|\mathbf{h}_i\|^2)^{-1}, i = 1, 2, \dots, 2Nt$ 
5: for  $i = 1, i \leq 2Nt$  do
6:    $r_i^{(1)} = (b_i - \mathbf{G}_i^T \mathbf{x}^{(1)})$ 
7: end for
8: for  $k = 1, k \leq L$  do
9:    $q_i = t_i r_i^{(k)}$ 
10:   $r_i^{(k)} \in \mathbf{r}^{(k)}, i = 1, 2, \dots, 2Nt$ 
11:  Order  $q_i \in \mathbf{q}$  in descending order,  $\mathcal{O}^{(k)} = \underset{i}{arg\ sort} \mid q_i \mid, i = 1, 2, \dots, 2Nt$ 
12:  for  $l = 1, l \leq 2Nt$  do
13:     $m = \mathcal{O}^{(k)}(l)$ 
14:     $x_m^{(k+1)} = x_m^{(k)} + \frac{1}{g_{m,m}} \left( b_m - \sum_{j \in \mathcal{O}^{(k)}(l), j \geq m} g_{m,j} x_j^{(k)} - \sum_{j \in \mathcal{O}^{(k)}(l), j < m} g_{m,j} x_j^{(k+1)} \right)$ 
15:     $\mathcal{L}_m^{(k)} = |x_m^{(k+1)} - \mathcal{Q}(x_m^{(k+1)})|$ 
16:    if  $\mathcal{L}_m^{(k)} \leq l_{th}$  then
17:       $x_m^{(k+1)} = \mathcal{Q}(x_m^{(k+1)})$ 
18:    else
19:       $x_m^{(k+1)} = \mathcal{V}(x_m^{(k+1)})$ 
20:    end if
21:     $r_{(m)}^{(k+1)} = r_{(m-1)}^{(k+1)} - g_{m,m} (x_m^{(k+1)} - x_m^{(k)})$ 
22:  end for
23: end for
24: Final output:  $\mathbf{x}^{(*)} = \mathbf{x}^{(L)}$ 

```



f

Figure 4.1: Flowchart of RFOD.

4.4 Reliability feedback mechanism

RFM is proposed to improve the quality of the solution estimated through QO based ordered detection. In RFM, at each iteration $(k+1)$, before feeding the estimated symbol $\hat{x}_i^{(k+1)}$ to the next iteration $(k+2)$, the reliability of the estimated symbol is checked. Suppose the unquantized symbol $\hat{x}_i^{(k+1)}$ lies between two constellation points \mathcal{Z}_1 and \mathcal{Z}_2 . The reliable regions are defined as

$$\mathcal{R}_t = \left\{ \hat{x}_i^{(k+1)} : \mathcal{Z}_t - l_{th} < \hat{x}_i^{(k+1)} < \mathcal{Z}_t + l_{th} \right\}, \quad t = 1, 2, \quad (4.20)$$

where l_{th} is the decision boundary of the reliable regions. The reliability of the unquantized symbol is checked by the metric defined as

$$\mathcal{L}_i^{(k+1)} = | \hat{x}_i^{(k+1)} - \mathcal{Q}(\hat{x}_i^{(k+1)}) | \quad (4.21)$$

After that, the symbol $\hat{x}_i^{(k+1)}$ is quantized according to the rule given below,

$$\hat{x}_i^{(k+1)} = \begin{cases} \mathcal{Q}\left(\hat{x}_i^{(k+1)}\right), & \text{if } \mathcal{L}_i \leq l_{th} \\ \mathcal{V}\left(\hat{x}_i^{(k+1)}\right) & \end{cases} \quad (4.22)$$

where $\mathcal{V}(x_i^{(k+1)}) = \frac{\mathcal{Z}_1 + \mathcal{Z}_2}{2}$ is considered as a virtual constellation point taken between two corresponding constellation points $\mathcal{Z}_1, \mathcal{Z}_2 \in \mathcal{A}$. Similar approach is performed for all the symbols $\hat{x}_i^{(k+1)} \in \hat{\mathbf{x}}^{(k+1)}$. Next, a hard quantization of the detected symbol vector $\hat{\mathbf{x}}^{(k+1)}$ is performed. Furthermore, in order to enhance the performance, multiple iterations (say $k \leq L$) of RFOD are performed. The pseudocode and flowchart of RFOD are presented in Algorithm 4.1 and Fig 4.1 respectively.

4.5 Convergence analysis

This section analyzes convergence of the RFOD algorithm. For mathematical tractability, RFM is not considered in this analysis. Without loss of generality, the symbol update rule (4.12) is represented as a matrix-vector equation,

$$\begin{aligned} \tilde{\mathbf{x}}^{(k+1)} &= \tilde{\mathbf{x}}^{(k)} + \tilde{\mathbf{D}}^{-1} \left(\mathbf{b} - \tilde{\mathbf{G}} \tilde{\mathbf{x}}^{(k)} \right) \\ &= \left(\mathbf{I} - \tilde{\mathbf{D}}^{-1} \tilde{\mathbf{G}} \right) \tilde{\mathbf{x}}^{(k)} + \tilde{\mathbf{D}}^{-1} \mathbf{b} \\ &= \mathbf{M} \tilde{\mathbf{x}}^{(k)} + \tilde{\mathbf{D}}^{-1} \mathbf{b} \end{aligned} \quad (4.23)$$

where $\tilde{\mathbf{x}} = \mathbf{P}\mathbf{x}$, $\tilde{\mathbf{G}} = \mathbf{G}\mathbf{P}^{-1}$, $\tilde{\mathbf{D}}^{-1} = \mathbf{P}\mathbf{D}^{-1}$ and \mathbf{P} is a $2Nt \times 2Nt$ row permutation matrix based on permutation defined by order \mathcal{O} . It is certain that the convergence of update rule (4.23) ensures the convergence of (4.12). For mathematical tractability, the row permutation matrix is assumed to obey the following properties [71].

- \mathbf{P} is nonsingular and $\mathbf{P}^{-1} = \mathbf{P}^T$.

- Matrix norm is invariant under permutation, i.e $\| \mathbf{PD} \| = \| \mathbf{DP}^{-1} \|$
 $= \| \mathbf{D} \|$

Equation (4.23) is a stationary iteration with iteration matrix $\mathbf{M} = (\mathbf{I} - \tilde{\mathbf{D}}^{-1}\tilde{\mathbf{G}})$. Hence, the convergence analysis of (4.23) is carried out based on the iteration matrix \mathbf{M} and iteration (4.23). Gram matrix \mathbf{G} is expressed as $\mathbf{G} = \mathbf{L} + \mathbf{L}^T + \mathbf{D}$ using standard matrix splitting [72], where \mathbf{L} is a $2Nt \times 2Nt$ strictly lower triangular matrix and \mathbf{D} is a $2Nt \times 2Nt$ diagonal matrix. The diagonal matrix \mathbf{D} is obtained using the diagonal elements of the matrix \mathbf{G} , while keeping the off-diagonal elements to zero. The strictly lower triangular matrix \mathbf{L} is obtained from \mathbf{G} by keeping both the diagonal and the off-diagonal elements above the main diagonal to zero. Taking the matrix norm of \mathbf{M} ,

$$\begin{aligned}
 \| \mathbf{M} \| &= \| \mathbf{I} - \tilde{\mathbf{D}}^{-1}\tilde{\mathbf{G}} \| \\
 &= \| \mathbf{I} - \mathbf{PD}^{-1}\mathbf{GP}^{-1} \| \\
 &= \| \mathbf{I} - \mathbf{PD}^{-1}(\mathbf{L}^T + \mathbf{L} + \mathbf{D})\mathbf{P}^{-1} \| \\
 &= \| \mathbf{I} - \mathbf{PD}^{-1}(\mathbf{L}^T + \mathbf{L})\mathbf{P}^{-1} - \mathbf{PD}^{-1}\mathbf{DP}^{-1} \| \\
 &= \| -\mathbf{PD}^{-1}(\mathbf{L}^T + \mathbf{L})\mathbf{P}^{-1} \| \\
 &= \| \mathbf{PD}^{-1}(\mathbf{L}^T + \mathbf{L})\mathbf{P}^{-1} \| \tag{4.24}
 \end{aligned}$$

Lemma 1 *Given a diagonally dominant matrix \mathbf{G} , the matrix norm of the iteration matrix, $\mathbf{M} = (\mathbf{I} - \tilde{\mathbf{D}}^{-1}\tilde{\mathbf{G}})$ is less than unity.*

Proof 1 *Given \mathbf{G} is diagonally dominant i.e $\sum_{j \neq i} |g_{i,j}| < |g_{i,i}|$ and hence,*

$$\sum_{j=1}^{2Nt} |m_{i,j}| = \frac{\sum_{j \neq i} |g_{i,j}|}{|g_{i,i}|} < 1 \tag{4.25}$$

Since the matrix norm is invariant under the permutation [73], using equation (4.24), $\| \mathbf{M} \|$ is simplified as

$$\begin{aligned} \|\mathbf{M}\| &= \|\mathbf{PD}^{-1}(\mathbf{L}^T + \mathbf{L})\mathbf{P}^{-1}\| \\ &= \|\mathbf{D}^{-1}(\mathbf{L}^T + \mathbf{L})\| \end{aligned} \quad (4.26)$$

Hence, (4.25) and (4.26) conclude that

$$\|\mathbf{M}\| < 1 \quad (4.27)$$

Theorem 2 *Given a nonsingular matrix \mathbf{G} and a permutation matrix \mathbf{P} , $\lim_{k \rightarrow \infty} \mathbf{x}^{(k)} \rightarrow \mathbf{x}^{(*)}$ if $\rho(\mathbf{M}) \leq 1$*

Proof 2 *At first, for mathematical tractability, the matrix $\mathbf{I} - \mathbf{M}$ is expressed in terms of matrices \mathbf{G} , \mathbf{P} and \mathbf{D} .*

$$\begin{aligned} \mathbf{I} - \mathbf{M} &= \mathbf{I} - (\mathbf{I} - \tilde{\mathbf{D}}^{-1}\tilde{\mathbf{G}}) \\ &= \tilde{\mathbf{D}}^{-1}\tilde{\mathbf{G}} \\ &= \mathbf{PD}^{-1}\mathbf{GP}^{-1} \end{aligned} \quad (4.28)$$

From the system model of mMIMO (given in Chapter 1), it is obvious that the Gram matrix $\mathbf{G} = \mathbf{H}^T\mathbf{H}$ and diagonal matrix \mathbf{D} are nonsingular. Since \mathbf{G} , \mathbf{D} and \mathbf{P} are nonsingular, hence, $\mathbf{I} - \mathbf{M}$ is also nonsingular and $(\mathbf{I} - \mathbf{M})^{-1}$ exists.

$$(\mathbf{I} - \mathbf{M})^{-1} = (\mathbf{I} + \mathbf{M} + \mathbf{M}^2 + \dots) \quad (4.29)$$

Hence, the stationary iterative update rule (4.23) is expressed as

$$\tilde{\mathbf{x}}^{(k+1)} = \mathbf{M}^{(k)}\tilde{\mathbf{x}}^{(1)} + \left(\sum_{i=0}^{k-1} \mathbf{M}^i\right)\tilde{\mathbf{D}}^{-1}\mathbf{b} \quad (4.30)$$

Taking $\lim_{k \rightarrow \infty}$ on both side of equation (4.30),

$$\begin{aligned} \lim_{k \rightarrow \infty} \tilde{\mathbf{x}}^{(k+1)} &= \lim_{k \rightarrow \infty} \mathbf{M}^{(k)} \tilde{\mathbf{x}}^{(1)} + \left(\mathbf{I} + \mathbf{M} + \mathbf{M}^2 + \dots \right) \tilde{\mathbf{D}}^{-1} \mathbf{b} \\ &= \lim_{k \rightarrow \infty} \mathbf{M}^{(k)} \tilde{\mathbf{x}}^{(1)} + \left(\mathbf{I} - \mathbf{M} \right)^{-1} \tilde{\mathbf{D}}^{-1} \mathbf{b} \end{aligned} \quad (4.31)$$

Hence, from Lemma 1 given in this Chapter, the spectral radius $\rho(\mathbf{M}) \leq \|\mathbf{M}\| < 1$. Further, $\lim_{k \rightarrow \infty} \mathbf{M}^{(k)} = \mathbf{0}$, Hence,

$$\begin{aligned} \lim_{k \rightarrow \infty} \tilde{\mathbf{x}}^{(k+1)} &= \left(\mathbf{I} - \mathbf{M} \right)^{-1} \tilde{\mathbf{D}}^{-1} \mathbf{b} \\ &= \mathbf{P} \mathbf{G}^{-1} \mathbf{b} \\ \lim_{k \rightarrow \infty} \mathbf{x}^{(k+1)} &= \mathbf{G}^{-1} \mathbf{b} = \mathbf{x}^{(*)} \end{aligned} \quad (4.32)$$

Thus, it is proved from (4.32) that the iteration (4.23) converges to the optimal solution $\mathbf{x}^{(*)}$ when the quality ordering \mathcal{O} is applied.

4.6 Simulation results

This section draws the simulation results for comparing the BER performance of RFOD with some of the existing algorithms for 128×64 and 128×74 mMIMO systems with 16-QAM modulation¹. An ensemble of 2×10^3 is considered to average the BER performance over the random channel and noise conditions.

BER performance comparison among contending detection algorithms:

Figs. 4.2 and 4.3 compare BER performance of RFOD with RI, CG, JSDJI and ISD for approximately equal number of multiplications of $20N_t^2$. As observed from Fig. 4.2, SNR gains of 5.3 dB for $\text{BER} = 4 \times 10^{-3}$ and 3.5 dB for $\text{BER} = 10^{-3}$ are observed in RFOD over CG and ISD respectively for 128×64 mMIMO system. Moreover, as depicted in Fig. 4.3, RFOD achieves

¹Both 128×74 and 128×64 systems have a system loading factor of approximately 2. Hence, the detection with such a large number of users is a more challenging task in these system models than the system models considered in the previous chapter.

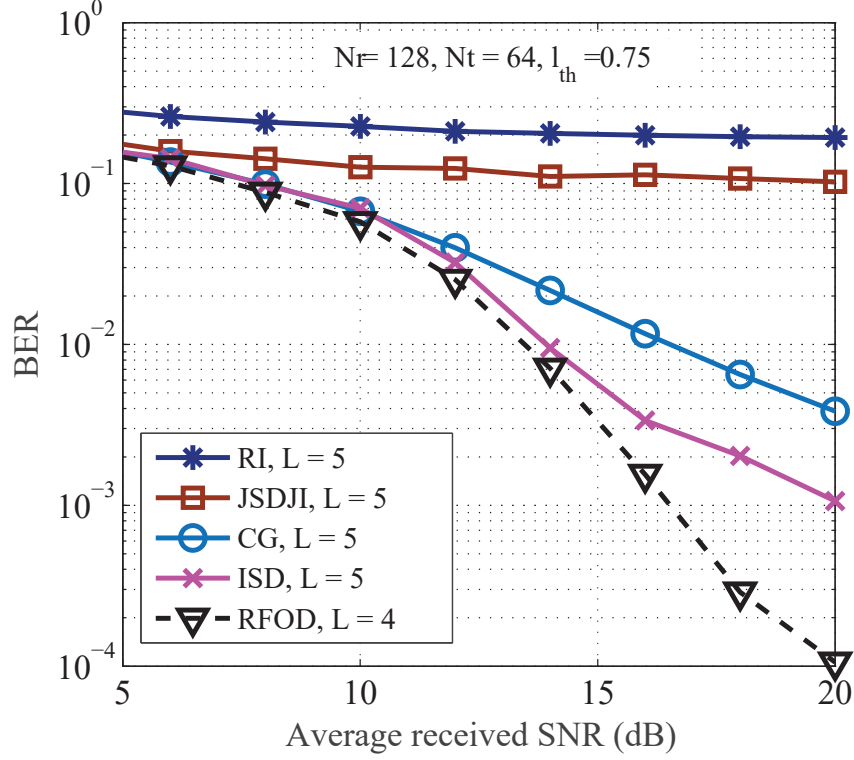


Figure 4.2: BER performance comparison for 128×64 mMIMO system with approximately equal real valued multiplications.

82.9% and 76.2% improvements in BER at SNR=20 dB as compared to CG and ISD respectively for 128×74 mMIMO systems.

Comparison of BER performance with increased number of antennas:

As depicted in Figs. 4.4-4.5, the BER performances of both CG and ISD improve when the number of iterations increases from $L = 4$ to $L = 6$. This proves that CG and ISD are not capable to reach global optima with $L = 4$ iterations in Figs 4.2-4.3. Hence, the number of iterations at $L = 4$ is not sufficient to justify and compare the contending algorithms' performance with RFOD. Hence, for fair comparisons, a higher number of iterations are explored.

In Figs. 4.4-4.5, RFOD with $L = 6$ outperforms MMSE, which requires approximately $28Nt^2$ real valued multiplications for both 128×64

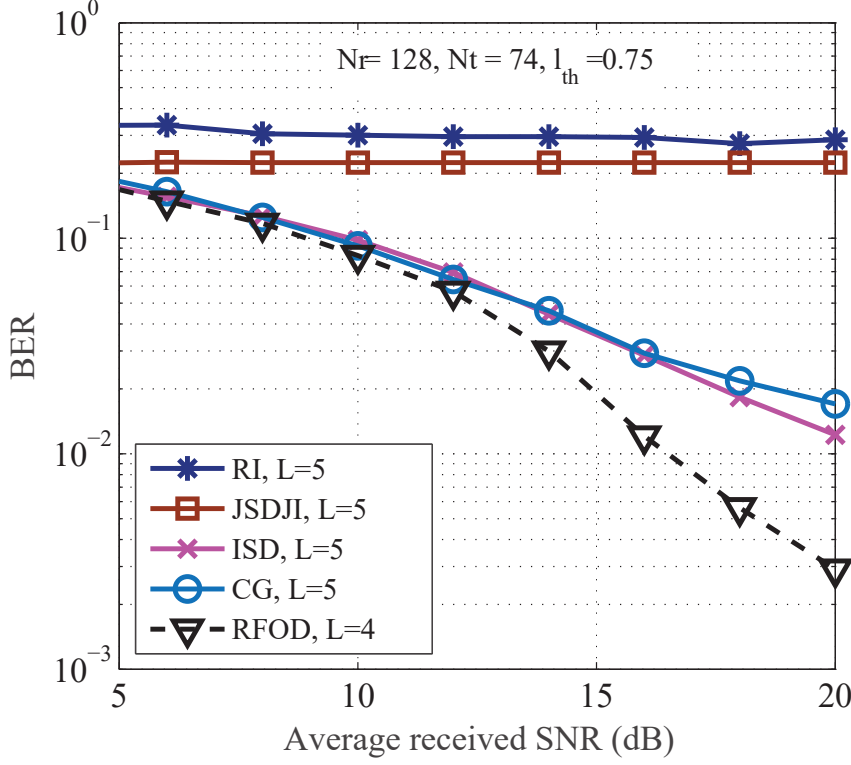


Figure 4.3: BER performance comparison for 128×74 mMIMO system with approximately equal real valued multiplications.

and 128×74 mMIMO systems. However, CG even with $L = 14$ archives near-MMSE performance and requires double number of multiplications (approximately $56Nt^2$) as compared to RFOD. Moreover, ISD with $56Nt^2$ multiplications yields inferior performance than RFOD for both 128×64 and 128×74 mMIMO systems. Hence, Figs. 4.2-4.5 prove the superiority of RFOD compared to RI, CG, JSDJI and ISD in terms of real valued operations.

Analysis of BER performance in terms of FLOPs: To further verify the viability of RFOD, BER performances of contending algorithms are compared in Figs. 4.6-4.7 in terms of the number of FLOPs. As depicted in Fig. 4.6-4.7, the BER performances of RI and JSDJI are far inferior as compared with RFOD. The RFOD algorithm with $L = 6$ outperforms MMSE and re-

4.6. SIMULATION RESULTS

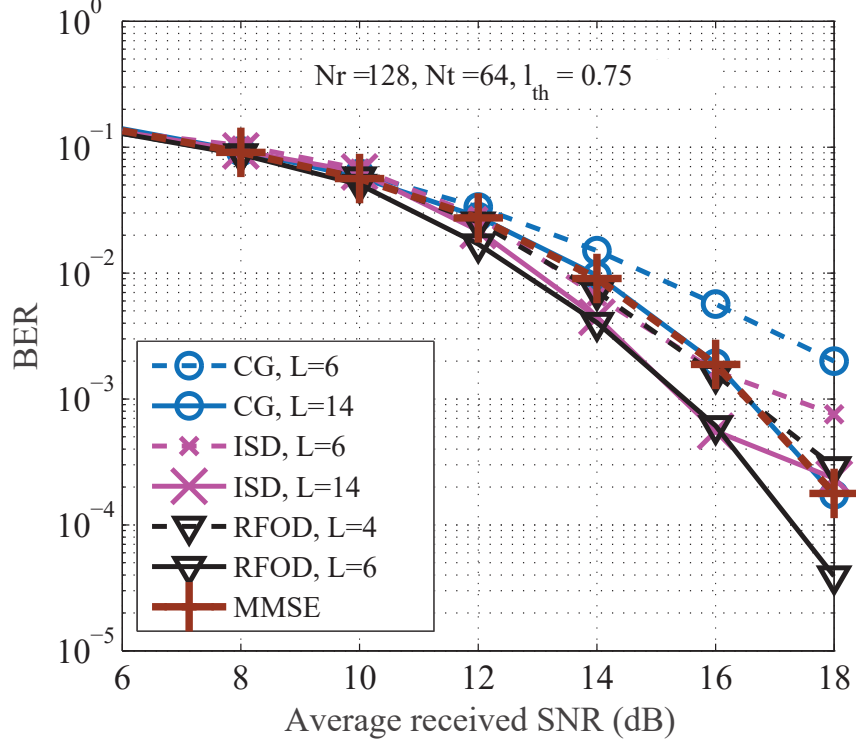


Figure 4.4: BER performance comparison for 128×64 mMIMO system with increased number of iterations.

quires 3.98×10^5 FLOPs for 128×64 and 5.31×10^5 FLOPs for 128×74 mMIMO system.

However, as shown in Fig. 4.6, CG requires $L = 14$ to achieve near-MMSE performance and consumes 7.5×10^4 more FLOPs as compared to the RFOD algorithm (with $L = 6$) for 128×64 mMIMO systems. On the other hand, CG requires 10^5 more FLOPs for 128×74 mMIMO system than RFOD (with $L = 6$) as depicted in Fig. 4.6. In Fig. 4.6, ISD with $L = 14$ requires 6.7×10^4 more FLOPs than RFOD (with $L = 6$) for 128×64 mMIMO systems. Furthermore, ISD at $L = 14$ consumes 9×10^4 more FLOPs as compared to RFOD at $L = 6$ for 128×74 mMIMO systems. Nevertheless, for both 128×64 and 128×74 mMIMO systems, ISD yields inferior performance than RFOD. Moreover, the performance of RFOD improves with the number of

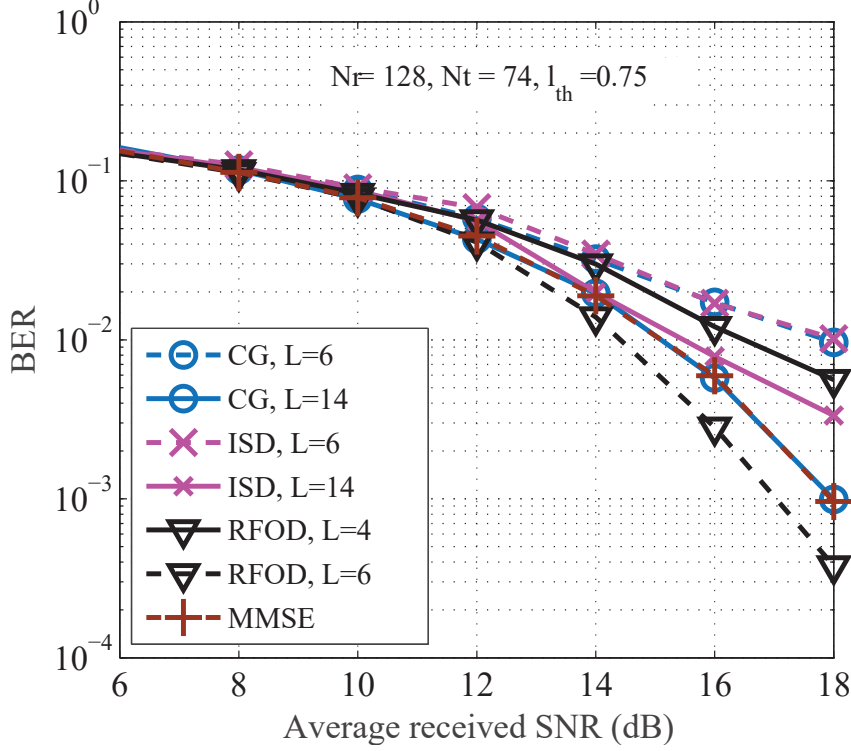


Figure 4.5: BER performance comparison for 128×74 mMIMO system with increased number of iterations.

iterations L . However, CG and ISD do not show significant improvement in BER after $L = 14$. Hence, from Figs. 4.6-4.7, the superiority of RFOD over RI, CG, JSDJI and ISD is again validated for both BER and computational complexity in terms of the number of FLOPs.

Influence of reliability feedback and quality ordering on BER performance:

Fig. 4.8 illustrates the effect of the proposed QO and RFM on detection, which are consequences of equations (4.8) and (4.22) respectively. Fig. 4.9 depicts that BER performance of RFOD improves with initial solutions. However, as depicted in Fig. 4.9, the RFOD algorithm even initialized with zero initial solution outperforms ISD with $\mathbf{x}^{(0)} = \mathbf{D}^{-1}\mathbf{b}$. Furthermore, SNR gain of approximately 1.7 dB is achieved in RFOD (initialized with zero initial solution) as compared to ISD (with $\mathbf{x}^{(0)} = \mathbf{D}^{-1}\mathbf{b}$) for a targeted BER of

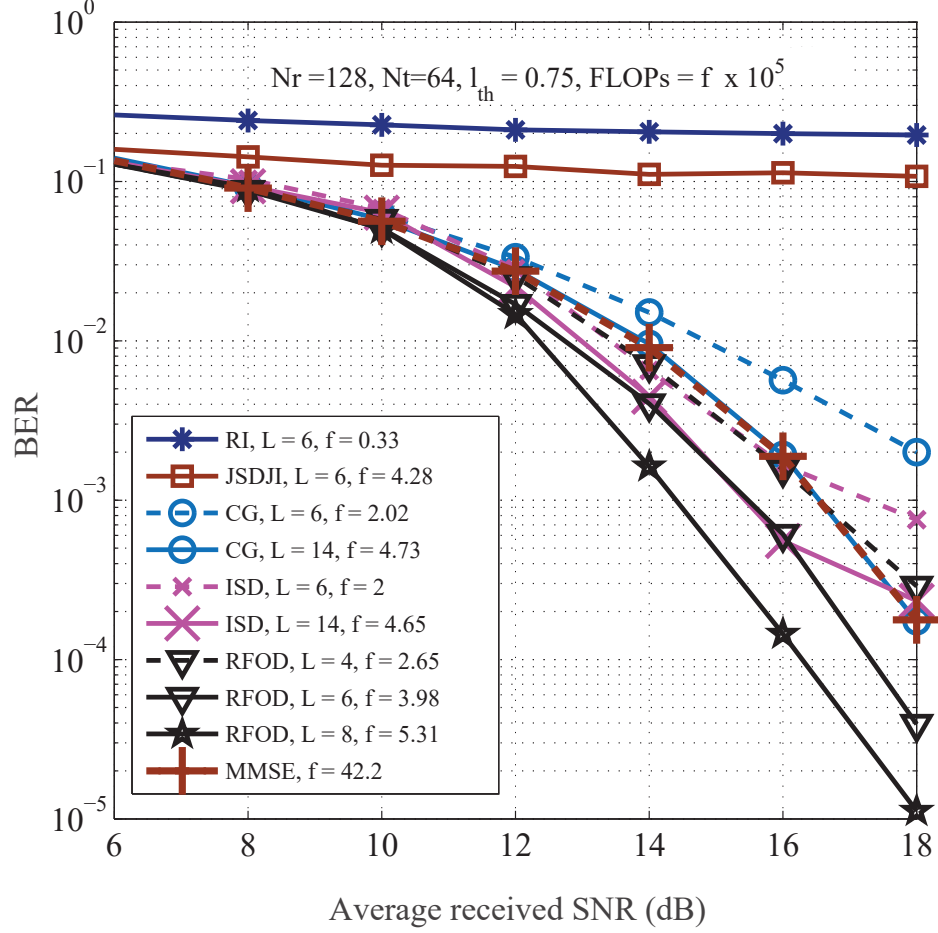


Figure 4.6: BER performance comparison for 128×64 mMIMO system with approximately equal number of FLOPs.

10^{-2} . Hence, it confirms viability of RFOD over ISD.

4.7 Complexity analysis

In this section, the computational complexity of various mMIMO detection techniques are compared in terms of both real-valued operations and FLOPs [74]. Both Table 4.1 and Table 4.2 compare the computational complexity of RFOD with other contending mMIMO detection algorithms [8, 38, 39,

Detectors	Multiplications	Additions
RI [65]	$4LNt^2 + 2LNt$	$4LNt^2 + 2LNt$
CG [39]	$4LNt^2 + 2LNt$	$4LNt^2 + 6LNt$
JSDJI [38]	$4(L+1)Nt^2 + 2(L+4)Nt$	$4LNt^2 + 4LNt$
ISD [8]	$4LNt^2 + 2(2L+1)Nt$	$4LNt^2 + 2LNt$
RFOD	$4(L+1)Nt^2 + 2(3L+1)Nt$	$4(L+1)Nt^2 + 6LNt$

Table 4.1: Number of real-valued operations required for detection.

	(Nr,Nt,L)	FLOPs ($\times 10^5$)	BER at SNR=20dB
RI [65]	(128,64,6)	0.33	1.95×10^{-1}
	(128,74,6)	0.44	2.74×10^{-1}
JSDJI [38]	(128,64,6)	4.28	1.07×10^{-1}
	(128,74,6)	5.72	2.24×10^{-1}
CG [39]	(128,64,14)	4.73	1.77×10^{-4}
	(128,74,14)	6.30	9.62×10^{-4}
ISD [8]	(128,64,14)	4.65	2.34×10^{-4}
	(128,74,14)	6.21	3.34×10^{-4}
RFOD	(128,64,6)	3.98	3.92×10^{-5}
	(128,74,6)	5.31	1.24×10^{-4}

Table 4.2: Average number of FLOPs ($\times 10^5$) required for detection.

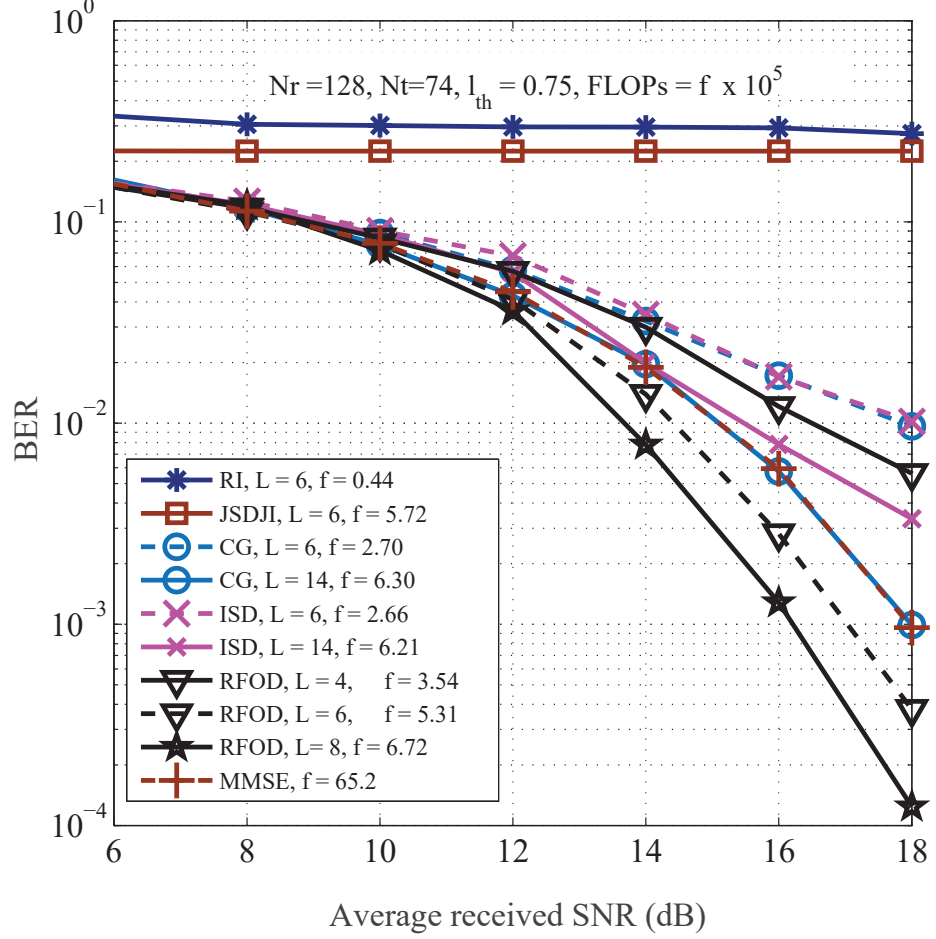


Figure 4.7: BER performance comparison for 128×74 mMIMO system with approximately equal number of FLOPs.

65]. However, the computational complexities in Table 4.1 are computed in terms of real valued multiplications and additions. On the other hand, the computational complexities in Table 4.2 are computed in terms of the number of FLOPs. Since the initial parameters like \mathbf{G} , \mathbf{A} , \mathbf{W} , \mathbf{W}^{-1} and \mathbf{b} are similar in all contending detection algorithms mentioned in this section, the number of real valued operations as well as FLOPs for calculating those initial parameters are neglected, while comparing the computational complexities. The values of real valued multiplication and real-valued additions given in

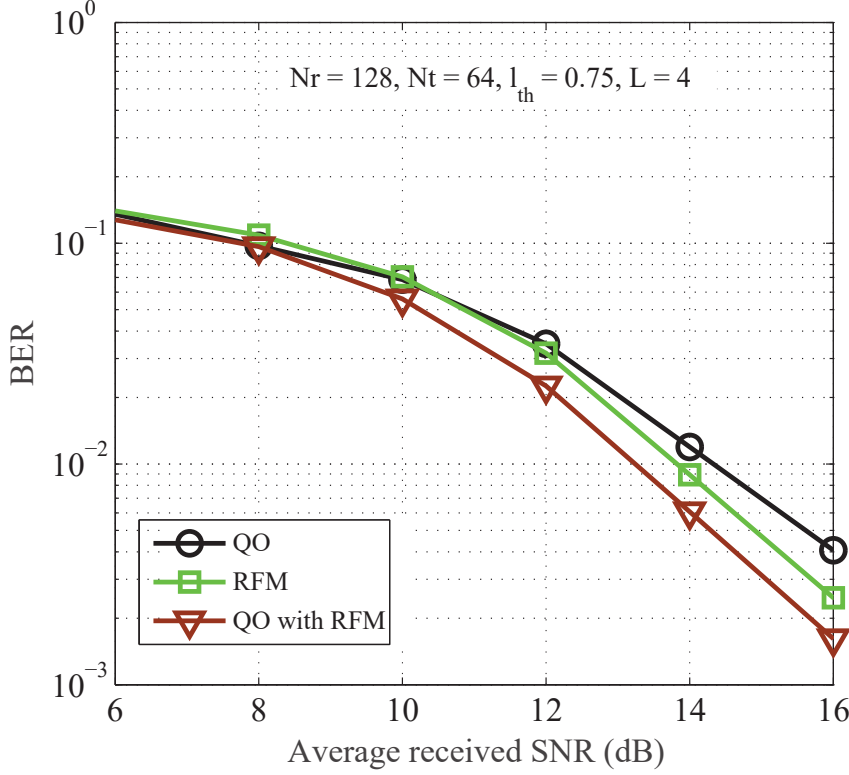


Figure 4.8: Effect of initial solution, reliability feedback and quality ordering on the BER performance of RFOD.

Table 4.1 for other contending algorithms are taken from their respective articles on symbol detection in mMIMO systems [8, 38, 39, 65]. However, the values for RFOD algorithm are computed from Algorithm 4.1 as shown in Table 4.3 [75]. In lines 12-14 of Table 4.3, m is the number of multiplications during m^{th} symbol update. Furthermore, the computations in lines 1-3 are ignored as these steps are common in all contending detection algorithms.

In order to further verify the computational efficiency of RFOD, the computational complexities of contending mMIMO detection techniques are also compared in terms of the number of FLOPs [58] in Table 4.2. The values given in Table 4.2 are computed using "FLOPs()" function available in the linear equations software package (LINPACK) software library [76]. It must be noted from both Table 4.1 and Table 4.2 that RFOD requires less

4.7. COMPLEXITY ANALYSIS

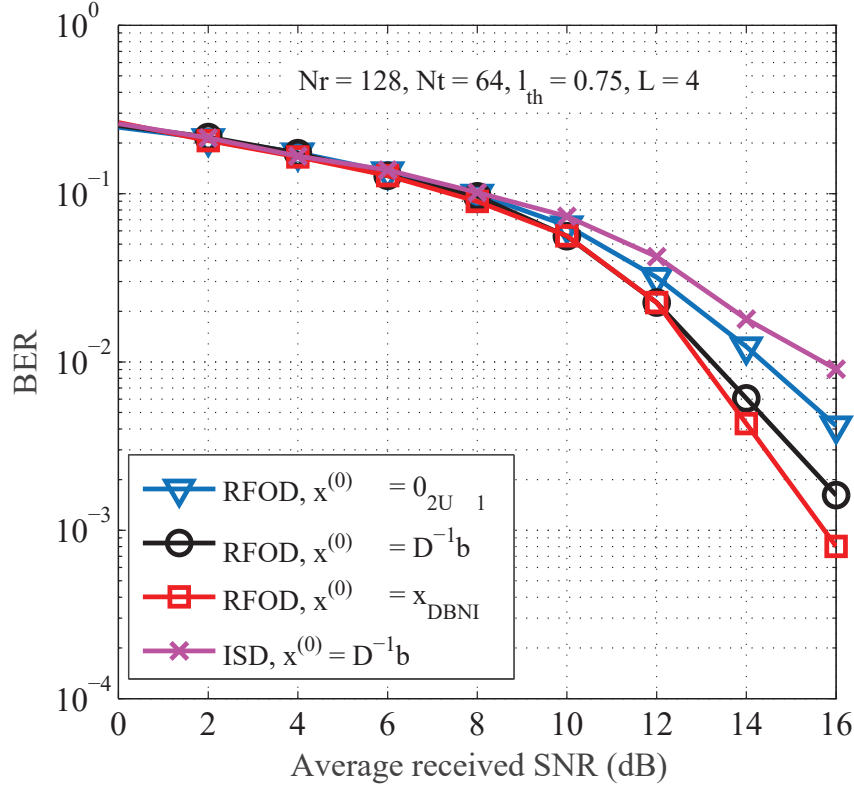


Figure 4.9: BER performance comparison for 128×64 mMIMO system with different initial solution.

Line Nos	No of multiplications	No of additions
1 – 3	Ignored	Ignored
4	$2Nt$	0
5-7	$2Nt \times 2Nt = 4Nt^2$	$((2Nt - 1) + 1) \times 2Nt = 4Nt^2$
8	0	0
9-11	$2NtL$	0
12-14	$((2Nt - m) + (m - 1)) \times 2Nt + 4Nt)L = 4Nt^2L + 2NtL$	$((2Nt - 1) \times 2Nt + 2Nt)L = 4Nt^2L$
15-20	0	$2NtL$
21	$2NtL$	$4NtL$
Total	$4(L + 1)Nt^2 + 2(3L + 1)Nt$	$4(L + 1)Nt^2 + 6LNt$

Table 4.3: Real valued operations.

computational complexity to yield significant BER improvement over other contending mMIMO detection algorithms.

4.8 Summary

In this Chapter, the RFOD algorithm is proposed for low-complexity symbol detection in mMIMO systems with a large number of users. In RFOD, an initial symbol estimate is iteratively refined in an ordered sequence obtained through QO, followed by reliability feedback aided detection of each symbol. While detecting a symbol, QO mitigates interference from other users, and RFM helps in improving the reliability of the detected symbol. Thus, the error propagation reduces, thereby resulting in enhanced BER performance. Simulation results validate the superiority of RFOD over recent state-of-the-art mMIMO detection algorithms in terms of both the BER performance as well as the computational complexity.

In Chapters 2 to 4, the symbol detection problem in uplink mMIMO is solved using model-driven approaches, where AMI and/or MII based techniques are utilized. Hence, the algorithms proposed in these chapters are not capable of learning high-level features from given data and constrained to provide fixed performance based on the inherent predefined mathematical model. In the next Chapter, a data-driven DL model is proposed for symbol detection in uplink mMIMO systems to circumvent these drawbacks of conventional iterative detection algorithms.

Chapter 5

Deep Unfolded Sparse Refinement Network Based Detection

5.1 Introduction

The promising detection techniques proposed in previous Chapters are based on specific mathematical models and have limitations in translating the theory into practical models. The complex signal processing involved in those algorithms may preclude the low latency requirement while achieving high BER performance in mMIMO systems. Those conventional algorithms are not data-driven approaches and cannot learn the interrelations of parameters where mathematical models of communication scenarios cannot be readily described. DL techniques can deliver high-quality results with maximum utilization of data, thereby drawing enormous attention from companies and international organizations such as the International communication union (ITU), Huawei and Qualcomm [77][78].

In this Chapter, a low complexity SRN based detection model is proposed for uplink mMIMO systems. SRN is designed by unfolding the conventional JI [40]. The computational complexity of SRN based symbol detection is

reduced by masking some 'unimportant' network connections of a , leading to a sparsely connected deep unfolded model. The theoretical convergence of SRN is analyzed, which is further validated through simulations. SRN's performance is compared with the state-of-the-art mMIMO detectors measured on BER performance and computational complexity.

The following terminology is used in this Chapter. α denotes the masking ratio. $\rho(\cdot)$ refers to the activation function. L is the number of hidden layers/iterations. μ denotes the step size. \mathcal{P}_e implies the probability of error. $\gamma(\cdot)$ refers to Fisher information.

The Chapter is organized as follows. SRN and symbol detection in SRN are discussed in Section 5.2. Convergence of SRN is performed in Section 5.3. Complexity analysis of SRN based symbol detection is performed in Section 5.4. Simulation results are drawn in Section 5.5. Finally, the summary is outlined in Section 5.6.

5.2 Network Model and Symbol Detection

This section briefly describes the proposed detection model for uplink mMIMO systems utilizing SRN.

5.2.1 Deep unfolded refinement network

The SRN architecture proposed for low complexity symbol detection in uplink mMIMO systems is a model-driven network, and is developed by deep unfolding of conventional JI [40]. JI is expressed as

$$\mathbf{x}^{(k+1)} = \mathbf{x}^{(k)} + \mathbf{D}^{-1}(\mathbf{b} - \mathbf{A}\mathbf{x}^{(k)}), \quad (5.1)$$

Each iteration of JI is a linear combination of $\mathbf{D}^{-1}\mathbf{G}$, $\mathbf{H}^T\mathbf{y}$ and $\mathbf{D}^{-1}\mathbf{H}^T$. To develop a detection network unfolding JI, the crucial components are $\mathbf{D}^{-1}\mathbf{G}$, $\mathbf{H}^T\mathbf{y}$ and $\mathbf{D}^{-1}\mathbf{H}^T$. Therefore, to achieve substantive performance

improvements with DL, the crucial components of JI are mapped to a higher-dimensional space, and standard nonlinearities are applied.

$$\mathbf{x}^{(k)} = \rho\left(\omega_1 \mathbf{D}^{-1} \mathbf{H}^T \mathbf{y} + \omega_2 \mathbf{D}^{-1} \mathbf{H}^T \mathbf{y} + \beta_1\right) \quad (5.2)$$

$$\mathbf{x}^{(k+2)} = \rho\left(\omega_3 \mathbf{D}^{-1} \mathbf{G} + (1 - t_k) \mathbf{x}^{(k+1)} + t_k \mathbf{x}^{(k)} + \beta_2\right), \quad (5.3)$$

where $0 < t_k < 1$. The proposed JI driven DL architecture utilizes an IDN (Fig. 5.1), which takes \mathbf{y} , \mathbf{H} and \mathbf{D}^{-1} as input and yields an estimation $\hat{\mathbf{x}}$. The estimate is later refined using multiple layers of RDN, where each hidden layer of RDN is represented as Fig. 5.2. Hence, trainable parameters of the proposed network are $\theta = \{\omega_1, \omega_2, \omega_3, \beta_1, \beta_2\}_{k=1}^L$.

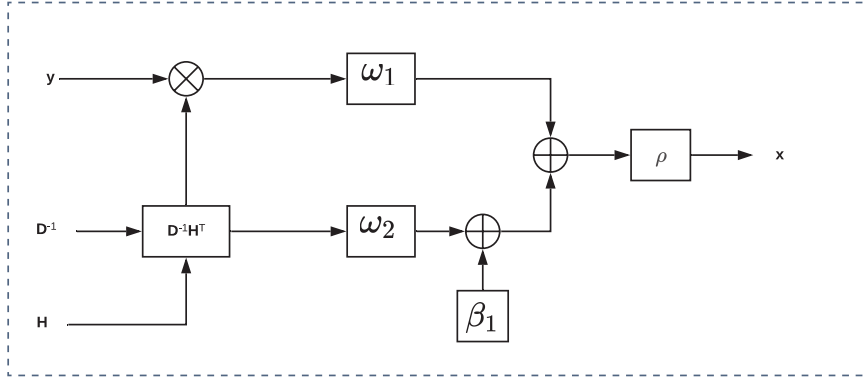


Figure 5.1: A hidden layer of IDN.

5.2.2 Sparsely connected refinement network

Detection networks are not considered fully connected to improve accuracy and reduce the models' computational complexity. A mask matrix ζ is considered that disables insignificant connections based on the masking ratio α , leading to a sparse network (Fig. 5.3). The sparse weight matrix ω_i is computed as

$$\omega_{si} = \omega_i \cdot \zeta \quad (5.4)$$

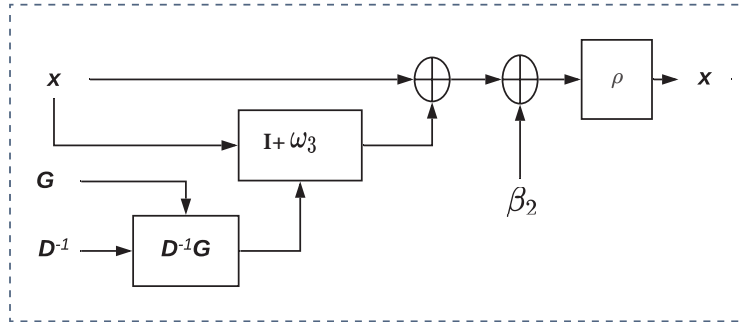


Figure 5.2: A hidden layer of RDN.

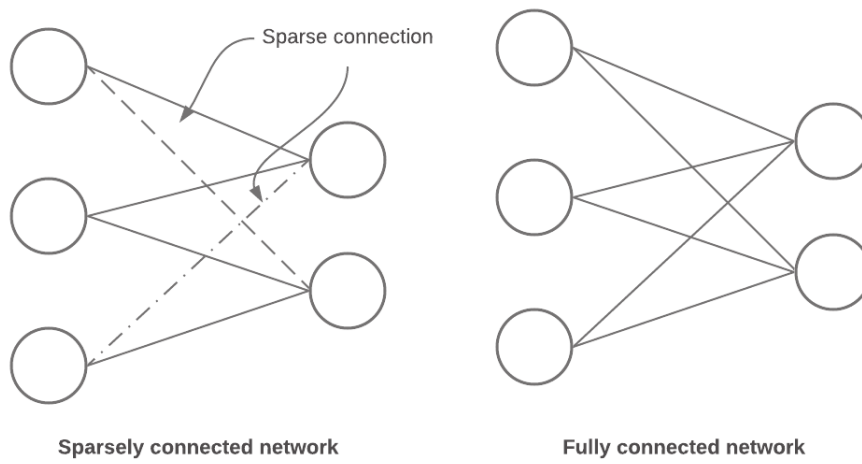


Figure 5.3: Differences between sparsely and fully connected networks.

where $\zeta_{m,n} \in \{0, 1\}$. Sparsely connected IDN and RDN models are expressed as

$$\mathbf{x}^{(k)} = \rho\left(\omega_{s1}\mathbf{D}^{-1}\mathbf{H}^T\mathbf{y} + \omega_{s1}\mathbf{D}^{-1}\mathbf{H}^T\mathbf{y} + \beta_1\right) \quad (5.5)$$

$$\mathbf{x}^{(k+2)} = \rho\left(\omega_{s3}\mathbf{D}^{-1}\mathbf{G} + (1 - t_k)\mathbf{x}^{(k+1)} + t_k\mathbf{x}^{(k)} + \beta_2\right) \quad (5.6)$$

The forward propagation and backward propagation derivatives are computed with respect to the sparse weight matrix ω_{si} . For convenience, the subscript s is discarded in the rest of the Chapter.

5.2.3 Symbol detection

IDN and RDN are available for use in the BS after an initial training phase. During the training phase, the networks are trained on all sets of potential constellations of the mMIMO system under study. Since the network considers CSI and the received symbol vector to be input parameters, it may also be deployed in a variety of CSI scenarios at BS. The theoretical upper bound on BER of the proposed detection technique can be stated as [60]

$$\begin{aligned} \mathcal{P}_e &\leq \frac{1}{\pi} \int_0^{\pi/2} \mathcal{Y}_\gamma\left(-\frac{\kappa^2}{2\sin^2\theta}\right) d\theta \\ &\leq c {}_2F_1\left(1, N_r + \frac{1}{2}; N_r + 1; \frac{N_r}{N_r + \kappa^2\tilde{\gamma}}\right), \end{aligned}$$

where $c = \frac{\sqrt{\kappa}\Gamma(N_r + \frac{1}{2})}{2\sqrt{\pi}(1+\kappa)^{m+\frac{1}{2}}\Gamma(N_r+1)}$. ${}_2F_1(\cdot, \cdot; \cdot; \cdot)$ refers to hypergeometric function, N_r is the number of receive antennas and κ is a modulation dependent parameter.

5.3 Convergence analysis

In this section, the convergence behaviour of SRN is analyzed theoretically. SRN consists of a single layer of IDN, followed by multilayer RDNs. The training of SRN involves two stages of propagation, namely forward and

5.3. CONVERGENCE ANALYSIS

backward propagations. Assume an error exists in the estimated symbol vector received from IDN. This estimated erroneous symbol vector $\hat{\mathbf{x}}$ is fed to the RDN. The RDN absorbs the erroneous input $\hat{\mathbf{x}}$ and tries to minimize the cost function $\psi(\hat{\mathbf{x}}, \mathbf{x})$ in the mean square sense. In forward propagation, $\hat{\mathbf{x}}$ is projected into an affine set defined by the bias β_2 and weight ω_3 of the RDN. The operations done in the forward propagation phase are expressed as

$$\hat{\mathbf{x}}^{(0)} = \rho\left(\omega_1 \mathbf{D}^{-1} \mathbf{H}^T \mathbf{y} + \omega_2 \mathbf{D}^{-1} \mathbf{H}^T \mathbf{y} + \beta_1\right) \quad (5.7)$$

$$\hat{\mathbf{z}}^{(k)} = \omega_3 \mathbf{D}^{-1} \mathbf{G} + (1 - t_k) \hat{\mathbf{x}}^{(k)} + t_k \hat{\mathbf{x}}^{(k-1)} + \beta_2 \quad (5.8)$$

$$\hat{\mathbf{x}}^{(k)} = \rho(\hat{\mathbf{z}}^{(k)}) \quad (5.9)$$

Once the output error is calculated, it is propagated through RDN to optimize the network parameters responsible for the error. Back-propagating operations are written as

$$\begin{aligned} \nabla_{\mathbf{z}^{(k)}} \psi(\hat{\mathbf{x}}, \mathbf{x}) &= \nabla_{\mathbf{x}^{(k)}} \psi(\hat{\mathbf{x}}, \mathbf{x}) \nabla_{\mathbf{x}^{(k)}} \mathbf{z}_k \\ \nabla_{\mathbf{x}^{(k-1)}} \psi(\hat{\mathbf{x}}, \mathbf{x}) &= \nabla_{\mathbf{z}^{(k)}} \psi(\hat{\mathbf{x}}, \mathbf{x}) \omega_{\mathbf{i}}^{(k)} \\ \nabla_{\omega^{(k)}} \psi(\hat{\mathbf{x}}, \mathbf{x}) &= \mathbf{y}^{(k-1)} \nabla_{\mathbf{z}^{(k)}} \psi(\hat{\mathbf{x}}, \mathbf{x}) \\ \nabla_{\beta_{\mathbf{i}}^{(k)}} \psi(\hat{\mathbf{x}}, \mathbf{x}) &= \nabla_{\mathbf{z}^{(k)}} \psi(\hat{\mathbf{x}}, \mathbf{x}), \end{aligned} \quad (5.10)$$

where $\nabla_{\mathbf{z}^{(k)}} \psi(\hat{\mathbf{x}}, \mathbf{x})$ denotes the gradient of $\psi(\hat{\mathbf{x}}, \mathbf{x})$ with respect to $\mathbf{z}^{(k)}$. Finally, the weights and biases are updated as follows.

$$\begin{aligned} \omega_i^{(k)} &= \omega_{\mathbf{i}}^{(k)} - \mu^{(k)} \nabla_{\omega_{\mathbf{i}}^{(k)}} \psi(\hat{\mathbf{x}}, \mathbf{x}) \\ \beta_{\mathbf{i}}^{(k)} &= \beta_{\mathbf{i}}^{(k)} - \mu^{(k)} \nabla_{\beta_{\mathbf{i}}^{(k)}} \psi(\hat{\mathbf{x}}, \mathbf{x}) \end{aligned} \quad (5.11)$$

Since $\psi(\hat{\mathbf{x}}, \mathbf{x})$ is non-negative; it can be shown to be bounded from below

$$\mathbb{E}(\mathbf{x} - \hat{\mathbf{x}})^2 \geq \frac{(\mathbf{I} + \tilde{\delta}_{\mathbf{x}}^{(k)})}{\gamma(\mathbf{x})} + \beta(\mathbf{x})^2 \quad (5.12)$$

$\tilde{\delta}_{\mathbf{x}} = \frac{\Delta\beta}{\Delta\mathbf{x}}$. In addition, it can also be shown that $\psi(\hat{\mathbf{x}}, \mathbf{x})$ is Lipschitz continuous.

$$\| \psi(\hat{\mathbf{x}}_1, \mathbf{x}_1) - \psi(\hat{\mathbf{x}}_2, \mathbf{x}_2) \|_2 \leq \| \psi(\hat{\mathbf{c}}, \mathbf{c}) \|_2 \| \mathbf{x}_1 - \mathbf{x}_2 \|_2,$$

where $\mathbf{x}_1 \leq \mathbf{c} \leq \mathbf{x}_2$. As $\psi(\hat{\mathbf{x}}, \mathbf{x})$ is Lipschitz continuous, it is obvious that $\nabla_{\mathbf{W}_k} \psi(\hat{\mathbf{x}}, \mathbf{x})$ and $\nabla_{\mathbf{b}_k} \psi(\hat{\mathbf{x}}, \mathbf{x})$ are bounded on \mathbf{W} and \mathbf{b} respectively. Accordingly, it is concluded that RDN converges if the following condition holds [79].

$$\sum_{k=0}^{\infty} \mu^{(k)} = \infty, \quad \sum_{k=0}^{\infty} (\mu^{(k)})^2 < \infty, \quad 0 < \mu^{(k)} \leq 1 \quad (5.13)$$

Consequently, RDN is able to refine the erroneous estimation of $\hat{\mathbf{x}}$. Hence, it concludes that

$$\| \mathbf{I} - \omega_3 \mathbf{D}^{-1} \mathbf{G} \| \leq 1 \quad (5.14)$$

This proves the convergence of SRN.

5.3. CONVERGENCE ANALYSIS

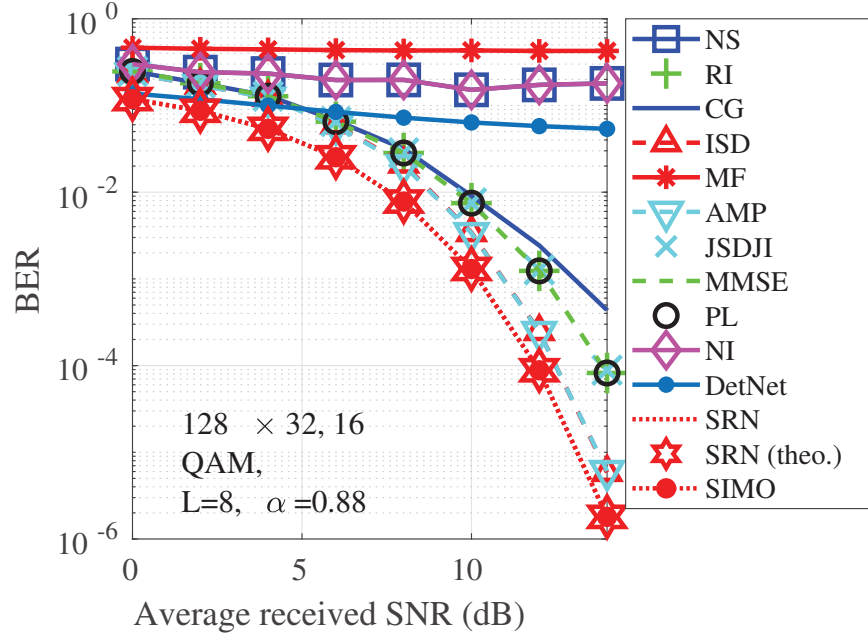


Figure 5.4: Comparison of BER performances of SRN with other contending algorithms for 128×32 massive MIMO system with 16 QAM modulation.

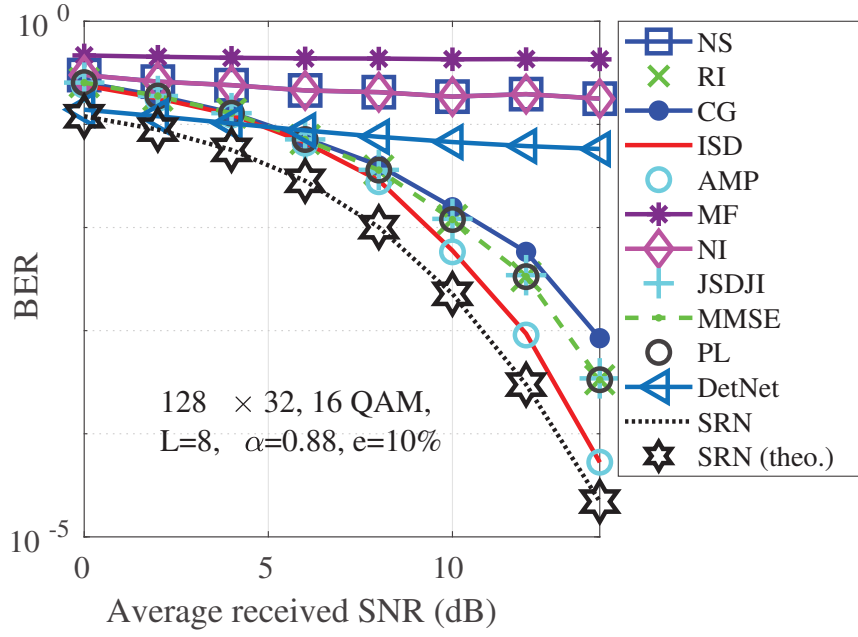


Figure 5.5: Comparison of BER performance of SRN with other contending algorithms for 128×32 massive MIMO system with channel estimation error $e = 10\%$ at the BS.

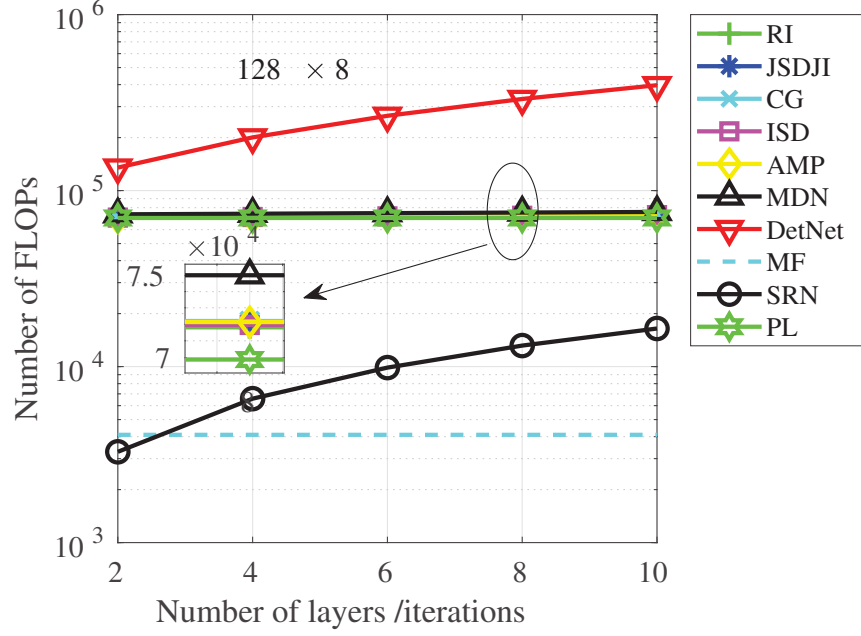


Figure 5.6: Comparison of computational complexity of SRN with other contending algorithms for different number of hidden layers / iterations with $N_t = 8$.

5.4 Complexity analysis

This section compares the computational complexity of SRN with other competing algorithms. Computational complexities of contending algorithms are shown in Fig. 5.6 in terms of FLOPs. It demonstrates that single layer of SRN is computationally more efficient compared to other contending algorithms.

5.5 Simulation results

In this section, SRN's performance is compared with several top-of-the-line detection techniques in terms of BER and computational complexity.

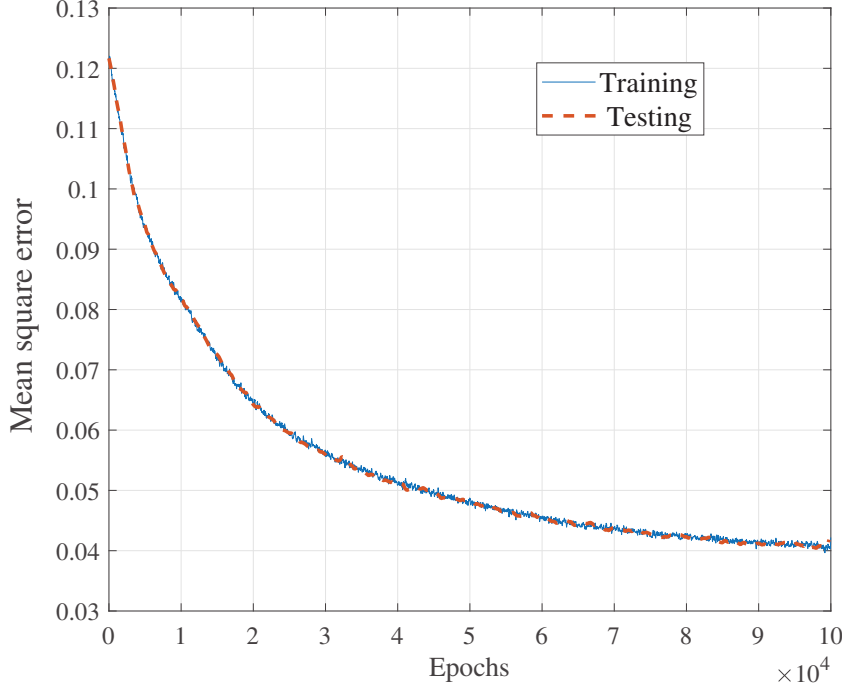


Figure 5.7: Learning curves of SRN.

5.5.1 Learning curves

Learning curves play a crucial role in diagnosing the performance of DL models. Learning curves of SRN are shown in Fig. 5.7. During the training phase, SRN yields an mean square error (MSE) loss of 4×10^{-2} with epochs of 9×10^4 . The ratio of training and test data is kept at 9 : 1, and Adam optimizer is used to optimize parameters. The best activation function (ρ) for SRN is the hyperbolic tangent. Real valued data are given directly to the network for training and testing, rather than using encoding techniques. As depicted in Fig. 5.7, the training and testing curves decrease towards the point of stability. Test curves are consistent with the training loss curves, indicating successful training of the network. Moreover, the difference between the training and testing loss is minimal. It implies that this learning curve plot shows a good fit, and the model has successfully optimized its

parameters with the given dataset.

5.5.2 BER performance

This subsection compares the BER performance of SRN with other contending detection algorithms.

In Fig. 5.4, the BER performance of the proposed SRN is compared with MMSE and DL-based algorithms and other state-of-the-art iterative detection algorithms for uplink massive MIMO systems. As depicted in Fig. 5.6, the computational complexity of a single layer of SRN is much less than the other contending iterative and DL based algorithms. Hence, for a fair comparison, we have chosen $L = 8$ for SRN and $L = 6$ for other contending algorithms. However, the proposed SRN with $L = 8$ exhibits at least 2.5×10^4 less computational complexity than other algorithms with $L = 6$. It is observed from Fig. 5.4 that the proposed SRN even with comparatively less computational complexity, provides an SNR gain of .7 dB over ISD and AMP for a targeted BER of 10^{-5} . Other contending algorithms have far inferior BER performance as compared to ISD and AMP. It proves superiority of the proposed SRN for low complexity symbol detection in uplink massive MIMO systems.

As depicted in Fig. 5.5, the proposed SRN outperforms several state-of-the-art algorithms for uplink symbol detection in a massive MIMO system. In a 128×32 massive MIMO system, proposed SRN even with $e = 10\%$ channel estimation error at the BS, yields and SNR gain of 0.7 dB over ISD for a targeted BER of 1.2×10^{-4} . The other contending algorithms shows far degraded BER performance as compared to SRN. It proves the robustness of SRN for symbol detection in uplink massive MIMO systems.

As depicted in Fig. 5.8, SRN exhibits a performance complexity trade-off. The performance of SNR improves with the number of hidden layers. However, computational complexity in symbol detection using SNR increases as the number of hidden layers increases.

Fig. 5.9 indicates the effect of parameter α in SRN. It is observed that

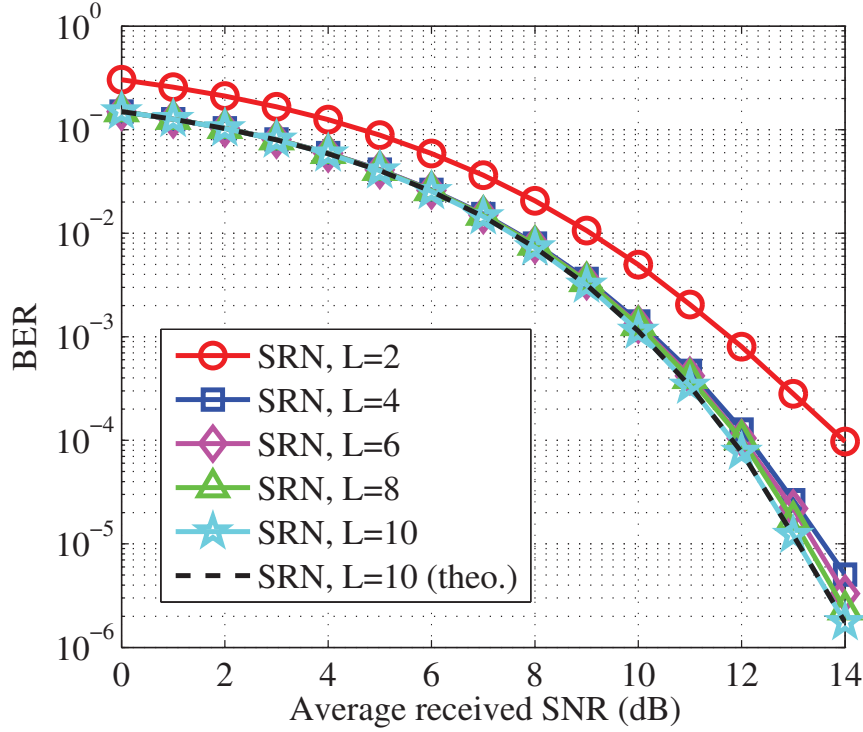


Figure 5.8: Comparison of BER performances of SRN with different number of hidden layers.

masking too many parameters leads to performance degradation in SRN. However, SRN shows significant performance improvement compared to unmasked SRN if the masking ratio, $\alpha \leq 0.5$. Therefore, the SRN uses significantly fewer trainable parameters, which results in an improved detection model compared to DetNet. It is found that SRN with $\alpha = 0.5$ utilizes 6×10^4 less parameters compared to DetNet for the same number of hidden layers $L = 30$.

5.6 Summary

In this Chapter, SRN based detection is proposed for uplink mMIMO. SRN prunes the insignificant parameters during training, giving a less complex detection network. The network can also fine-tune an initial estimate of the

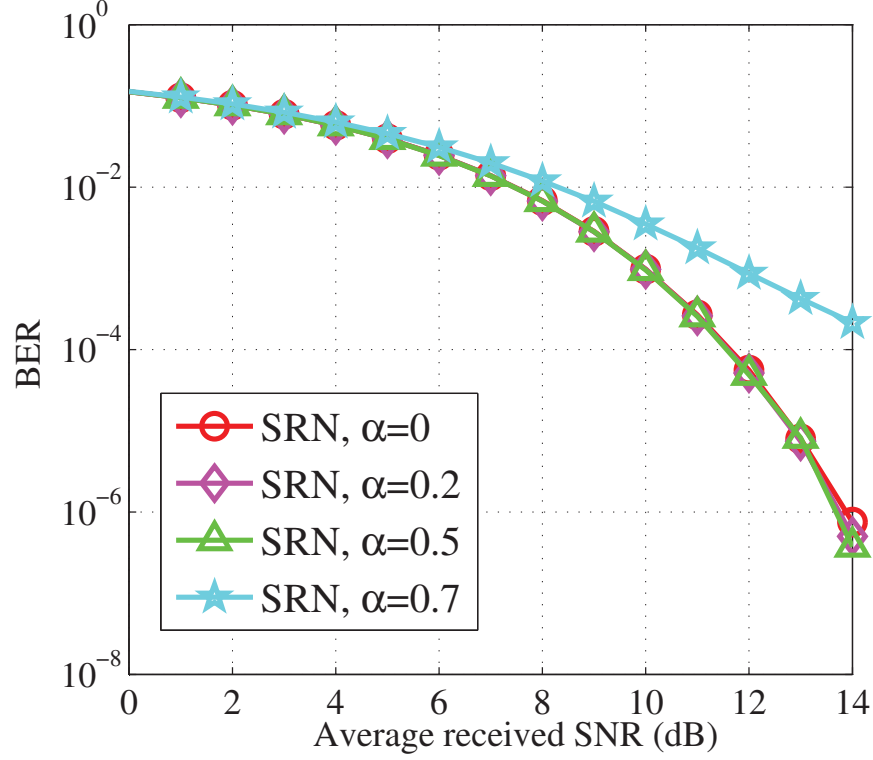


Figure 5.9: Comparison of BER performances of SRN with different values of masking ratio.

transmit symbol vector of mMIMO. Simulations are carried out to compare the performance of SRN with state-of-the-art mMIMO detection techniques measured on computational complexity and BER performance. The convergence characteristic of SRN is analysed, and the simulations are substantiated by a derived upper bound on the error performance. Simulation results validate the viability of SRN against several detection techniques for symbol detection in uplink mMIMO systems.

Chapters 3 to 5 essentially address the detection of symbols in mMIMO systems. In mMIMO, multiplexing gain limits the supreme diversity because of the diversity multiplexing tradeoff, and depends on the rank of the channel matrix. One cost-effective technique for further enhancing the spectral efficiency of the mMIMO system is the incorporation of MBM into the

CHAPTER 5. DEEP UNFOLDED SPARSE REFINEMENT NETWORK BASED DETECTION

mMIMO. Hence, the problem of symbol detection in the MBM-mMIMO system is investigated in the following Chapters, and appropriate low-complexity detection algorithms, SID, MEPD and MEPDRS, are proposed.

Chapter 6

Detection Algorithms for Uplink MBM-mMIMO Systems

6.1 Introduction

In the previous Chapters, mMIMO systems are taken into account, which provides high spectral efficiency in comparison with SISO systems. In the case of a static fading channel, diversity in an mMIMO system is achieved at the expense of the reduction in spectral efficiency due to the diversity-multiplexing trade-off. The spectral efficiency of the mMIMO system is further enhanced when integrated with the MBM [47–49].

MBM [80] is a novel modulation technique that places multiple RF mirrors near the transmit antennas in a rich scattering environment and creates different channel fade realizations. In MBM, the set of indices of RF mirrors corresponding to the different possible channel fade realizations is called the channel modulation alphabet. The set of information bits to be transmitted is divided into two parts; one corresponding to the channel modulation alphabet and the other corresponding to the conventional modulation alphabet. If N_{RF} is the number of RF mirrors and \mathcal{A} is the conventional modulation alphabet, the spectral efficiency of single-user MBM is $N_{RF} + \log_2 \#\mathcal{A}$ bits per channel use. MBM has the inherent diversity in dealing with slow fading. It

is a promising candidate for a rich scattering multipath fading environment to yield high-speed data communication beyond 5G and 6G wireless communications without demanding excess transmit energy and resources. Though being limited to low mobility or static communication scenarios, MBM with N_r receiver antennas over a static multipath channel is capable of asymptotically achieving the channel capacity of N_r parallel AWGN channels [5].

In the previous Chapters, symbol detection in mMIMO systems with conventional modulation techniques is explored. However, algorithms proposed in the preceding Chapters fail to detect the sparse transmit symbol vectors in MBM-mMIMO systems. In this Chapter, symbol detection in MBM-mMIMO is analyzed and modelled as a graph traversing problem. A graph-traversal aided low-complexity symbol detection algorithm is proposed inspired by socio-cognitive learning of swarm optimization.

The following terminology is used in this Chapter. $h_{j,i,k}$ denotes the element in the i^{th} row and the k^{th} column of the sub-matrix \mathbf{H}_j . $\mathbf{h}_{j,k}$ denotes the k^{th} column of \mathbf{H}_j . \mathbf{H}_j refers to the matrix corresponding to the j^{th} user. $x_{j,i}$ refers to the i^{th} element of \mathbf{x}_j . \mathcal{W} denotes the moment generating function (MGF). x_{j,l_1} refers to the l_1^{th} non-zero element of \mathbf{x}_j . $\mathbb{E}(\cdot)$ denotes the expectation operator. κ_1 and κ_2 respectively, refer to the Lagrangian multiplier and the step size. $\mathbb{P}_{\mathcal{M}}(\cdot)$ denotes projection onto a set \mathcal{M} . $\mathcal{D}(\cdot, \cdot)$ is the Hamming distance operator.

The Chapter is organized as follows: System model of MBM-mMIMO is presented in Section 6.2. Section 6.4.1 specifies the initialization requirements for SID. SID algorithm is discussed in Section 6.4.2. Minim error pursuit algorithm is proposed in Section 6.5. Finally, Section ?? summarizes the Chapter.

6.2 System Model of MBM-mMIMO

The system model of MBM-mMIMO is briefly explained in this section. An uplink MBM-mMIMO system model is considered with N_r BS antennas and

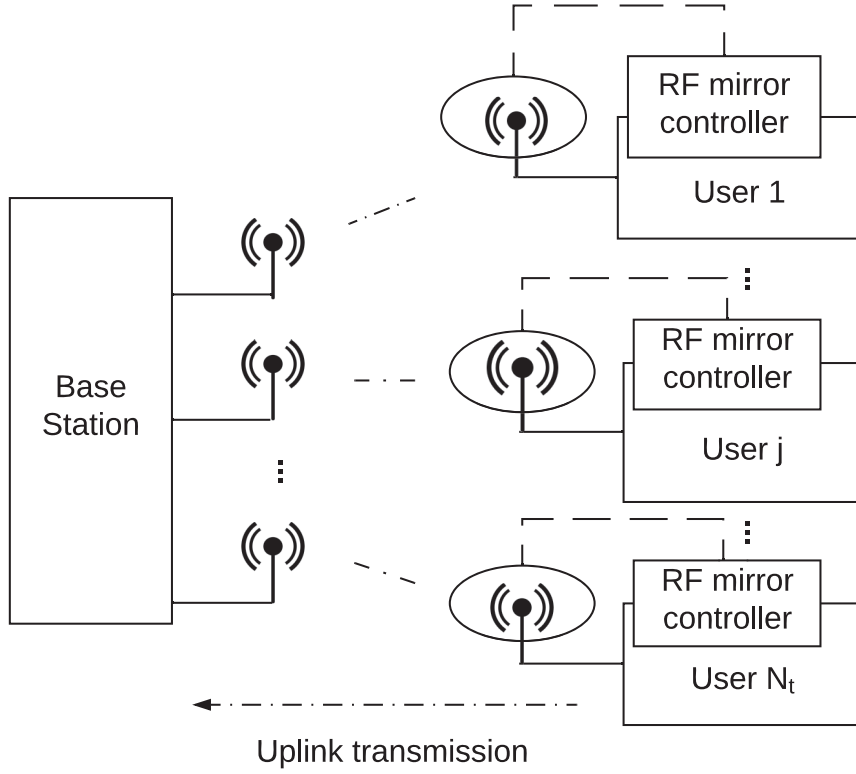


Figure 6.1: MBM-mMIMO system model.

N_t single antenna users with N_{RF} RF mirrors placed before each transmit antenna (Fig. 6.1). After demodulation and sampling, the received symbol vector \mathbf{y} at the BS is expressed as¹ [47, 48]

$$\mathbf{y} = \sum_{j=1}^{N_t} \mathbf{H}_j \mathbf{x}_j + \mathbf{n}, \quad (6.1)$$

¹In mMIMO and large MIMO systems (system model (1.1) of Chapter 1), each user transmits a symbol from the QAM constellation set \mathcal{A} . However, in MBM-mMIMO, a single RF mirror creates multiple channel realizations before each transmit antenna. Hence, each user transmits a sparse vector corresponding to the MBM constellation set \mathcal{M} . Consequently, symbol detection in MBM-mMIMO at the BS is more difficult compared to mMIMO systems.

6.3. EXISTING STATE-OF-THE-ART DETECTORS FOR MBM-MMIMO

where $\mathbf{x}_j \in \mathbb{C}^{M \times 1}$ is the transmit MBM symbol vector from the j^{th} user, and $M = 2^{N_{RF}}$. \mathbf{H}_j is defined as the channel matrix corresponding to the j^{th} user. All channel gains are assumed to be i.i.d. Gaussian random variables with zero mean and unit variance. Each element of noise vector $\mathbf{n} \in \mathbb{C}^{N_r \times 1}$ is additive white Gaussian distributed with zero mean and variance σ^2 . The MBM signal set \mathcal{M} is expressed as $\mathcal{M} = \{\mathbf{m} : m_i \in \mathcal{A} \cup \{0\}, \|\mathbf{m}\|_0 = 1\}$, where \mathbf{m} is $M \times 1$ vector. For example, if $N_{RF} = 1$ and $\#\mathcal{A} = 2$, MBM signal set with BPSK for each user can be expressed as $\mathcal{M} = \left\{ \begin{bmatrix} 1 \\ 0 \end{bmatrix}, \begin{bmatrix} -1 \\ 0 \end{bmatrix}, \begin{bmatrix} 0 \\ -1 \end{bmatrix}, \begin{bmatrix} 0 \\ 1 \end{bmatrix} \right\}$. Each of N_t users transmit a symbol vector from \mathcal{M} . The ML detection for system model (6.1) is expressed as

$$\hat{\mathbf{x}} = \arg \min_{\mathbf{x} \in \mathcal{M}^{N_t}} \|\mathbf{y} - \mathbf{H}\mathbf{x}\|_2^2 \quad (6.2)$$

It is worth noting that, the computational complexity of ML detection ² is exponential in N_{RF} and N_t , $\mathcal{O}((2^{N_{RF}} \#\mathcal{A})^{N_t})$. Consequently, ML detection is not suitable for MBM-mMIMO.

6.3 Existing state-of-the-art detectors for MBM-mMIMO

6.3.1 MMSE Detection

The estimated symbol vector at the base station is computed as

$$\hat{\mathbf{x}} = \mathbf{A}^{-1}\mathbf{b},$$

where $\mathbf{A} = \mathbf{G} \frac{\sigma^2}{E_x} \mathbf{I}$ is the MMSE filter matrix, and $\mathbf{G} = \mathbf{H}^H \mathbf{H}$ is called the Gram matrix. $\mathbf{b} = \mathbf{H}^H \mathbf{y} \cdot \sigma^2$ denotes the noise variance and E_x is the average energy per symbol. Due to channel hardening phenomenon, the

²As shown in Chapter 1, there are no RF mirrors employed in large MIMO and mMIMO systems. Hence, ML detection's computational complexity in mMIMO and large MIMO systems exponentially increases only with the number of users N_t .

gram matrix \mathbf{G} becomes diagonally dominant. As a consequence, MMSE yields near-optimal BER performance for mMIMO systems. However, in MBM-mMIMO, the transmit symbol vector is sparse. As MMSE detector fails to utilize the sparsity of the transmit MBM-mMIMO symbol vector, it shows poor BER performance for MBM-mMIMO systems. Moreover, MMSE involves high dimensional matrix inversion, and hence, MMSE is also not suitable for mMIMO systems due to cubic order computational complexity.

6.3.2 IESP Detection

IESP [48] is a sparsity exploiting detection algorithm which utilizes the inclusion-exclusion sparse structure of transmit MBM-mMIMO symbol vector. The transmit MBM-mMIMO symbol vector is sparse as all the possible channel realizations are not utilized. However, the transmit MBM-mMIMO symbol vector have an additional structure that only element in each block corresponding to each user has a non-zero entity. IESP exploits this additional structure to yield low-complexity symbol detection in the uplink MBM-mMIMO. IESP generates the initial estimate through orthogonal matching pursuit (OMP) algorithm, followed by the computation of residual error. At each iteration, IESP restricts estimated non-zero index to be from the set of possible values of non-zero indices, \mathcal{B} . Thus, IESP maintains the inclusion-exclusion sparsity structure of the estimated MBM-mMIMO symbol vector. IESP stops iterating when the residual error is more than the previous error. IESP updates non-zero locations of the estimated MBM-mMIMO symbol vector as follows:

$$l_i^{(k)} = \begin{cases} l_i^{(k)}, & z_{l_k^{(k-1)}} > z_{l_k} \\ l'_i & \end{cases}$$

where $l'_i = \underset{i \in \mathcal{B}}{\operatorname{argmax}} \mathbf{h}_{j,i}^H \mathbf{r}_j$, and \mathbf{r}_j refers the residual vector corresponding to the j th user. $\mathbf{z} = (\mathbf{H}_{\mathcal{S}^{(k)}}^H \mathbf{H}_{\mathcal{S}^{(k)}})^{-1} \mathbf{H}_{\mathcal{S}^{(k)}}^H \mathbf{y} \cdot \mathcal{S}^{(k)}$ denotes the set of non-zero indices at iteration k and $\mathbf{H}_{\mathcal{S}^{(k)}}$ is a submatrix of \mathbf{H} . Though IESP exhibits lower computational complexity as compared to ML detection, however, the BER

6.4. GRAPH TRAVERSAL AIDED DETECTION IN UPLINK MBM-MMIMO BASED ON SOCIO-COGNITIVE KNOWLEDGE OF SWARM OPTIMIZATION

performance of IESP degrades with the increase in the number of antennas.

6.4 Graph Traversal Aided Detection in Uplink MBM-mMIMO based on Socio-Cognitive Knowledge of Swarm Optimization

6.4.1 Initialization

The sparsity level $\|\mathbf{x}\|_0$ (the number of nonzero indices) of the transmit symbol vector \mathbf{x} is assumed to be known at BS. However, exact indices of the nonzero elements of \mathbf{x} are unknown. Hence, estimating the initial transmit vector involves identifying both the nonzero indices and the values in those nonzero locations. A set T of the nonzero indices of \mathbf{x} are called the support set. The initial estimate of the support set T is designed based on Q -thresholding algorithm [81]

$$T = \{\text{Indices of } N_t \text{ largest elements of } \mathbf{h}_i^T \mathbf{y}, i = 1, 2, \dots, MN_t\}, \quad (6.3)$$

The elements of T correspond to nonzero indices of the initial estimate $\mathbf{x}^{(0)}$. Thus, the initial estimate of the transmit symbol vector $\mathbf{x}^{(0)}$ is computed as

$$\hat{x}_i^{(0)} = \begin{cases} \mathbf{h}_i^T \mathbf{y} & \text{if } i \in T \\ 0, & \text{otherwise} \end{cases} \quad (6.4)$$

The above initial solution is iteratively improved in SID. Moreover, all users in MBM-mMIMO are not equally affected by the noise. Hence, for efficient and robust symbol detection, users are ordered based on the channel gain and the initial solution. Thus, to achieve significant performance benefits, the users are ordered based on the following set O

$$O = \arg \underset{i}{\text{sort}} \|\mathbf{y} - \mathbf{H}_i \mathbf{x}_i^{(0)}\|_2, \quad (6.5)$$

where $\hat{\mathbf{x}}_i^{(0)}$ and \mathbf{H}_i respectively refer to the estimate of initial symbol vector, and the channel matrix corresponds to the i^{th} user. The elements in \mathbf{O} are sorted in descending order of $\|\mathbf{y} - \mathbf{H}_i \mathbf{x}_i^{(0)}\|_2$ [82]. After that, a tree traversal aided sequential detection approach based on social and cognitive knowledge of swarm optimization has been considered to detect the users based on the order mentioned in \mathbf{O} .

6.4.2 Tree traversal aided symbol detection

SID which transforms and solves the uplink symbol detection problem in MBM-mMIMO as minimum spanning tree (MST) is discussed in this section.

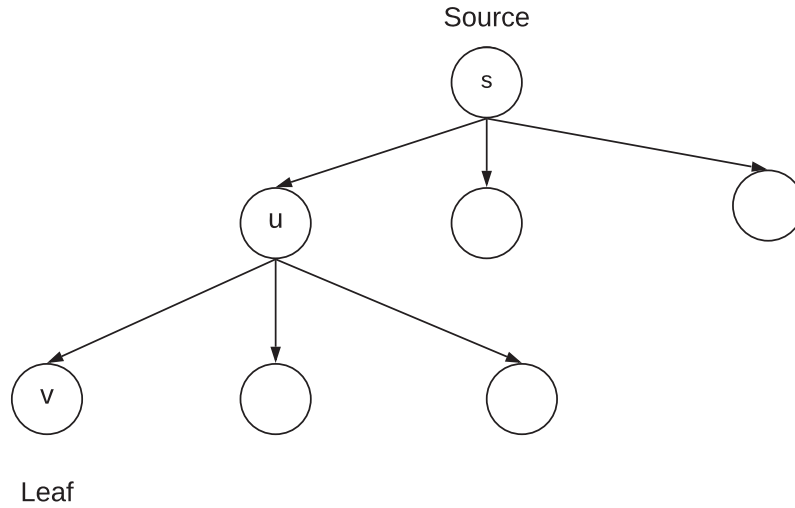


Figure 6.2: MBM-mMIMO symbol detection as a spanning tree.

Symbol detection as MST: The symbol detection problem at the BS in uplink MBM-mMIMO system is modelled as finding an MST from an undirected graph (Fig. 6.2). The undirected graph $G = (V, E)$ is formed as follows. The depth of G is equal to the number of users N_t . The root is chosen as a dummy vertex at depth zero. The number of vertices at j^{th} level is $|\mathcal{A}|^j - 1$, thereby making the total number of vertices at each level as $\frac{|\mathcal{A}|^j - 1}{|\mathcal{A}| - 1}$.

6.4. GRAPH TRAVERSAL AIDED DETECTION IN UPLINK MBM-MMIMO BASED ON SOCIO-COGNITIVE KNOWLEDGE OF SWARM OPTIMIZATION

From the root s , SID performs a depth-first search with a probability metric based on the residual error from the source node to the current node. SID is initialized at the root with the initial solution (6.4) obtained in the Section 6.4.1. Each child vertex of a parent represents a possible MBM constellation point under the MBM with single input single output (SISO) scenario.

Edge weight and Cost function: The complete weight function is considered as the ML cost defined as

$$\phi(\mathbf{x}) = \mathbf{r}^H \mathbf{r}, \quad (6.6)$$

where the residual error, $\mathbf{r} = \mathbf{b} - \mathbf{G}\mathbf{x}$ and $\mathbf{G} = \mathbf{H}^H \mathbf{H}$. $(\cdot)^H$ denotes matrix Hermitian. Hence, at level i , the partial weight function of an edge $(s, u) \in E$ is defined as

$$\mathbf{w}_{i,(s,u)} = \mathbf{b} - \sum_{j=1, \neq i}^{N_t} \mathbf{G}_j \mathbf{x}_j - \mathbf{G}_i \mathbf{s}_{i \in u} \quad (6.7)$$

where $\mathbf{s}_{i \in u} \in \mathcal{M}$. \mathbf{G}_i is the i^{th} sub-matrix of \mathbf{G} , corresponding to the i^{th} user.

Update strategy: SID first computes the initial solution $\mathbf{x}^{(0)}$ and performs user-ordering as defined in equation (6.5). For each parent node, SID chooses the child node corresponding to the next user's transmit symbol vector in \mathcal{O} . A probabilistic approach is taken to compute the attractiveness of a child node towards a parent node. The child node selected at the i^{th} level becomes the parent node for the $(i+1)^{th}$ level. The probability metric must be chosen. The probability at each node leads to the minimization of the overall square loss penalty between the estimated transmit vector and receive symbol vector defined in equation (6.6). The minimization of the square loss penalty also must ensure the minimization of the BER at BS. Following minimum bit error rate (MBER) criteria [83], the probability metric of correct detection

is computed as

$$\begin{aligned}\tanh\left(\beta(\mathbf{r}^H\mathbf{r} + 1)\right) + \tanh\left(\beta(\mathbf{r}^H\mathbf{r} - 1)\right) &= 0 \\ \frac{\exp(\beta\mathbf{r}^H\mathbf{r}) - \exp(-\beta\mathbf{r}^H\mathbf{r})}{\exp(\beta\mathbf{r}^H\mathbf{r}) + \exp(-\beta\mathbf{r}^H\mathbf{r})} &= 0 \\ \exp(2\beta\mathbf{r}^H\mathbf{r}) &= 1,\end{aligned}\tag{6.8}$$

where \mathbf{r} denotes the residual error and $\beta = \frac{\sigma^2}{2}$. The equation (6.8) infers that the probability metric becomes unity when MBER is achieved. Hence, the probability metric for selecting the correct vertex v for the i^{th} user is chosen as

$$\mathcal{P}(\mathbf{s}_{i \in v}) = \exp\left(-\mathbf{r}^T(\sigma_v^2\mathbf{I})^{-1}\mathbf{r}\right),\tag{6.9}$$

where \mathbf{I} is $M \times M$ identity matrix. The symbol vector at the i^{th} level for the i^{th} user is estimated by choosing the maximum value of the probability metric.

$$\hat{\mathbf{x}}_{i \in v} = \arg \max_{\mathbf{s}_{i \in v} \in \mathcal{M}} \mathcal{P}(\mathbf{s}_{i \in v})\tag{6.10}$$

The choice of an exponential probability metric can also be explained from the attractiveness parameter proposed in the swarm and evolutionary computation literature [84]. In case of FA, where two fireflies refer to two candidate solutions, the attractiveness between two fireflies reduces with the increase in their distance and is represented by an exponential function (discussed in Chapter 2). Hence, a candidate solution (a possible transmit vector for a user) that is nearest to the previously estimated transmit vector of another user is more likely to be chosen. Consequently, as the detection of a transmit vector for a user is considered as a multiclass classification from the MBM-SISO constellation set, a softmax function that depends on the residual error vector is considered as the probability metric. This probability metric refers to attractiveness of the particle $\hat{\mathbf{x}}_{i \in v}$ towards a candidate solution $\mathbf{s}_{i \in v}$. The

6.4. GRAPH TRAVERSAL AIDED DETECTION IN UPLINK MBM-MMIMO BASED ON SOCIO-COGNITIVE KNOWLEDGE OF SWARM OPTIMIZATION

performance of SID improves if the social and cognitive knowledge of the search space is considered by keeping track of the global best and local best solutions, respectively. To further enhance SID's performance, L iteration of SID is performed. Conventional iterative techniques do not utilize the social and cognitive knowledge of the set of solutions achieved from different iterations. Hence, to improve the exploration and exploitation capability of SID, the local best solution is computed at each iteration. At iteration k , once the symbol vector/position corresponding to the i^{th} swarm is computed at vertex u , the fitness of that solution $\hat{\mathbf{x}}_i$ is computed as

$$\phi(\hat{\mathbf{x}}_{i \in u}^{(k+1)}) = || \mathbf{w}_{i,(s,u)}^{(k+1)} ||_2^2, \quad (6.11)$$

where $\mathbf{w}_{i,(s,u)}^{(k+1)} = \mathbf{w}_{i,(s,u)}^{(k)} + \mathbf{G}_i(\mathbf{x}_{i \in u}^{(k)} - \mathbf{x}_{i \in u}^{(k+1)})$. If the fitness of present solution $\hat{\mathbf{x}}_i^{(k+1)}$ is better than the previous solution $\left(\phi(\hat{\mathbf{x}}_{i \in u}^{(k+1)}) < \phi(\hat{\mathbf{x}}_{i \in u}^{(k)}) \right)$, $\hat{\mathbf{x}}_{i \in u}^{(k+1)}$ is chosen as the local best solution of i^{th} user. Finally, the global best solution obtained from the local best solutions of L iterations are declared as the output of SID. The flowchart and pseudocode of SID are given in Fig. 6.3 and Algorithm 6.1 respectively.

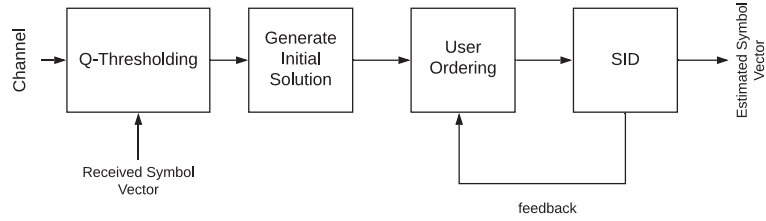


Figure 6.3: Flowchart of SID.

6.4.3 Theoretical analysis

In this section, the convergence analysis and analytical upper bound on BER performance of SID are provided.

Algorithm 6.1 Proposed SID algorithm

Input: $N_r, N_t, M, \mathbf{H}, \mathbf{y}, L, \sigma_v$
Output: \mathbf{x}_{gBest}
Preprocessing: $\mathbf{G} = \mathbf{H}^T \mathbf{H}, \mathbf{b} = \mathbf{H}^T \mathbf{y}$
 Compute initial estimate using (6.4)
while iteration $\leq L$ **do**
 for $i = 1, i \leq 2N_t$ **do**
 Perform user ordering based on (6.5)
 Calculate probability metric using (6.9)
 Calculate fitness using (6.11)
 Update local best solution \mathbf{x}_{lBest}
 end for
end while
 Update global best solution \mathbf{x}_{gBest}
 Update fitness using (6.11)

Convergence analysis

The convergence of SID is analysed based on the proposed MST detection model. Suppose SID detects a symbol vector from the i^{th} user and reaches node u . $(s, u) \in E$. The error vector \mathbf{t}_i after detection of the symbol vector from the i^{th} user at the i^{th} level is expressed as

$$\mathbf{t}_i = \mathbf{y} - \sum_{j \neq i, i \in u}^{N_t} \mathbf{H}_j \mathbf{x}_j - \mathbf{H}_i \hat{\mathbf{x}}_{i \in u}, \quad (6.12)$$

where $\mathbf{r} = \mathbf{H}^H \mathbf{t}$. While traversing the tree, suppose vertex v is selected at the $(i+1)^{th}$ level and there exists an edge $(u, v) \in E$. From equation (6.12), the error vector \mathbf{t} at the $(i+1)^{th}$ level after detection of symbol vector from the $(i+1)^{th}$ user is computed as

$$\begin{aligned} \mathbf{t}_{i+1} &= \mathbf{t}_i + \mathbf{H}_{i+1} (\mathbf{x}_{i+1} - \hat{\mathbf{x}}_{i+1 \in v}) \\ &= \mathbf{t}_i + \mathbf{H}_{i+1} \mathbf{d}_{i+1}, \end{aligned} \quad (6.13)$$

6.4. GRAPH TRAVERSAL AIDED DETECTION IN UPLINK MBM-MMIMO BASED ON SOCIO-COGNITIVE KNOWLEDGE OF SWARM OPTIMIZATION

where $\mathbf{d}_{i+1} = \mathbf{x}_{i+1} - \hat{\mathbf{x}}_{i+1 \in v}$. Applying the square of L2-norm on both sides of equation (6.13),

$$\begin{aligned} \|\mathbf{t}_{i+1}\|_2^2 &= \|\mathbf{t}_i\|_2^2 + \|\mathbf{H}_{i+1}\mathbf{d}_{i+1}\|_2^2 + 2(\mathbf{H}_{i+1}\mathbf{d}_{i+1})^H (\mathbf{t}_{i+1} - \mathbf{H}_{i+1}\mathbf{d}_{i+1}) \\ &= \|\mathbf{t}_i\|_2^2 - \|\mathbf{H}_{i+1}\mathbf{d}_{i+1}\|_2^2 \end{aligned} \quad (6.14)$$

Since $\mathbf{H}_{i+1}^H \mathbf{t}_{i+1} = \mathbf{0}$ [58], from (6.14),

$$\|\mathbf{t}_{i+1}\|_2^2 < \|\mathbf{t}_i\|_2^2 \quad (6.15)$$

Hence, the error associated with the estimated symbol decreases while traversing the tree. Thus, it concludes that SID achieves the minimum residual error when it reaches the tree's leaf node level. It proves convergence of SID.

BER analysis

An analytical upper bound on BER performance of SID is computed as follows. The approximate received SNR for the j^{th} user at the iteration k is calculated as

$$\gamma_j^{(k)} = \frac{1}{\sigma^2 + \sum_{i=1, i \neq j}^{N_t} \|\mathbf{x}_i^{(k)} - \hat{\mathbf{x}}_i^{(k)}\|_2^2}$$

Hence, MGF corresponds to the average instantaneous received SNR $\tilde{\gamma}$ under CSI mismatch scenario at the BS is computed as

$$\mathcal{W}_\gamma(s) = \left(1 - s(1 + e^2)\tilde{\gamma}\right)^{-N_r}, \quad (6.16)$$

where e is the channel estimation error. Hence, the probability of error \mathcal{P}_e is computed as [60]

$$\begin{aligned}\mathcal{P}_e &= \frac{1}{\pi} \int_0^\pi \mathcal{W}_\gamma\left(-\frac{1}{2\sin^2\theta}\right) d\theta \\ &= \frac{1}{\pi} \int_0^\pi \left(\frac{\sin^2\theta}{\frac{(1+e^2)\tilde{\gamma}}{2N_r} + \sin^2\theta} \right) d\theta \\ &\leq \left(\frac{1-\mu(c)}{2} \right)^{N_r} \sum_{k=0}^{N_r-1} \binom{N_r+k-1}{k} \left(1 + \frac{\mu(c)}{2} \right)^k, \quad (6.17)\end{aligned}$$

where $\mu(c) = \sqrt{\frac{(1+e^2)\tilde{\gamma}}{2N_r+(1+e^2)\tilde{\gamma}}}$. Setting $e = 0$ in expressions (6.16) and (6.17) gives the expression of \mathcal{P}_e for the perfect CSI at the BS.

6.4.4 Simulation results

This section compares SID with IESP [48] and MMSE in terms of BER performance and computational complexity. Simulation parameters are listed in Table. 6.1.

Table 6.1: Table of parameters

Parameter	Value
N_{RF}	2, 3, 4
N_r	128
N_t	16
e	0%, 0.5%, 10%, 30%
$\#\mathcal{A}$	4

In Fig. 6.4, BER performance of SID is compared with MMSE and IESP detection techniques for an MBM-mMIMO system with $N_r = 128$, $N_t = 16$ and $N_{RF} = 2$. In an MBM-mMIMO system with $N_r = 128$, $N_t = 16$ and $N_{RF} = 2$, the overall channel matrix formed between the users and BS is tall. Hence, the MBM-mMIMO system becomes an overdetermined system with a system loading factor ($\alpha = \frac{N_r}{2N_{RF}N_t}$) of 2. As observed in Fig. 6.4, SID outperforms both MMSE and IESP for such overdetermined MBM-mMIMO

6.4. GRAPH TRAVERSAL AIDED DETECTION IN UPLINK MBM-MMIMO BASED ON SOCIO-COGNITIVE KNOWLEDGE OF SWARM OPTIMIZATION

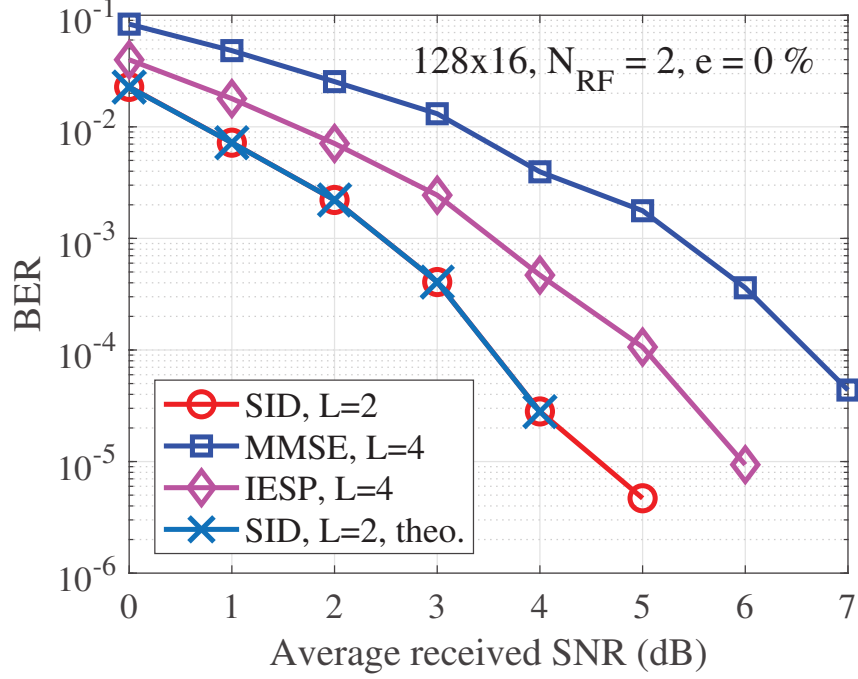


Figure 6.4: Comparison of BER performance of SID with other contending techniques for $N_r = 128$, $N_t = 16$ and $N_{RF} = 2$

systems. SID even with $L=2$ has superior BER performance as compared to MMSE with $L=4$ and IESP with $L=4$. Moreover, even with half number of iterations, proposed SID is capable of achieving SNR gains of 1.5 dB and 3 dB as compared to IESP and MMSE respectively for a targeted BER of 10^{-4} . It shows that SID not only converges faster but also yields better BER performance compared to both MMSE and IESP. This proves the viability of SID for symbol detection in an overdetermined MBM-mMIMO with less number of RF mirrors placed before each user.

As discussed in Section 6.1, the spectral efficiency of MBM-mMIMO systems improves with the number of RF mirrors placed before each user [80]. Hence, the viability of SID over MMSE and IESP needs to be justified for a large number of RF mirrors. Accordingly, a determined and underdetermined MBM-mMIMO systems are also considered with the number of RF mirrors chosen for each user as $N_{RF} = 3$ and $N_{RF} = 4$, respectively.

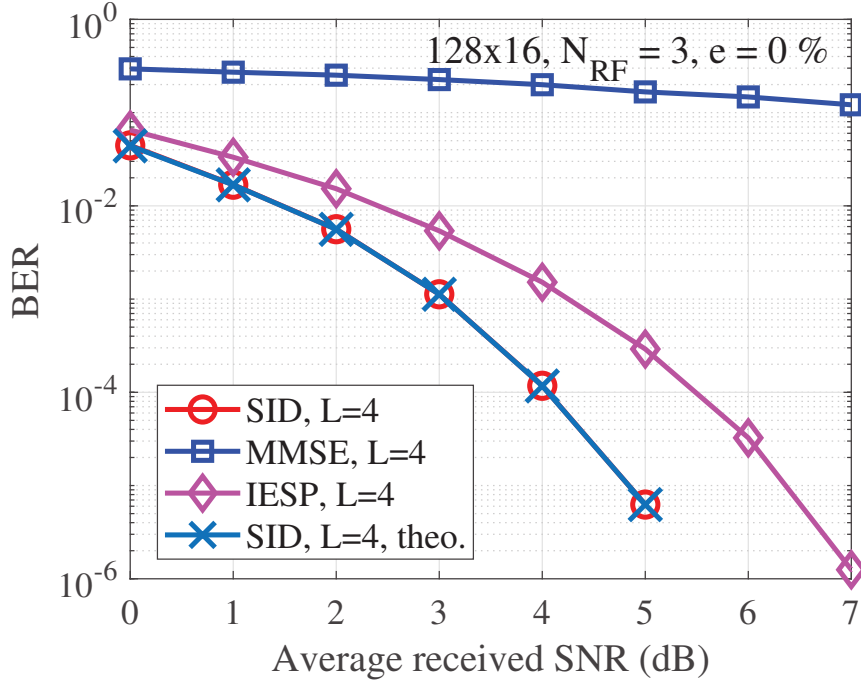


Figure 6.5: Comparison of BER performance of SID with other contending techniques for $N_r = 128$, $N_t = 16$ and $N_{RF} = 3$.

Fig. 6.5 depicts BER performance of SID compared with MMSE and IESP detection techniques for an determined MBM-mMIMO system with $N_r = 128$, $N_t = 16$ and $N_{RF} = 3$. In an MBM-mMIMO system with $N_r = 128$, $N_t = 16$ and $N_{RF} = 3$, the overall channel matrix formed between the users and BS becomes a square matrix, eventually converting MBM-mMIMO system to a determined system with a system loading factor of unity. For a fair comparison, the number of iterations is kept the same ($L = 4$) for all the contending detection techniques. Fig. 6.5 shows that SID achieves an SNR gain of 1.5 dB as compared to IESP for a targeted BER of 10^{-4} . Furthermore, MMSE yields far inferior BER performance as compared to SID. It concludes that SID is a promising technique for symbol detection in determined MBM-mMIMO systems.

As MBM-mMIMO provides comparatively more spectral efficiency than mMIMO, SID needs to be efficient under massive number of users. Hence,

6.4. GRAPH TRAVERSAL AIDED DETECTION IN UPLINK
MBM-MMIMO BASED ON SOCIO-COGNITIVE KNOWLEDGE OF
SWARM OPTIMIZATION

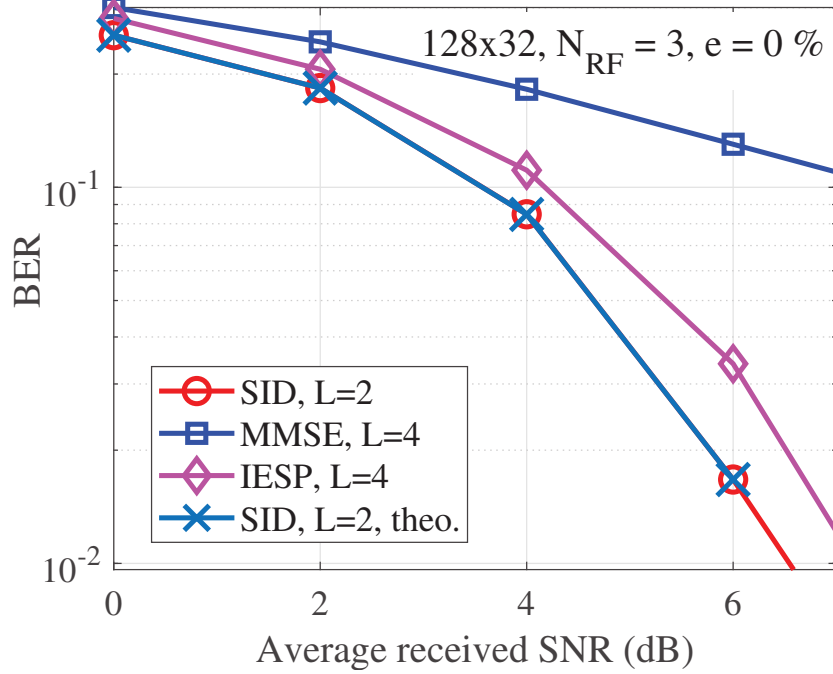


Figure 6.6: Comparison of BER performance of SID with other contending techniques for $N_r = 128$, $N_t = 32$ and $N_{RF} = 3$.

in Fig. 6.6, the BER performance of SID is compared with MMSE and IESP for a scenario where the number of users scales up in the system. In Fig. 6.6, the number of BS-antennas and RF mirrors are kept the same as in Fig. 6.5, and the number of users is increased to $N_t = 32$. Fig. 6.6, depicts that SID outperforms MMSE and IESP even for a large number of active users in the MBM-mMIMO system. Hence, SID is a more suitable candidate compared to MMSE and IESP for uplink symbol detection in MBM-mMIMO systems for 5G and beyond wireless communications.

In Fig. 6.7, the number of RF mirrors for each user is further increased to $N_{RF} = 4$. As the dimension of the transmit MBM-mMIMO symbol detector is more than the number of BS-antennas, the MBM-mMIMO system considered in Fig. 6.7 is underdetermined with a system loading factor (α) of 0.5, making the symbol-detection more challenging. However, even under such a challenging scenario, SID achieves an SNR gain of 1.5 dB over IESP

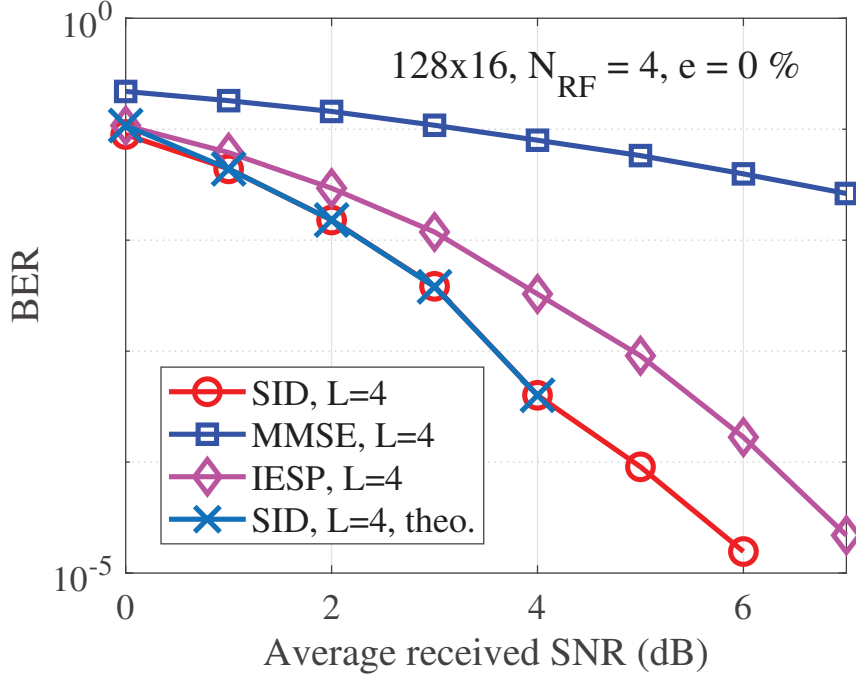


Figure 6.7: BER performance comparison of SID with other contending detection techniques under perfect CSI scenarios, $N_r = 128$, $N_t = 16$ and $N_{RF} = 4$.

for the same number of iterations. In Fig. 6.7, MMSE shows substantial degradation in BER compared to SID. Hence, from Fig. 6.4 to Fig. 6.7, it is proven that SID is a more efficient detection technique in terms of BER performance as compared to MMSE as well as IESP, justified against any number of RF mirrors for each user.

From Fig. 6.4-Fig. 6.7, it is assumed that the CSI is perfectly known at the BS, and there is no CSI error. However, BS has imperfect CSI due to pilot contamination problem in practical wireless communication systems. SID technique is suitable to be deployed for practical wireless scenarios if the robustness of SID is validated under both perfect and imperfect CSI scenarios. Hence, from Fig. 6.8 to Fig. 6.9, BER performance of SID is compared with MMSE, and SID under CSI mismatch scenarios.

Fig. 6.8 compares the BER performance of SID under different CSI mis-

6.4. GRAPH TRAVERSAL AIDED DETECTION IN UPLINK MBM-MMIMO BASED ON SOCIO-COGNITIVE KNOWLEDGE OF SWARM OPTIMIZATION

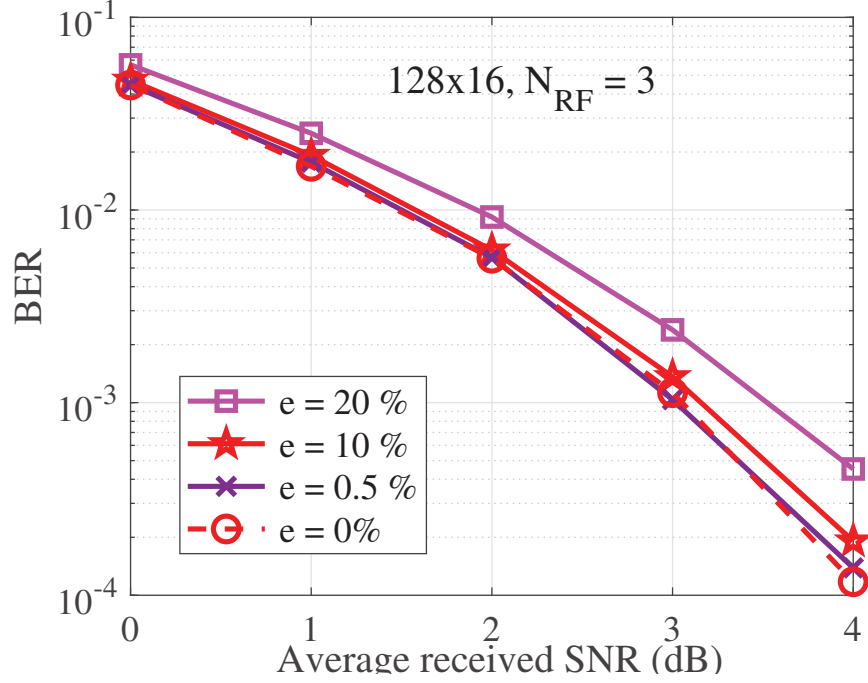


Figure 6.8: BER performances of SID under different CSI mismatch scenarios for $N_r = 128$, $N_t = 16$ and $N_{RF} = 3$.

match conditions. It is found through simulations that SID shows minimal degradation in BER performance if there exists CSI mismatch at the BS. It corroborates robustness of SID under CSI mismatch scenarios.

To prove superiority of SID under CSI mismatch scenario, the Fig. 6.9 compares BER performance of the contending detection techniques for channel estimation error of $e = 30\%$. SID attains an SNR gain of approximately 2 dB over IESP for a targeted BER of 4×10^{-5} , even for a high value of channel estimation error of $e = 30\%$ at the BS. MMSE shows very poor BER performance under such CSI error scenario. SID detection technique is more robust to even higher CSI estimation errors as compared to both MMSE and IESP. Moreover, it is already proved from Fig. 6.8 that the BER performance of SID with small CSI errors at BS does not degrade much compared to the perfect CSI conditions. Hence, SID is more efficient and robust MBM-MMIMO symbol detection technique compared to the MMSE and the IESP

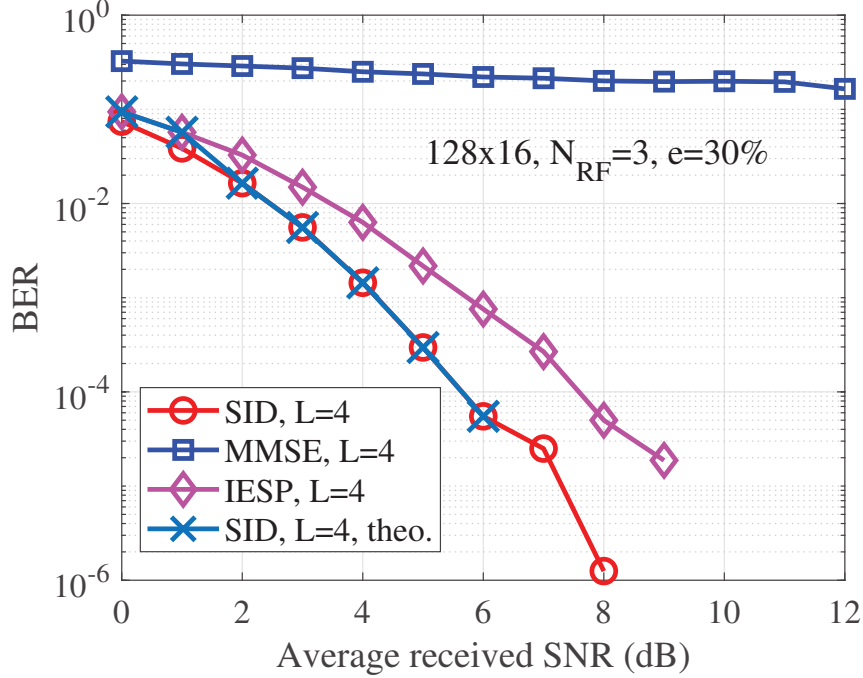


Figure 6.9: BER performance comparison of proposed detection technique with other contending detection techniques under imperfect CSI scenario, $N_r = 128$, $N_t = 16$ and $N_{RF} = 3$.

from BER performance perspective.

The computational complexities of the competing detection techniques are compared in Fig. 6.10-Fig. 6.11 in terms of FLOPs. Less number of FLOPs of A detection technique which requires less number of FLOPs helps faster processing in the floating point unit (FPU). Hence, a detection technique with less number of FLOPs per iteration is computationally more efficient for symbol detection in MBM-mMIMO systems.

As illustrated in Fig. 6.10, a single iteration of SID is computationally more efficient as compared to both MMSE and IESP. Moreover, as shown in Fig. 6.11, SID requires a significantly fewer number of FLOPs in symbol detection than IESP and MMSE for the same number of BS antennas in the system. Hence, it is proved from Fig. 6.10 and Fig. 6.11 that SID is computationally more viable than MMSE and IESP for uplink MBM-

6.4. GRAPH TRAVERSAL AIDED DETECTION IN UPLINK MBM-MMIMO BASED ON SOCIO-COGNITIVE KNOWLEDGE OF SWARM OPTIMIZATION

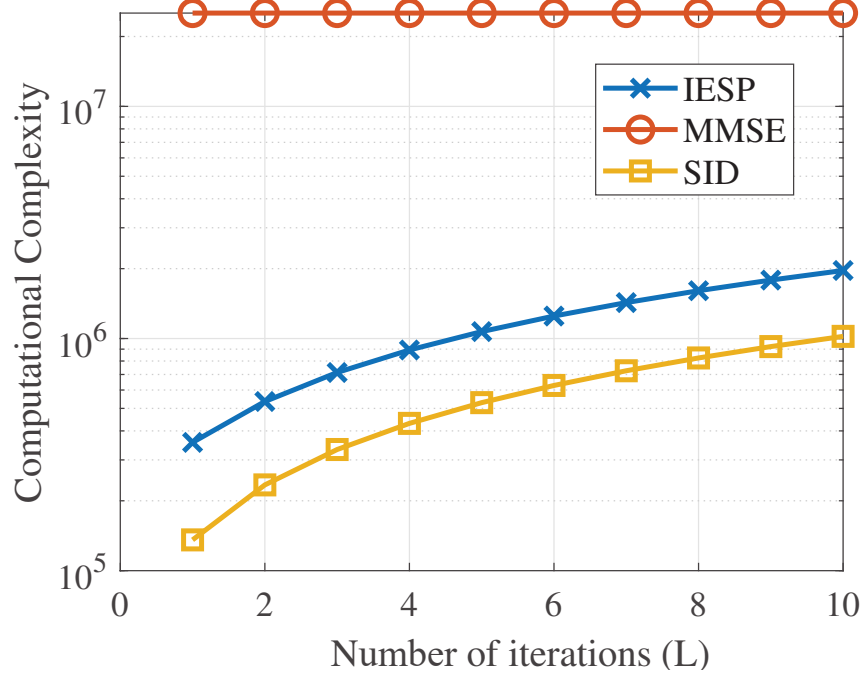


Figure 6.10: Comparison of computational complexity under different number of iterations for $N_r = 128$, $N_t = 16$ and $N_{RF} = 4$.

mMIMO.

SID technique detects the transmitted symbol vector from each user sequentially. It utilizes socio-cognitive knowledge from all iterations, which prunes the interuser interference and provides superior performance. The convergence of SID is analyzed theoretically in this Chapter. Simulation results reveal that SID outperforms existing state-of-the-art detection techniques in terms of both BER performance and computational complexity, which are further validated through an analytic expression of upper bound on BER. Moreover, SID's robustness is also verified under imperfect CSI scenarios at BS. It concludes that SID is a promising low-complexity candidate for uplink symbol detection in MBM-mMIMO systems with a large number of users in terms of error performance, as well as robustness. However, except for the initial Q thresholding step, SID does not take advantage of the transmit MBM-mMIMO symbol vector's sparse nature. Such sparse

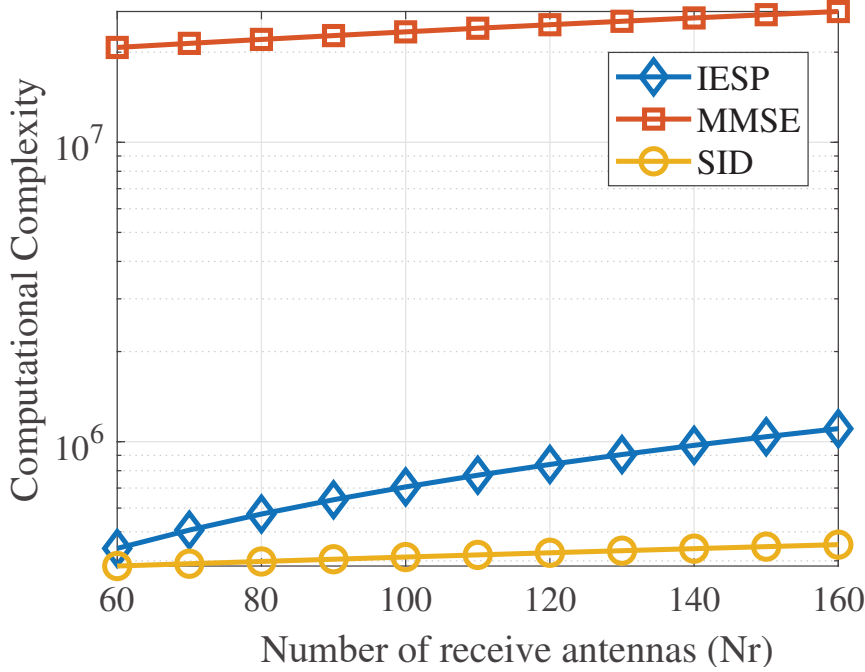


Figure 6.11: Comparison of computational complexity under different number of BS antennas for $N_{RF} = 4$, $N_t = 16$ and $L = 4$.

signal detectors' performance can further be improved if the actual support set is retrieved at each iteration. Hence, the symbol detection problem in MBM-mMIMO needs to be reconsidered. An efficient criteria needs to be introduced to recover true support of the transmit MBM-mMIMO vector at each iteration. In the subsequent algorithm, MSRE criteria-based enhanced detectors, MEPD and MEPDRS, are proposed to achieve near-ML performance for symbol detection MBM-mMIMO systems.

6.5 Minimum Error Pursuit Detection Algorithm for MBM-mMIMO

The SID technique utilizes a graph-traversal-based probabilistic approach to update the symbol vectors while maintaining a swarm intelligence-based

6.5. MINIMUM ERROR PURSUIT DETECTION ALGORITHM FOR MBM-MMIMO

exploration-exploitation trade-off. Consequently, SID outperforms IESP and MMSE detection algorithms. However, SID does not ensure recovery of true support set at each iteration, resulting in inferior performance compared to ML detection. Hence, the design of low complexity algorithms for uplink MBM-mMIMO systems considering the structured sparsity of the transmit MBM-mMIMO symbol vector is crucial. Hence, at first, MSRE criteria based low-complexity sequential symbol detection technique MEPD is proposed for the uplink of MBM-mMIMO system. Another improved low complexity detection technique, MEPDRS is devised by enhancing MEPD's exploration capability to a limited message space. Comparisons of the proposed techniques are drawn with other state-of-the-art techniques for the uplink MBM-mMIMO systems.

The following terminology is used in this chapter. x_{j,l_1} refers to the l_1^{th} non-zero element of \mathbf{x}_j . $\mathbb{E}(\cdot)$ denotes the expectation operator. κ_1 and κ_2 respectively, refer to the Lagrangian multiplier and the step size. $\mathbb{P}_{\mathcal{M}}(\cdot)$ denotes projection onto a set \mathcal{M} . $\mathcal{D}(\cdot, \cdot)$ is the Hamming distance operator.

6.5.1 Problem Formulation and Symbol Detection

In this section, a support recovery (SR) technique is discussed first, followed by the introduction of MSRE criteria.

Support Recovery

Suppose \mathbf{x}_j is the symbol vector transmitted by the j^{th} user. The support δ_j of \mathbf{x}_j is defined as the number of nonzero elements in the vector \mathbf{x}_j , as $\delta_j = \|\mathbf{x}_j\|_0$. Since the signal of interest \mathbf{x}_j contains both zero and nonzero elements, exact recovery of nonzero locations of \mathbf{x}_j at the BS is crucial for reliable estimation of \mathbf{x}_j . If \mathcal{T}_j is the set of all indices of \mathbf{x}_j , \mathcal{T}_j can be expressed as $\mathcal{T}_j = \mathcal{V}_j \cup \emptyset_{(M-\delta_j) \times 1}$, where \mathcal{V}_j and $\emptyset_{(M-\delta_j) \times 1}$ respectively refer to the support set and the set of zero locations of the transmitted signal \mathbf{x}_j . δ_j and $M - \delta_j$ respectively, denote the cardinalities of \mathcal{V}_j and the set $\emptyset_{(M-\delta_j) \times 1}$. The received symbol vector \mathbf{y} is simplified as $\mathbf{y} = \mathbf{H}_j \mathbf{x}_j + \mathbf{e}_j$, where

$\mathbf{e}_j = \sum_{u=1, u \neq j}^{N_t} \mathbf{H}_u \mathbf{x}_u + \mathbf{n}$ is the interference and noise term associated with the j^{th} user. Hence, the support set \mathcal{V}_j is recovered as $\mathcal{V}_j = \{\arg \min_k 1 - |\mathbf{h}_{j,k}^\dagger \mathbf{y}_j|, k = 1, 2, \dots, M\}$.

MSRE Criteria

As the transmit MBM-mMIMO symbol vector exhibits structured sparsity, \mathbf{H}_j satisfies the restricted isometry property (RIP) [5, 80, 85]. To ensure recovery of true support from \mathcal{V}_j , the channel matrix \mathbf{H}_j must follow the following criteria [86], $\max_{k \neq i} |\mathbf{h}_{j,k}^\dagger \mathbf{y}_j| \leq |\mathbf{h}_{j,i}^\dagger \mathbf{y}_j|$, where $\mathbf{y}_j = \mathbf{H}_j \mathbf{x}_j + \mathbf{n}_j$. Hence, the probability of support recovery error (SRE) is expressed as

$$\mathcal{P}_{SRE} \leq \sum_{k \neq i} \mathcal{P}(\mathbf{h}_{j,k}^\dagger \mathbf{y}_j > x_i) \quad (6.18)$$

In noise-free environment, $\mathbf{h}_{j,k}^\dagger \mathbf{y}_j$ is simplified as $\mathbf{h}_{j,k}^\dagger \mathbf{y}_j = \sum_{l_1=1}^M s_{j,l_1}$, where $s_{j,l_1} = \sum_{l_2=1}^{N_r} h_{j,l_2,k} h_{j,l_1,l_2} x_{j,l_1}$. Assume that $\mathcal{P}(|s_{j,l_1}| < \mu_{j,max}) = 1$ and $\mathbb{E}(s_{j,l_1}^2) \leq \frac{\mu_{j,max}^2}{N_t}$, where $\mu_{j,max}$ is the maximum cross-correlation on \mathbf{H}_j , which is defined as $\mu_{j,max} = \max_{i \neq k} |\mathbf{h}_{j,i}^\dagger \mathbf{h}_{j,k}|$. Hence, applying Markov's inequality [87] on equation (6.18), the probability of error in support recovery is computed as

$$\mathcal{P}_{SRE} \leq 2(1 - M) \left(1 - \frac{3x_{j,i}^2}{6v + 2cx_{j,i}} \right), \quad (6.19)$$

where $c = \mu_{j,max}$, $M = 2^{N_{RF}}$ and $v = \frac{c^2}{M}$. Hence, to corroborate error-free support-recovery and detection, the detection technique must minimize the upper bound on support-recovery error-rate computed in the equation (6.19), termed as MSRE criteria.

6.6 MSRE criteria based detection

In this section, the MSRE criteria derived in subsection 6.5.1 is utilised to develop an efficient detection technique for MBM-mMIMO, which ensures

6.6. MSRE CRITERIA BASED DETECTION

minimum SRE. Based on the inequality constraint (6.19), the symbol detection problem at the BS is formulated as

$$\begin{aligned} \min_{\hat{x}_{j,i}} & \|\mathbf{y}_j - \mathbf{H}_j \hat{\mathbf{x}}_j\|_2^2 \\ \text{s.t } & 2(1-M) \left(1 - \frac{3\hat{x}_{j,i}^2}{6v + 2c\hat{x}_{j,i}}\right) = 0 \end{aligned} \quad (6.20)$$

To solve problem (6.20) which exploits sparsity by incorporating SRE as a constraint, Lagrangian function $\phi(x_{j,i}, \kappa_1)$ is formed as $\phi(x_{j,i}, \kappa_1) = g(x_{j,i}) + \kappa_1 f(x_{j,i})$, where $g(x_{j,i}) = \|\mathbf{y}_j - \mathbf{H}_j \mathbf{x}_j\|_2^2$, $f(x_{j,i}) = 2(1-M) \left(1 - \frac{3x_{j,i}^2}{6v + 2cx_{j,i}}\right)$. Solving (6.20), the symbol update strategy for the proposed MEPD is obtained as $\hat{x}_{j,i}^{(k+1)} = \mathbb{P}_{\mathcal{M}} \left(\hat{x}_{j,i}^{(k)} - \kappa_2 \nabla_i \phi(\hat{x}_{j,i}, \mu_1) \right)$. Thus, the i^{th} symbol of the j^{th} user, $\hat{x}_{j,i}$ is updated based on a stochastic gradient descent method. $\mathbb{P}_{\mathcal{M}}(\cdot)$ projects the updated symbol vector to the nearest MBM constellation. Although MEPD considers the multi-user interference as noise, it neither performs an exhaustive search for each user nor updates the symbol using a greedy approach. Moreover, to achieve a fast convergence rate, MEPD keeps track of the global best cost Δ and symbol vector $\hat{\mathbf{u}}$. After maximum iteration, L , the global best symbol vector $\hat{\mathbf{u}}$ is declared as the final estimated output of the proposed detection technique. The pseudocode and receiver block diagram of MEPD are given in Algorithm 6.2 and Fig. 6.12, respectively.

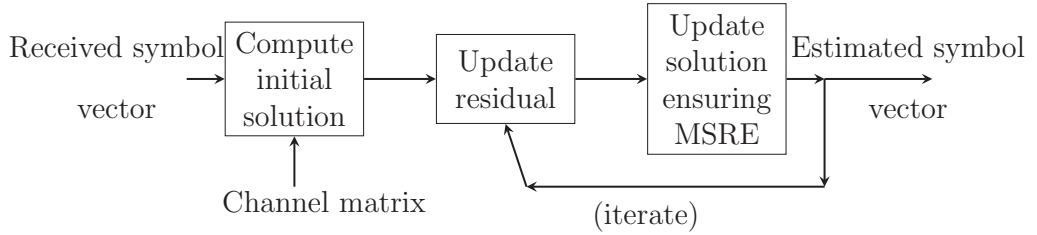


Figure 6.12: Block Diagram of MEPD Technique.

MEPD is an iterative technique which does not explore the MBM constellations. However, performance of MEPD is improved in MEPDRS with restricted search by introducing a restricted exploration in a comparatively

Algorithm 6.2 Proposed MEPD algorithm

```

1: Inputs:  $\hat{\mathbf{x}}^{(1)}$ ,  $L$ ,  $\mathbf{H}$ ,  $\mathbf{y}$ ,  $\mu_1$ ,  $\mu_2$ ,  $\mu_{max}$ ,  $k = 1$ ,  $M$ ,  $N_t$ 
2: Output:  $\hat{\mathbf{u}}$ 
3: for  $j = 1 : N_t$  do
4:   Compute residual  $\mathbf{r} = \mathbf{H}_j^+ \mathbf{y}$ 
5:   Choose index  $l = \arg \max_{i=1,2,\dots,M} |r_i|$ 
6:   Update  $\hat{x}_{j,l} = (\|\mathbf{h}_{j,l}\|_2^2)^{-1} \mathbf{h}_{j,l}^+ \mathbf{y}$ 
7: end for
8: Update residual  $\mathbf{r} = \mathbf{y} - \mathbf{H}\hat{\mathbf{x}}$ 
9:  $\Delta = \|\mathbf{r}\|_2^2$ 
10: while  $k \leq L$  do
11:   for  $j = 1 : N_t$  do
12:      $\mathbf{y}_j = \mathbf{r} + \mathbf{H}_j \hat{\mathbf{x}}_j^{(k)}$ 
13:      $l_j \in \mathcal{V}_j$ 
14:     Update  $\hat{x}_{j,l_j}^{(k+1)} = \mathcal{P}_{\mathcal{M}}(\hat{x}_{j,l_j}^{(k)} - \mu_2 \nabla_l \phi(\hat{x}_{j,l_j}, \mu_1))$ 
15:      $\mathbf{c}^{(k)} = \mathbf{r}^{(k)} + \mathbf{H}_j(\hat{\mathbf{x}}_j^{(k)} - \hat{\mathbf{x}}_j^{(k+1)})$ 
16:     if  $\Delta > \|\mathbf{c}^{(k)}\|_2^2$  then
17:        $\mathbf{r}^{(k+1)} = \mathbf{c}^{(k)}$ 
18:        $\Delta = \|\mathbf{c}^{(k)}\|_2^2$ 
19:        $\hat{\mathbf{u}}_j = \hat{\mathbf{x}}_j^{(k+1)}$ 
20:     end if
21:      $\hat{\mathbf{x}}_j^{(k+1)} = \hat{\mathbf{u}}_j$ 
22:   end for
23:    $k = k + 1$ 
24: end while

```

Algorithm 6.3 Proposed MEPDRS algorithm

```

1: Inputs:  $\hat{\mathbf{x}}^{(1)}$ ,  $L$ ,  $\mathbf{H}$ ,  $\mathbf{y}$ ,  $\mu_1$ ,  $\mu_2$ ,  $k = 1$ ,  $M$ ,  $N_t$ 
2: Output:  $\hat{\mathbf{u}}$ 
3: for  $j = 1 : N_t$  do
4:   Compute residual  $\mathbf{r} = \mathbf{H}_j^+ \mathbf{y}$ 
5:   Choose index  $l = \arg \max_{i=1,2,\dots,M} |r_i|$ 
6:   Update  $\hat{x}_{j,l} = (\|\mathbf{h}_{j,l}\|_2^2)^{-1} \mathbf{h}_{j,l}^+ \mathbf{y}$ 
7: end for
8: Update residual  $\mathbf{r} = \mathbf{y} - \mathbf{H}\hat{\mathbf{x}}$ 
9:  $\Delta = \|\mathbf{r}\|_2^2$ 
10: while  $k \leq L - 1$  do
11:   for  $j = 1 : N_t$  do
12:      $\mathbf{y}_j = \mathbf{r} + \mathbf{H}_j \hat{\mathbf{x}}_j^{(k)}$ 
13:      $l_j \in \mathcal{V}_j$ 
14:     Update  $\hat{x}_{j,l_j}^{(k+1)} = \mathbb{P}_{\mathcal{M}}(\hat{x}_{j,l_j}^{(k)} - \mu_2 \nabla_l \phi(\hat{x}_{j,l_j}, \mu_1))$ 
15:     for  $i = 1 : \#\mathcal{N}_{RS}$  do
16:        $\mathbf{c}^{(k)} = \mathbf{r}^{(k)} + \mathbf{H}_j(\hat{\mathbf{x}}_j^{(k)} - \hat{\mathbf{x}}_{i \in \mathcal{N}_{RS}}^{(k+1)})$ 
17:       if  $\Delta > \|\mathbf{c}^{(k)}\|_2^2$  then
18:          $\mathbf{r}^{(k+1)} = \mathbf{c}^{(k)}$ 
19:          $\Delta = \|\mathbf{c}^{(k)}\|_2^2$ 
20:          $\hat{\mathbf{u}}_j = \hat{\mathbf{x}}_j^{(k+1)}$ 
21:       end if
22:     end for
23:      $\hat{\mathbf{x}}_j^{(k+1)} = \hat{\mathbf{u}}_j$ 
24:   end for
25:    $k = k + 1$ 
26: end while
27: for  $j = 1 : N_t$  do  $\mathbf{y}_j = \mathbf{r} + \mathbf{H}_j \hat{\mathbf{x}}_j^{(k)}$ 
28:   for  $i = 1 : \#\mathcal{M}$  do
29:      $\mathbf{c}_i^{(k)} = \mathbf{r}^{(k)} + \mathbf{H}_j(\hat{\mathbf{x}}_j^{(k)} - \hat{\mathbf{x}}_{i \in \mathcal{M}}^{(k+1)})$ 
30:   end for
31:    $l = \arg \min_{i \in \mathcal{M}} \mathbf{c}_i^{(k)}$ 
32:   if  $\Delta > \|\mathbf{c}_l^{(k)}\|_2^2$  then
33:      $\mathbf{r}^{(k+1)} = \mathbf{c}_l^{(k)}$ 
34:      $\Delta = \|\mathbf{c}_l^{(k)}\|_2^2$ 
35:      $\hat{\mathbf{u}}_j = \mathbf{x}_l^{(k+1)}$ 
36:   end if
37: end for

```

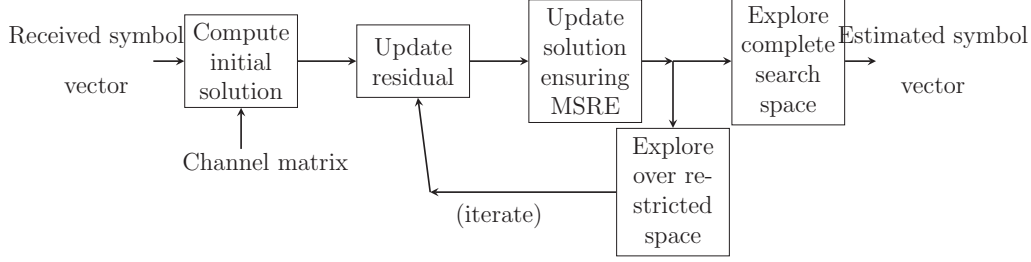


Figure 6.13: Block Diagram of MEPDRS Technique.

small search space. The search space for restricted search (RS) is defined as $\mathcal{N}_{RS} = \{\hat{\mathbf{x}}_i, \mathbf{s}_i \in \mathcal{M} | \mathcal{D}(\tilde{\mathbf{s}}_i, \hat{\mathbf{x}}_i) = 1\}$, where $\hat{\mathbf{x}}_i$ is the MEPD estimated symbol vector for the i^{th} user. MEPDRS explores the least number of vectors during RS when $\mathcal{D}(\tilde{\mathbf{s}}_i, \hat{\mathbf{x}}_i) = 1$. Hence, exploration with RS requires less computational cost ($\mathcal{O}(\#\mathcal{A})$) as compared to the computational cost ($\mathcal{O}(2^{N_{RF}} \#\mathcal{A})$) of exploration over all the MBM constellations. Finally, to avoid getting stuck into a local optima due to RS, MEPDRS performs a single exploration over all MBM constellations. However, multiple explorations over all MBM constellations do not substantially improve the BER performance of MEPDRS, rather increasing the computational complexity. The pseudocode and receiver block diagram of MEPDRS are shown in Algorithm 6.3 and Fig. 6.13, respectively. Moreover, theoretical upper bound on the probability of error of MEPDRS is computed as [88] $P_e \leq \left(\frac{1-\kappa(c)}{2}\right)^{N_r} \sum_{k=0}^{N_r-1} \binom{N_r+k-1}{k} \left(1 + \frac{\kappa(c)}{2}\right)^k$, where $\kappa(c) = \sqrt{\frac{\tilde{\gamma}}{2N_r + \tilde{\gamma}}}$ and $\tilde{\gamma}$ is the average received SNR.

6.6.1 Simulation results and discussion

The computational complexity and BER performances of MEPD and MEPDRS are analysed and compared with MMSE, IESP and IIC detection techniques in this section.

Computational complexity: The computational complexities of ML, MMSE, IESP, IIC, MEPD and MEPDRS are listed in Table 6.2 in terms of the number of FLOPs. $T = \#\mathcal{M}$ denotes cardinality of MBM constellation set \mathcal{M} .

It is observed from Table 6.2 that a single iteration of IIC significantly

Table 6.2: Computational complexity

Detection tech- niques	FLOPs
ML	$(2^{N_{RF}} \#\mathcal{A})^{N_t}$
MMSE [89]	$4N_t^3 + 8N_t^2 + 4(N_t^2 + N_t)N_r$
IESP [48]	$(L+1)N_tN_rM + 4(L+1)N_t^2N_r + 2(L+1)N_t^3 + (2L+3)N_tN_r + (2L+1)N_r$
IIC [47]	$3LTN_tN_rM + 3N_t^2N_r + LN_t^2 + 2LN_tN_r + N_r(N_t + 1)$
MEPD	$(2L+1)N_tN_rM + 0.5N_t^2N_r + (6L+2.5)N_tN_r + ((M+2T+15)L+3)N_t + 2N_r$
MEPDRS	$(2L + 3MT - 1)N_tN_rM + 0.5N_t^2N_r + (6L - 0.5)N_tN_r + ((M+2T+15)L - ((T+1)M + 2(T+7)))N_t + 2N_r$

requires more number of FLOPs compared to IESP, MEPD and MEPDRS. However, the computational complexities of IESP and MEPDRS are comparable.

BER Performance: In Fig. 6.14, the BER performances of MEPD and MEPDRS are compared with MMSE, IESP and IIC detection techniques for an MBM-mMIMO system with $N_r = 128$, $N_t = 16$ and $N_{RF} = 4$. It is observed that MPED outperforms MMSE, IESP and IIC with the same number of iterations. An SNR gain of approximately 1 dB is achieved in MEPD over IIC with the same number of iterations ($L=2$) for a targeted BER of 4×10^{-4} . It is already proved from Table 6.2 that a single iteration of MEPD requires substantially less number of computations as compared to a single iteration of IIC. As mentioned in Section 6.6, MEPDRS is designed to outperform MEPD for the same number of iterations and achieves an SNR gain of approx. 0.5 dB over MEPD for a targeted BER of 3×10^{-4} .

In Fig. 6.15, the BER performance of MEPDRS is compared for large

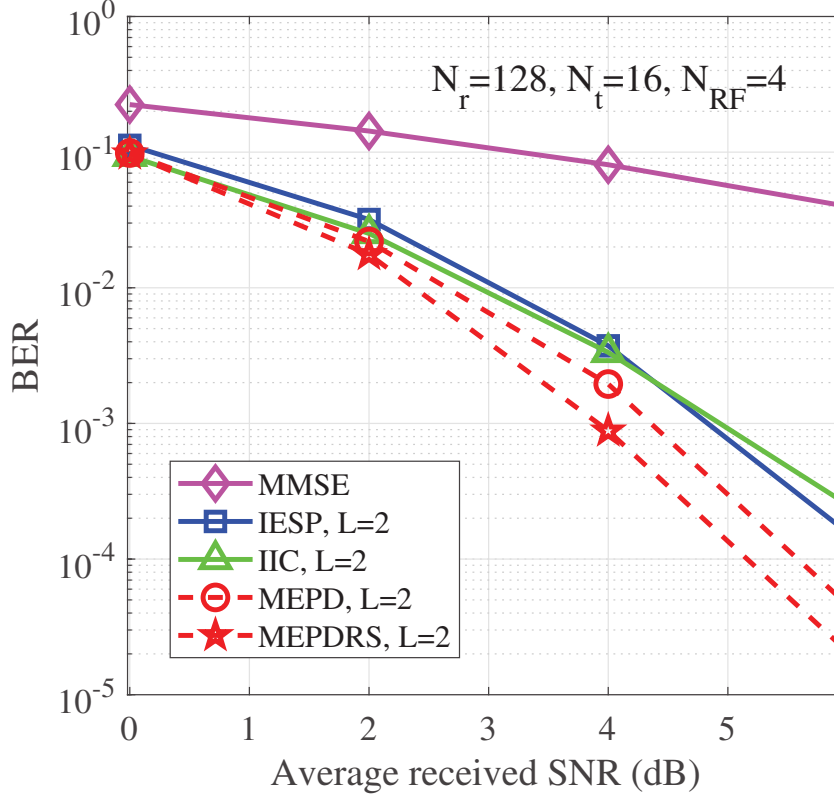


Figure 6.14: BER performance comparison of MEPD with MMSE, IESP and IIC.

number of iterations with ML, IIC and IESP. It is found that the performances of IESP and IIC do not improve after $L = 20$ and $L = 4$ respectively. Fig. 6.15 depicts that MEPD with $L=4$ outperforms IESP with $L = 20$, with an SNR gain of 0.6 dB for a targeted BER of 3×10^{-3} . MEPDRS with $L = 4$ reaches hypothetical lower bound (LB), giving IIC equivalent BER performance. Moreover, MEPDRS with $L = 4$ yields near-ML performance for MBM-mMIMO with $N_r = 128, N_t = 16$ and $N_{RF} = 4$. Hence, it is proved from Figs. 6.14-6.15 and Table 6.2 that MEPD and MEPDRS are more viable candidates for uplink symbol detection in MBM-mMIMO as compared to MMSE, IESP and IIC. For $L \leq 2$, both MEPD and MEPDRS outperform IIC. For $L \geq 3$, MEPDRS requires comparatively less number of

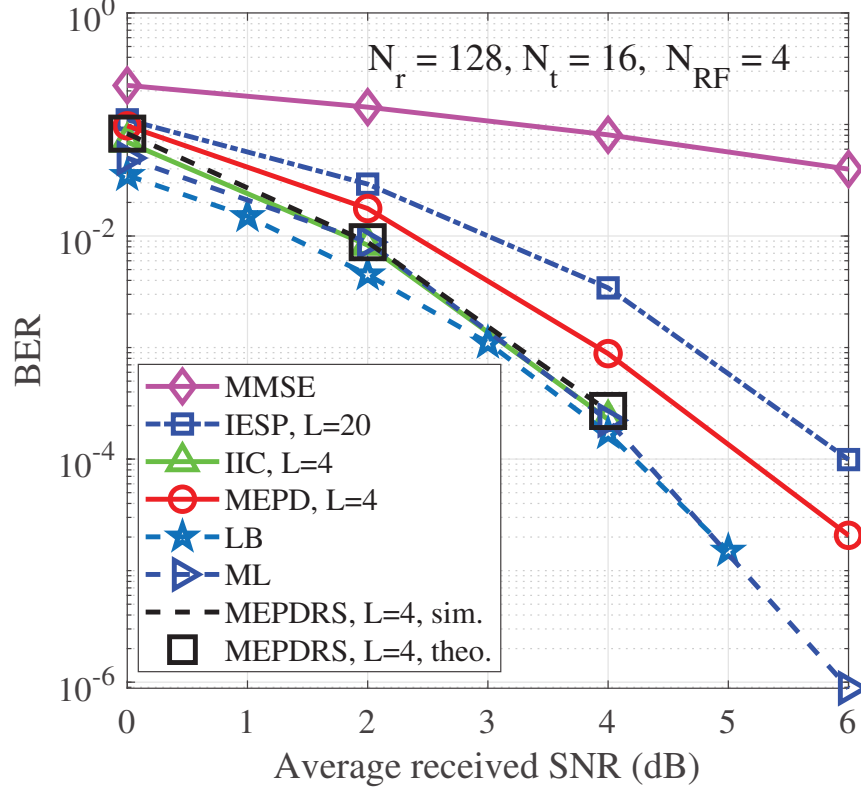


Figure 6.15: BER performance comparison of MEPDRS with MMSE, IESP and IIC.

FLOPs than IIC to achieve equivalent BER performance.

The comparison of BER performance among contending algorithms is shown in Figs. 6.16-6.17 for different number of RF mirrors for MBM-mMIMO systems with $N_r = 128$ and $N_t = 16$. It is drawn from Figs. 6.16-6.17 that both MEPD and MEPDRS significantly outperform IESP and IIC for $N_{RF} = 2$, $N_{RF} = 3$ and $N_{RF} = 4$. The simulation results in Figs. 6.16-6.17 validate the superiority of MEPD and MEPDRS over IESP and IIC for any number of RF mirrors placed before the transmit antennas. It is also observed from Figs. 6.16-6.17 that the performance gains of MEPD and MEPDRS over IIC are more significant when the number of RF mirrors increases in the system. It concludes the superiority of MEPD and MEPDRS

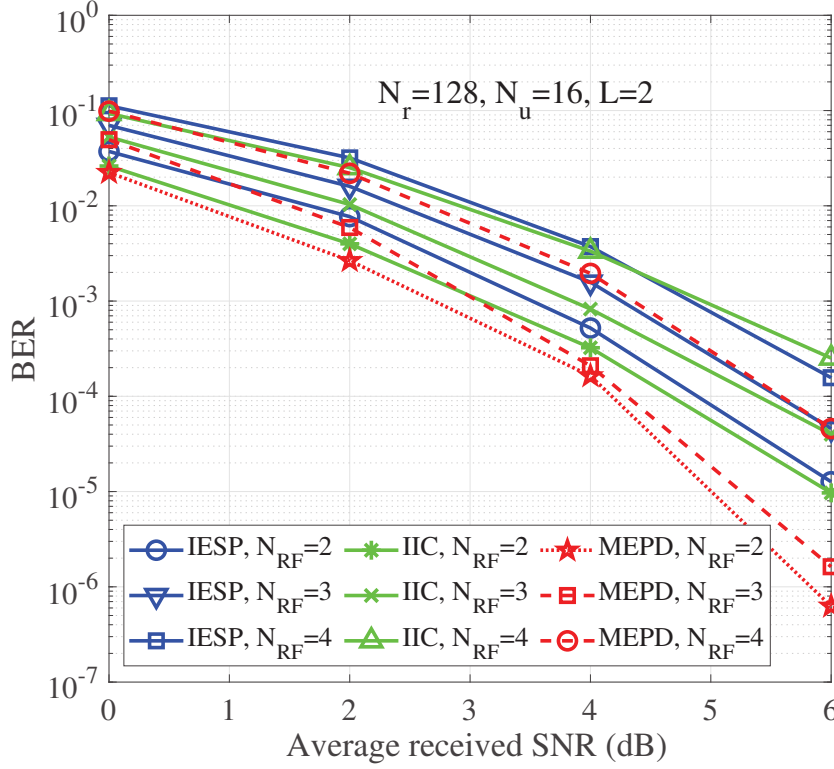


Figure 6.16: BER performance comparison of MEPD, IESP and IIC for different number of RF mirrors.

over IESP and IIC for symbol detection in MBM-mMIMO incorporated in high data rate wireless communications.

In Fig. 6.18, the BER performances of MEPD, MEPDRS, IESP and IIC are analyzed for different numbers of BS antennas. It is depicted in Fig. 6.18 that IIC with the same number of iterations $L=2$ requires a greater number of BS antennas to achieve BER equivalent to MEPD and MEPDRS. As shown in Fig. 6.18, IIC achieves BER of 10^{-4} with $N_r = 150$ BS antennas; however, MEPD and MEPDRS require only $N_r = 135$ and $N_r = 130$ respectively BS antennas to achieve approximately equal BER performance.

It is observed in Figs. 6.19-6.20, MEPD and MEPDRS require less number of FLOPs compared to IIC for the same number of iterations as well as the number of BS antennas. As shown in Fig. 6.20, IESP is computationally

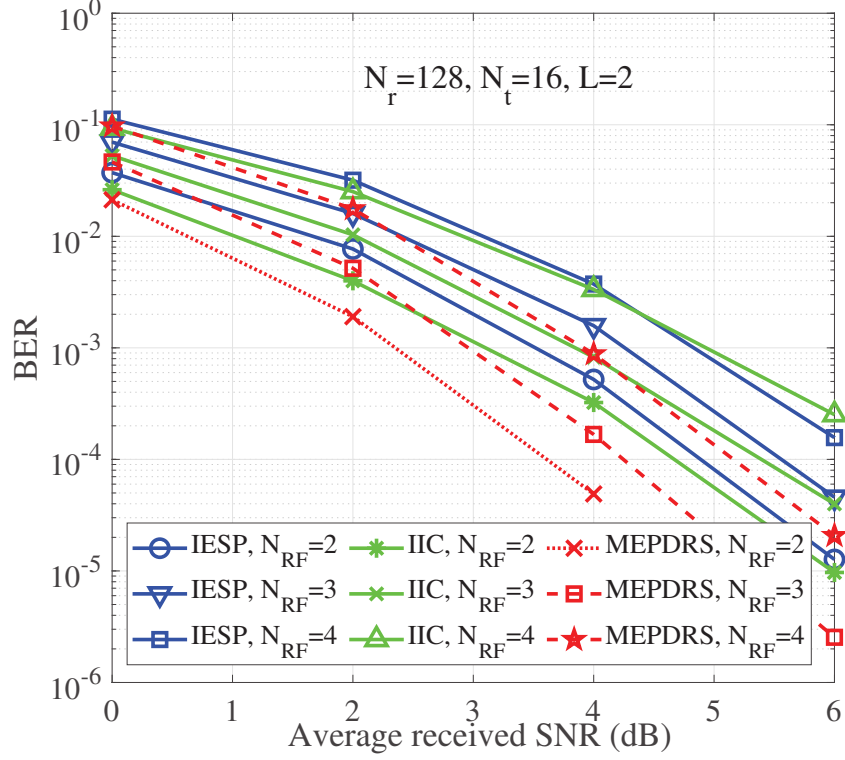


Figure 6.17: BER performance comparison of MEPDRS, IESP and IIC for different number of RF mirrors.

comparable to MEPDRS in terms of the number of BS antennas. It is already proved from Fig. 6.15 that the performance of IESP does not significantly increase with the number of iterations.

Fig. 6.21 shows that IIC requires more number of FLOPs as compared to both MEPD and MEPDRS for different system configurations with different RF mirrors. This proves the cost-effectiveness of MEPD and MEPDRS in terms of less BS antenna requirement, RF mirrors and computational complexity.

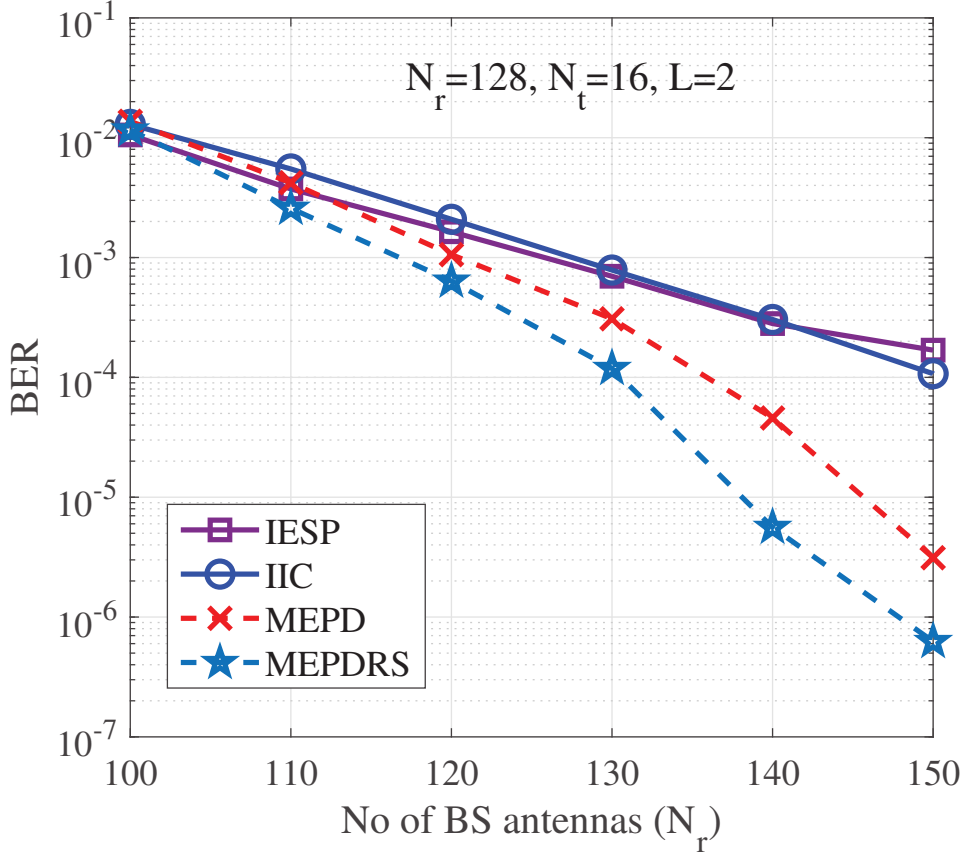


Figure 6.18: BER performance comparison of MEPD, MMSE, IESP and IIC with different number of BS antennas.

6.7 Summary

In this Chapter, low complexity MBM-mMIMO symbol detection techniques, MEPD and MEPDRS, are proposed. MEPD exploits MSRE criteria and sequentially detects the symbol vector transmitted by each user. The error rate performance of MEPD is further enhanced with exploration in a restricted search space. Both MEPD and MEPDRS detection techniques are analysed through simulations, which demonstrate substantial viability over state-of-the-art MBM-mMIMO symbol detection techniques in terms of error rate performance as well as the computational complexity. Hence, MEPD and

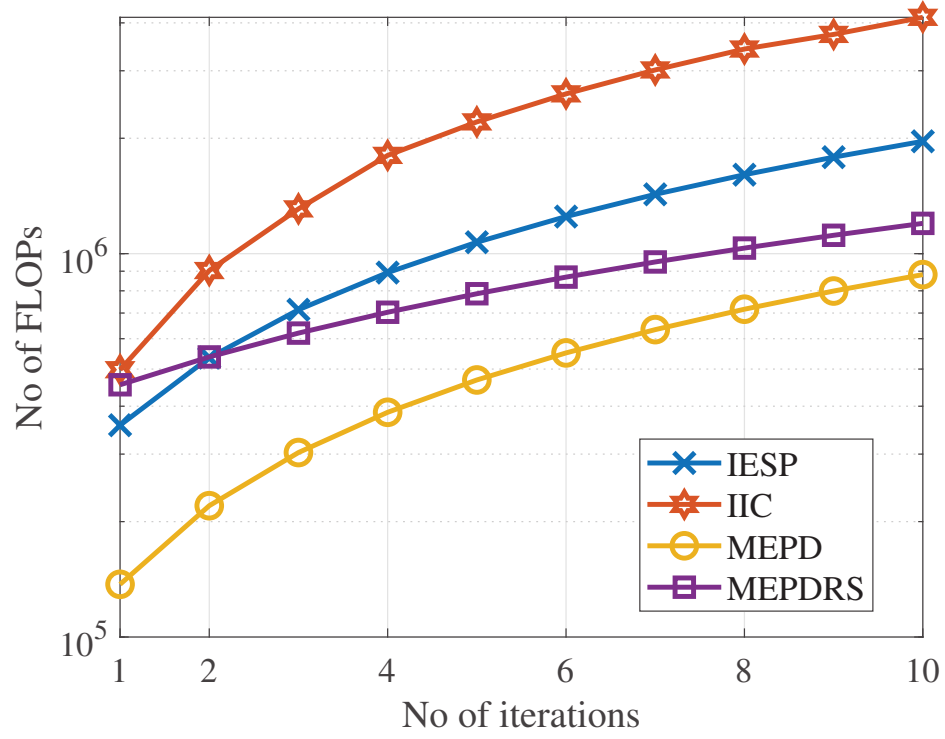


Figure 6.19: Comparison of computational complexity of contending detection techniques for different number of iterations.

MEPDRS are promising candidates for uplink symbol detection in MBM-mMIMO systems for beyond 5G and 6G wireless communication systems.

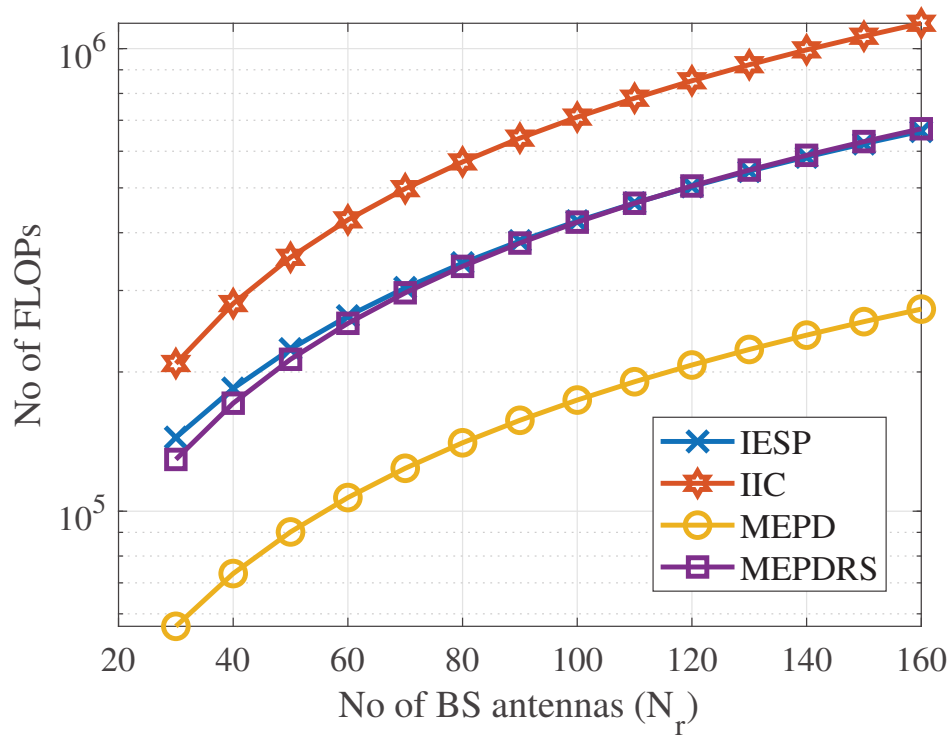


Figure 6.20: Comparison of computational complexity of contending detection techniques for different number of BS antennas.

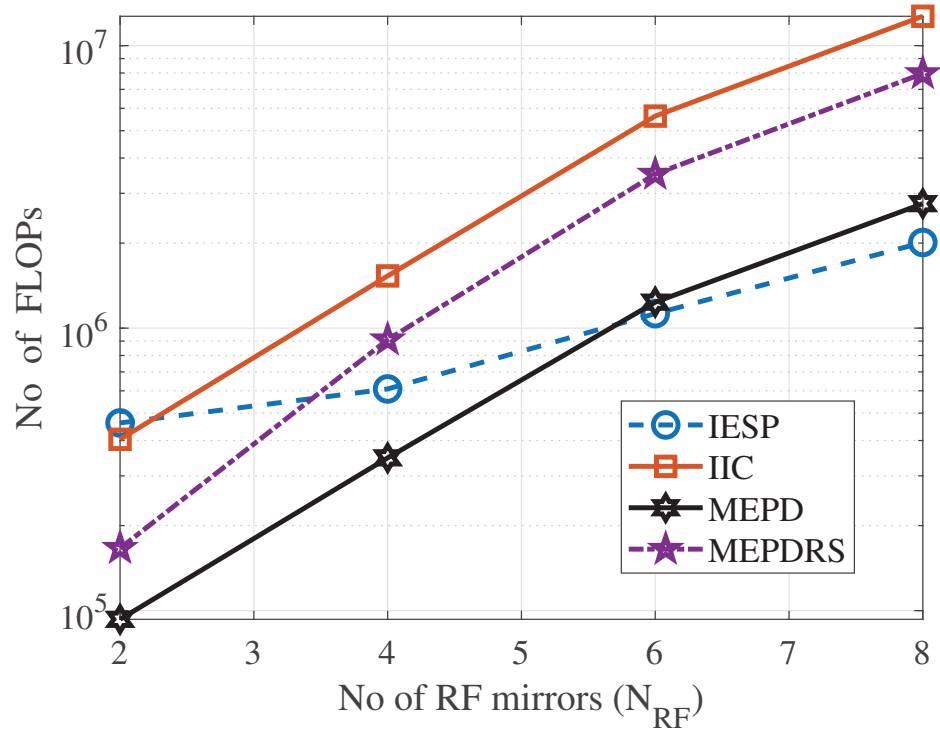


Figure 6.21: Computational complexity of contending techniques with number of RF mirrors.

Chapter 7

Conclusion and Future Work

An in-depth study on the design and analysis of novel detection techniques for uplink mMIMO systems is accomplished in this thesis. This chapter presents the conclusions, the key points of this thesis and the future directions of the work.

7.1 Conclusion

This thesis has extensively studied the design and analysis of novel detection techniques for uplink mMIMO systems. The proposed novel techniques have been presented in this thesis in six chapters.

In the second chapter, evolutionary algorithms are explored for symbol detection, and a novel MFA is proposed for symbol detection in uplink large MIMO systems. The proposed MFA utilises a probabilistic approach to estimate the symbols and is capable of maintaining a balance between exploration and exploitation. Simulation results and convergence analysis of MFA prove the viability of the algorithm compared against several conventional large MIMO systems.

In the third chapter, AMI and MII techniques are investigated for uplink massive MIMO systems. Two novel algorithms, pseudo stationary iteration-based HA and nonstationary iteration based ILS are proposed for uplink

mMIMO detection. Analyses on the convergence of the proposed algorithms are also performed. Simulations are carried out to verify HA and ILS algorithms' superiority compared to several state-of-the-art mMIMO detection techniques. Both HA and ILS are capable of reaching a near-MMSE solution with comparatively less computational complexity than several state-of-the-art detection algorithms. Analyses on the convergences of HA and ILS are also performed.

In the fourth chapter, RFOD is proposed for mMIMO systems with a large number of users. RFOD utilizes a quality metric for ordering the symbols before detection and applies RFM to improve the estimated solution. The convergence of RFOD is theoretically analyzed, which is further corroborated through simulation results. RFOD outperforms several state-of-the-art uplink mMIMO detectors, including MMSE, even when the users scale-up in mMIMO systems.

DL-based techniques are surveyed in the fifth chapter. A sparsely connected SRN is proposed for uplink mMIMO systems, which obtains better performance in terms of computational complexity and BER compared to iterative detection techniques.

Finally, existing detectors for systems are explored in the sixth chapter, and two low complexity detectors, SID and MEPDRS are proposed for symbol detection in uplink MBM-mMIMO systems. SID transforms the MBM-mMIMO symbol detection as graph traversal problem and outperforms several existing detectors for MBM-mMIMO systems. MEPDRS uses a projected gradient descent-based update rule formed from MSRE constraint and is able to achieve near-ML BER performance.

In conclusion, MFA is found to obtain superior performance than several state-of-the-art detectors for large MIMO systems. However, MFA is not suitable for symbol detection in mMIMO systems due to degraded BER performance and high computational complexity. As an alternative, stationary and pseudo-stationary iteration based detection techniques, ILS and HA outperform several existing detectors for mMIMO systems. However,

they can only reach near-MMSE performance and show suboptimal performance when users scale up in the system. RFOD is a promising solution for symbol detection in mMIMO systems with a large number of users. However, being a model-based approach, it is capable of providing fixed performance benefits based on the predefined mathematical model. Hence, deep unfolding based detection SRN is proposed which outperforms precedent detectors and provides superior performance than previously proposed detectors for an mMIMO system with a large number of users. While SRN is a promising detection technique for mMIMO systems, the performance benefits of mMIMO systems improve when incorporated with MBM. Having said that, SRN shows degraded BER performance when deployed for sparse transmitted vector detection in MBM-mMIMO systems. Consequently, SID and MEPDRS are proposed, which outperforms several competing detection techniques for MBM-mMIMO systems. The superior BER performance and improved computational complexities of the algorithms proposed in the thesis corroborate that the proposed detection algorithms are convenient and promising for the practical realisation of beyond 5G and 6G wireless communication systems.

7.2 Limitations and Future Work

As future work, the algorithms proposed and the results discussed in the thesis can be extended as follows.

- Swarm intelligence-based algorithms are promising for symbol detection in large MIMO systems. The MFA algorithms proposed in Chapter 2 outperforms several swarm intelligence based detection algorithms for large MIMO systems. However, the computational complexity of MFA presented in Chapter 2 is relatively high for symbol detection in mMIMO systems. Further reduction in the computational complexity of MFA for mMIMO systems remains an open problem.

- DL techniques outperform conventional AMI and MII techniques. However, traditional DL techniques possess high memory requirements and training time. Model-driven DL techniques fuse principled algorithms with DL, giving improved performance and computational complexity. Iterative algorithms proposed in this thesis are constrained to specific mathematical models with non-trainable parameters. They may be explored to design computationally efficient model-driven DL networks for mMIMO systems.
- Fixed-point analysis (FPA) of the algorithms proposed in this is crucial for practical implementation of the proposed algorithms. Fixed point refers to the fixed number of digits after the decimal point. Hence, FPA plays a crucial role in the successful hardware realization of the proposed algorithms to maintain a fixed precision of the estimated solution. Hence, FPA of the proposed detection algorithm needs to be completed before their hardware implementation.
- The proposed algorithms can be extended to cell-free mMIMO (CF-mMIMO) systems targetted for beyond 5G wireless communications. CF-mMIMO system is an energy-efficient and cost-effective technology for realising high-speed data communication in 6G wireless communication systems. In CF-mMIMO, a massive number of individually controllable access points (APs) are deployed to simultaneously serve a comparatively few numbers of user equipments (UEs) in a time division duplex (TDD) mode. As a massive number of APs are deployed in CF-mMIMO, the distance between an arbitrary UE and the closest AP substantially reduces, resulting in approximately uniform quality of service (QoS) for all users in comparison with mMIMO systems. The proposed detection techniques show promising results for low complexity detection in conventional mMIMO systems. Hence, this project should explore detection techniques proposed in this thesis and possibly extend for low complexity symbol detection in uplink CF-mMIMO

systems.

- Quadrature channel modulation (QCM) is an emerging area of research in wireless communications. Quadrature channel modulation is a novel modulation technique that combines QSM with MBM. Consequently, QCM has better spectral efficiency than both MBM and QSM. QSM exploits the in-phase and quadrature components of the information symbols and transfers additional information through the channel states generated through RF mirrors. Furthermore, when incorporated with mMIMO, QSM-mMIMO yields far superior data rates than mMIMO, QSM-mMIMO and MBM-mMIMO. As QCM-mMIMO fuses QSM-mMIMO and MBM-mMIMO, the symbol detection at the BS in QCM-mMIMO is comparatively challenging due to the sparse nature of the transmitted symbol vector and interuser interference. Hence, it will be interesting to investigate the performance of proposed MBM-mMIMO detection algorithms for QCM-mMIMO systems.
- The achievable data rate in diffusion-based molecular communication is slow as diffusion plays the primary role in information propagation. Consequently, communication with a massive number of molecular transmitters and receivers provides a superior data rate than conventional molecular communication. Hence, the algorithms proposed in this thesis can be explored and investigated for low complexity detection in molecular mMIMO communication.
- Recent developments in meta-materials make the intelligence reflecting surfaces (IRS) emerge as a suitable solution for high-speed communication. IRS aided mMIMO systems are capable of reconfiguring the phase shifts in real-time, providing high link reliability with high spectral efficiency for 5G and beyond wireless communication systems. The mMIMO detection algorithms in this thesis are yet to be studied for IRS assisted mMIMO systems. It remains an exciting area of future research.

- The proposed detected algorithms are yet to be investigated for index modulation and quadrature spatial modulation (QSM) based symbol detection in uplink mMIMO systems. QSM is a novel modulation technique that extends the conventional spatial modulation (SM) constellation using real and imaginary dimensions. Hence, when incorporated with mMIMO, it provides improved throughput as compared to conventional SM-mMIMO systems. However, the transmitted symbol vector in SM-mMIMO is sparse, making the symbol detection more challenging in uplink QSM-mMIMO systems. Consequently, the algorithms proposed in this thesis for MBM-mMIMO systems can be further extended for QSM-mMIMO systems for symbol detection in uplink QSM-mMIMO systems.
- The novel detectors proposed in this thesis for mMIMO can further be extended for visible light communication (VLC). With the extensive use of light-emitting diodes (LED), visible light communication (VLC) has emerged as a promising solution for high speed and short-range communication. When multiple LEDs are deployed in a coordinated multi-point network, mMIMO-VLC provides several advantages such as low electromagnetic interference, high security, and high spectral efficiency as compared to its radio-frequency counterpart in conventional mMIMO systems. Consequently, the study of the proposed detectors for mMIMO-VLC systems remains a future research direction.

References

- [1] L. Lu, G. Y. Li, A. L. Swindlehurst, A. Ashikhmin, and R. Zhang, “An overview of massive MIMO: Benefits and challenges,” *IEEE Journal of Selected Topics in Signal Processing*, vol. 8, no. 5, pp. 742–758, 2014.
- [2] F. Rusek, D. Persson, B. K. Lau, E. G. Larsson, T. L. Marzetta, O. Edfors, and F. Tufvesson, “Scaling up MIMO: Opportunities and challenges with very large arrays,” *IEEE Signal Processing Magazine*, vol. 30, no. 1, pp. 40–60, 2012.
- [3] J. G. Andrews, S. Buzzi, W. Choi, S. V. Hanly, A. Lozano, A. C. Soong, and J. C. Zhang, “What will 5G be?” *IEEE Journal on Selected Areas in Communications*, vol. 32, no. 6, pp. 1065–1082, 2014.
- [4] E. G. Larsson, O. Edfors, F. Tufvesson, and T. L. Marzetta, “Massive MIMO for next generation wireless systems,” *IEEE Communications Magazine*, vol. 52, no. 2, pp. 186–195, 2014.
- [5] A. K. Khandani, “Media-based modulation: Converting static Rayleigh fading to AWGN,” *2014 IEEE International Symposium on Information Theory*, pp. 1549–1553, 2014.
- [6] M. Wu, B. Yin, G. Wang, C. Dick, J. R. Cavallaro, and C. Studer, “Large-scale MIMO detection for 3GPP LTE: Algorithms and FPGA implementations,” *IEEE Journal of Selected Topics in Signal Processing*, vol. 8, no. 5, pp. 916–929, 2014.

REFERENCES

- [7] E. G. Larsson, “MIMO detection methods: How they work [Lecture notes],” *IEEE Signal Processing Magazine*, vol. 26, no. 3, pp. 91–95, 2009.
- [8] M. Mandloi and V. Bhatia, “Low-complexity near-optimal iterative sequential detection for uplink massive MIMO systems,” *IEEE Communications Letters*, vol. 21, no. 3, pp. 568–571, 2017.
- [9] F. Yang, P. Cai, H. Qian, and X. Luo, “Pilot contamination in massive MIMO induced by timing and frequency errors,” *IEEE Transactions on Wireless Communications*, vol. 17, no. 7, pp. 4477–4492, 2018.
- [10] V. Bhatia and B. Mulgrew, “Non-parametric likelihood based channel estimator for Gaussian mixture noise,” *Signal Processing*, vol. 87, no. 11, pp. 2569–2586, 2007.
- [11] O. Raeesi, A. Gokceoglu, Y. Zou, E. Björnson, and M. Valkama, “Performance analysis of multi-user massive MIMO downlink under channel non-reciprocity and imperfect CSI,” *IEEE Transactions on Communications*, vol. 66, no. 6, pp. 2456–2471, 2018.
- [12] M. Mandloi and V. Bhatia, “Congestion control based ant colony optimization algorithm for large MIMO detection,” *Expert Systems with Applications*, vol. 42, no. 7, pp. 3662–3669, 2015.
- [13] B. Hassibi and B. M. Hochwald, “How much training is needed in multiple-antenna wireless links?” *IEEE Transactions on Information Theory*, vol. 49, no. 4, pp. 951–963, 2003.
- [14] T. L. Marzetta, “BLAST training: Estimating channel characteristics for high capacity space-time wireless,” in *Proceedings of the Annual Allerton Conference on Communication Control and Computing*, vol. 37. Citeseer, 1999, pp. 958–966.
- [15] A. Chockalingam and B. S. Rajan, *Large MIMO systems*. Cambridge University Press, New York, 2014.

REFERENCES

- [16] P. W. Wolniansky, G. J. Foschini, G. Golden, and R. A. Valenzuela, "V-BLAST: An architecture for realizing very high data rates over the rich-scattering wireless channel," in *Signals, Systems, and Electronics, 1998. ISSSE 98. 1998 URSI International Symposium on*. IEEE, 1998, pp. 295–300.
- [17] L. G. Barbero and J. S. Thompson, "Performance of the complex sphere decoder in spatially correlated MIMO channels," *IET Communications*, vol. 1, no. 1, pp. 122–130, 2007.
- [18] T. Datta, N. Srinidhi, A. Chockalingam, and B. S. Rajan, "Random-restart Reactive Tabu Search Algorithm for Detection in Large-MIMO Systems," *IEEE Communications Letters*, vol. 14, no. 12, pp. 1107–1109, 2010.
- [19] P. Som, T. Datta, A. Chockalingam, and B. Sundar Rajan, "Improved large-MIMO detection based on damped belief propagation," in *IEEE Information Theory Workshop 2010, ITW 2010*, 2010, pp. 311–315.
- [20] S. K. Mohammed, A. Chockalingam, and B. S. Rajan, "A low-complexity near-ML performance achieving algorithm for large MIMO detection," in *IEEE International Symposium on Information Theory - Proceedings*, no. 4, 2008, pp. 2012–2016.
- [21] C. Blum and A. Roli, "Metaheuristics in combinatorial optimization: Overview and conceptual comparison," *ACM Computing Surveys (CSUR)*, vol. 35, no. 3, pp. 268–308, 2003.
- [22] A. Das, D. Mandal, S. Ghoshal, and R. Kar, "An efficient side lobe reduction technique considering mutual coupling effect in linear array antenna using bat algorithm," *Swarm and Evolutionary Computation (2017)*, 2017, doi:10.1016/j.swevo.2017.02.004.
- [23] M. J. Islam, M. M. Islam, and A. A. Al Islam, "Intelligent dynamic spec-

REFERENCES

- trum access using hybrid genetic operators,” *Swarm and Evolutionary Computation (2017)*, 2017, doi:10.1016/j.swevo.2017.03.004.
- [24] N. Taspinar and M. Yildirim, “A novel parallel artificial bee colony algorithm and its PAPR reduction performance using SLM scheme in OFDM and MIMO-OFDM systems,” *IEEE Communications Letters*, vol. 19, no. 10, pp. 1830–1833, 2015.
- [25] P. M. Pradhan and G. Panda, “Pareto optimization of cognitive radio parameters using multiobjective evolutionary algorithms and fuzzy decision making,” *Swarm and Evolutionary Computation*, vol. 7, pp. 7–20, 2012.
- [26] R. Eberhart and J. Kennedy, “A new optimizer using particle swarm theory,” in *Micro Machine and Human Science, 1995. MHS’95., Proceedings of the Sixth International Symposium on*. IEEE, 1995, pp. 39–43.
- [27] M. Dorigo and T. Stützle, “The ant colony optimization metaheuristic: Algorithms, applications, and advances,” in *Handbook of metaheuristics*. Springer, 2003, pp. 250–285.
- [28] A. Khan, S. Bashir, M. Naeem, S. I. Shah, and A. Sheikh, “Binary ant colony algorithm for symbol detection in a spatial multiplexing system,” in *International Conference on Unconventional Computation*. Springer, 2007, pp. 115–126.
- [29] K. Khurshid, S. Irteza, and A. A. Khan, “Application of ant colony optimization based algorithm in MIMO detection,” *IEEE Congress on Evolutionary Computation*, pp. pp.1–7, 2010.
- [30] J. K. Lain and J. Y. Chen, “Near-MLD MIMO detection based on a modified ant colony optimization,” *IEEE Communications Letters*, vol. 14, no. 8, pp. 722–724, 2010.

REFERENCES

- [31] J. C. Marinello and T. Abrão, “Lattice reduction aided detector for MIMO communication via ant colony optimisation,” *Wireless Personal Communications*, vol. 77, no. 1, pp. 63–85, 2014.
- [32] A. A. Khan, M. Naeem, and S. I. Shah, “A particle swarm algorithm for symbols detection in wideband spatial multiplexing systems,” in *Proceedings of the 9th annual conference on Genetic and evolutionary computation*. ACM, 2007, pp. 63–69.
- [33] C. Tang, C. Liu, L. Yuan, and Z. Xing, “High precision low complexity matrix inversion based on Newton iteration for data detection in the massive MIMO,” *IEEE Communications Letters*, vol. 20, no. 3, pp. 490–493, 2016.
- [34] L. Fang, L. Xu, and D. D. Huang, “Low complexity iterative MMSE-PIC detection for medium-size massive MIMO,” *IEEE Wireless Communications Letters*, vol. 5, no. 1, pp. 108–111, 2015.
- [35] M. A. Albreem, M. Juntti, and S. Shahabuddin, “Massive mimo detection techniques: A survey,” *IEEE Communications Surveys & Tutorials*, vol. 21, no. 4, pp. 3109–3132, 2019.
- [36] J. Jin, Y. Xue, Y.-L. Ueng, X. You, and C. Zhang, “A split pre-conditioned conjugate gradient method for massive MIMO detection,” in *2017 IEEE International Workshop on Signal Processing Systems (SiPS)*. IEEE, 2017, pp. 1–6.
- [37] H. J. COSTA and V. O. RODA, “A scalable soft Richardson method for detection in a massive MIMO system,” *Networks*, vol. 2, p. 3, 2016.
- [38] X. Qin, Z. Yan, and G. He, “A near-optimal detection scheme based on joint steepest descent and Jacobi method for uplink massive MIMO systems,” *IEEE Communications Letters*, vol. 20, no. 2, pp. 276–279, 2016.

REFERENCES

- [39] B. Yin, M. Wu, J. R. Cavallaro, and C. Studer, “Conjugate gradient-based soft-output detection and precoding in massive MIMO systems,” in *2014 IEEE Global Communications Conference*. IEEE, 2014, pp. 3696–3701.
- [40] C. T. Kelley, *Iterative methods for linear and nonlinear equations*. SIAM, Philadelphia, 1995.
- [41] G. Cocchi, G. Liuzzi, S. Lucidi, M. Sciandrone *et al.*, “On the convergence of steepest descent methods for multiobjective optimization,” *Computational Optimization and Applications*, pp. 1–27, 2020.
- [42] G. Strang, *Linear algebra and learning from data*. Wellesley-Cambridge Press, Massachusetts, 2019.
- [43] H. Zhang, G. Peng, and L. Liu, “Low complexity signal detector based on Lanczos method for large-scale MIMO systems,” in *2016 6th International Conference on Electronics Information and Emergency Communication (ICEIEC)*, 2016, pp. 6–9.
- [44] X. Jing, A. Li, and H. Liu, “A low-complexity Lanczos-algorithm-based detector with soft-output for multiuser massive MIMO systems,” *Digital Signal Processing*, vol. 69, pp. 41–49, 2017.
- [45] C. Xiao, X. Su, J. Zeng, L. Rong, X. Xu, and J. Wang, “Low-complexity soft-output detection for massive MIMO using SCBiCG and Lanczos methods,” *China Communications*, vol. 12, pp. 9–17, 2015.
- [46] L. Dai, X. Gao, X. Su, S. Han, I. Chih-Lin, and Z. Wang, “Low-complexity soft-output signal detection based on Gauss–Seidel method for uplink multiuser large-scale MIMO systems,” *IEEE Transactions on Vehicular Technology*, vol. 64, no. 10, pp. 4839–4845, 2015.
- [47] L. Zhang, M. Zhao, and L. Li, “Low-complexity multi-user detection for MBM in uplink large-scale MIMO systems,” *IEEE Communications Letters*, vol. 22, no. 8, pp. 1568–1571, 2018.

REFERENCES

- [48] B. Shamasundar and A. Chockalingam, "Multiuser media-based modulation for massive MIMO systems," *2017 IEEE 18th International Workshop on Signal Processing Advances in Wireless Communications (SPAWC)*, pp. 1–5, 2017.
- [49] M. K. Kavunkal, S. Jacob, and A. Chockalingam, "Message passing receivers for generalized media-based modulation signals," *IEEE Transactions on Wireless Communications*, vol. 18, no. 5, pp. 2607–2622, 2019.
- [50] M. R. Hestenes, E. Stiefel *et al.*, *Methods of conjugate gradients for solving linear systems*. NBS Washington, DC, 1952, vol. 49, no. 1.
- [51] D. P. Maya and A. C. Kandiyil, "Blind inter carrier interference compensation in MIMO SC-IFDMA system using firefly algorithm," *AEU-International Journal of Electronics and Communications*, vol. 70, no. 6, pp. 857–865, 2016.
- [52] H. Su, Y. Cai, and Q. Du, "Firefly-algorithm-inspired framework with band selection and extreme learning machine for hyperspectral image classification," *IEEE Journal of Selected Topics in Applied Earth Observations and Remote Sensing*, vol. 10, no. 1, pp. 309–320, 2017.
- [53] S. Ranganathan, M. S. Kalavathi *et al.*, "Self-adaptive firefly algorithm based multi-objectives for multi-type facts placement," *IET Generation, Transmission & Distribution*, vol. 10, no. 11, pp. 2576–2584, 2016.
- [54] X. S. Yang, "Firefly algorithm, stochastic test functions and design optimisation," *International Journal of Bio-Inspired Computation*, vol. 2, no. 2, pp. 78–84, 2010.
- [55] M. C. Goldberg, *Luminescence Applications: in Biological, Chemical, Environmental, and Hydrological Sciences*. ACS Publications, 1989.
- [56] I. Fister, X.-S. Yang, and J. Brest, "A comprehensive review of firefly algorithms," *Swarm and Evolutionary Computation*, vol. 13, pp. 34–46, 2013.

REFERENCES

- [57] T. H. Cormen, C. E. Leiserson, R. L. Rivest, and C. Stein, *Introduction to algorithms*. MIT press, 2009.
- [58] G. H. Golub and C. F. Van Loan, *Matrix computations*. Johns Hopkins University Press Baltimore, 2012, vol. 3.
- [59] G. L. Turin, “The characteristic function of hermitian quadratic forms in complex normal variables,” *Biometrika*, vol. 47, no. 1/2, pp. 199–201, 1960.
- [60] M. K. Simon and M.-S. Alouini, *Digital Communication over Fading Channels*. John Wiley & Sons. 2005, vol. 95.
- [61] A. Khan, M. Naeem, S. Bashir, and S. Shah, “Optimized detection in multi-antenna system using particle swarm algorithm,” in *Third International Conference on Intelligent Systems*, 2006, pp. 25–27.
- [62] A. A. Khan, S. Bashir, M. Naeem, S. I. Shah, and X. Li, “Symbol detection in spatial multiplexing system using particle swarm optimization meta-heuristics,” *International Journal of Communication Systems*, vol. 21, no. 12, pp. 1239–1257, 2008.
- [63] H. Wang, W. Wang, X. Zhou, H. Sun, J. Zhao, X. Yu, and Z. Cui, “Firefly algorithm with neighborhood attraction,” *Information Sciences*, vol. 382, pp. 374–387, 2017.
- [64] C. B. M. J. J. Dongarra, J. R Bunch and G. W. Stewart, “Linpack user’s guide,” SIAM, 1979.
- [65] X. Gao, L. Dai, Y. Ma, and Z. Wang, “Low-complexity near-optimal signal detection for uplink large-scale MIMO systems,” *Electronics Letters*, vol. 50, no. 18, pp. 1326–1328, 2014.
- [66] T. L. Narasimhan and A. Chockalingam, “Channel hardening-exploiting message passing (CHEMP) receiver in large-scale MIMO systems,”

REFERENCES

- IEEE Journal of Selected Topics in Signal Processing*, vol. 8, no. 5, pp. 847–860, 2014.
- [67] C. Lee and C. Lee, *Convolutional coding: fundamentals and applications*. Artech House Boston, MA, 1997.
- [68] T. Tao, *Topics in random matrix theory*. American Mathematical Society, Providence, RI, 2012, vol. 132.
- [69] C. Tang, C. Liu, L. Yuan, and Z. Xing, “Approximate iteration detection with iterative refinement in massive MIMO systems,” *IET Communications*, vol. 11, no. 7, pp. 1152–1157, 2017.
- [70] J. O. Rawlings, S. G. Pantula, and D. A. Dickey, *Applied regression analysis: a research tool*. Springer Science & Business Media, 2001.
- [71] G. Strang, *Introduction to linear algebra*. Wellesley-Cambridge Press, Massachusetts, 1993, vol. 3.
- [72] A. Bjorck, *Numerical methods for least squares problems*, 1st ed. SIAM, Philadelphia, 1996, vol. 51.
- [73] R. A. Horn and C. R. Johnson, “Matrix analysis,” *Cambridge University Press, Baltimore*,, 1985.
- [74] R. Hunger, *Floating point operations in matrix-vector calculus*. Munich University of Technology, Inst. for Circuit Theory and Signal Processing, 2005.
- [75] C. H. Papadimitriou, *Computational complexity*. John Wiley and Sons Ltd., 2003.
- [76] J. R. B. J. J. Dongarra, C. B. Moler and G. W. Stewart, *LINPACK Users’ Guide*. SIAM, 1979.
- [77] J. Kaur, M. A. Khan, M. Iftikhar, M. Imran, and Q. E. U. Haq, “Machine Learning Techniques for 5G and Beyond,” *IEEE Access*, 2021.

REFERENCES

- [78] H. Zhao, “AI and machine learning in 5G—the ITU Challenge 2020,” *ITU News Magazine*, 2020.
- [79] O. L. Mangasarian and M. V. Solodov, “Backpropagation convergence via deterministic nonmonotone perturbed minimization,” in *Advances in Neural Information Processing Systems*, 1994, pp. 383–390.
- [80] E. Basar, “Media-based modulation for future wireless systems: A tutorial,” *IEEE Wireless Communications*, vol. 26, no. 5, pp. 160–166, 2019.
- [81] M. Shokri and H. R. Tizhoosh, “ $Q(\lambda)$ -based image thresholding,” *IEEE First Canadian Conference on Computer and Robot Vision, 2004. Proceedings.*, pp. 504–508, 2004.
- [82] M. Mandloi and V. Bhatia, “Error recovery based low-complexity detection for uplink massive MIMO systems,” *IEEE Wireless Communications Letters*, vol. 6, no. 3, pp. 302–305, 2017.
- [83] M. Gong, F. Chen, H. Yu, Z. Lu, and L. Hu, “Normalized adaptive channel equalizer based on minimal symbol-error-rate,” *IEEE Transactions on Communications*, vol. 61, no. 4, pp. 1374–1383, 2013.
- [84] X.-S. Yang, *Nature-Inspired Metaheuristic Algorithms*. Luniver Press Frome, UK. 2008, vol. 20.
- [85] S. Dhakal and A. Bayesteh, “Sparse space codes for multi-antenna systems,” in *2011 12th Canadian Workshop on Information Theory*. IEEE, 2011, pp. 159–164.
- [86] J. A. Tropp and A. C. Gilbert, “Signal recovery from random measurements via orthogonal matching pursuit,” *IEEE Transactions on information theory*, vol. 53, no. 12, pp. 4655–4666, 2007.
- [87] J. Uspensky, “Introduction to mathematical probability, New York, 1937,” *University of Birmingham*.

REFERENCES

- [88] E. Basar and I. Altunbas, “Space-time channel modulation,” *IEEE Transactions on Vehicular Technology*, vol. 66, no. 8, pp. 7609–7614, 2017.
- [89] E. Seifi, M. Atamanesh, and A. K. Khandani, “Media-based mimo: A new frontier in wireless communications,” *arXiv preprint arXiv:1507.07516*, 2015.

List of Publications

Journal Papers:

1. Arijit Datta, and Vimal Bhatia. “A near maximum likelihood performance modified firefly algorithm for large MIMO detection.” Elsevier Swarm and evolutionary computation 44 (2019): 828-839.
2. Arijit Datta, Manish Mandloi, and Vimal Bhatia. “Reliability feedback-aided low-complexity detection in uplink massive MIMO systems.” Wiley International Journal of Communication Systems 32.15 (2019): e4085.
3. Arijit Datta, Manish Mandloi, and Vimal Bhatia. “Minimum Error Pursuit Algorithm for Symbol Detection in MBM Massive-MIMO.” IEEE Communications Letters (2020).
4. Arijit Datta, Manish Mandloi, and Vimal Bhatia. “Graph Traversal Aided Detection in Uplink Massive MIMO MBM based on Socio-Cognitive Knowledge of Swarm Optimization.” Wiley International Journal of Communication Systems (2021): e4720.

Conference Papers:

1. Arijit Datta, Manish Mandloi, and Vimal Bhatia. “Error Refinement based Iterative Line Search for Symbol Detection in Uplink Massive MIMO.” 2019 IEEE 30th Annual International Symposium on Personal, Indoor and Mobile Radio Communications (PIMRC). IEEE, 2019.
2. Arijit Datta, Manish Mandloi, and Vimal Bhatia. “Hybrid Pseudostationary Iterative Detection Algorithm for Uplink Massive MIMO Systems.” 2018 IEEE International Conference on Advanced Networks and Telecommunications Systems (ANTS). IEEE, 2018.

Book Chapters

REFERENCES

1. Arijit Datta, Manish Mandloi and Vimal Bhatia. “Detection Techniques in Uplink Massive MIMO Systems.” 5G and Beyond Wireless Systems, Springer, 2020.
2. Arijit Datta, Manish Mandloi and Vimal Bhatia. “Swarm Intelligent Based Detection in the Uplink of Large-Scale MIMO Wireless Communication Systems.” Design Frameworks for Wireless Networks, Springer, 2019.

Publications apart from thesis

Journal Papers

1. Arijit Datta, Vimal Bhatia, Sudhir Dixit and Josef Noll. “Bridging the Digital Divide for the Elderly and Socially Disadvantaged.” IEEE Consumer Electronics Magazine (2018).

Conference Papers

1. Arijit Datta, and Vimal Bhatia. “A near-ML performance hybrid dijkstra and firefly algorithm for large MIMO detection.” 2017 8th International Conference on Computing, Communication and Networking Technologies (ICCCNT). IEEE, 2017.
2. Arijit Datta, and Vimal Bhatia. “A robust MIMO detection algorithm using gravitationally co-ordinated swarm.” 2017 Conference on Information and Communication Technology (CICT). IEEE, 2017.
3. Arijit Datta, and Vimal Bhatia. “Social spider optimizer based large MIMO detector.” 2017 IEEE International Conference on Advanced Networks and Telecommunications Systems (ANTS). IEEE, 2017.
4. Arijit Datta, Manekar Tushar Deo, and Vimal Bhatia. “Collaborative Learning based Symbol Detection in Massive MIMO.” 2020 European Signal Processing Conference (EUSIPCO). IEEE, 2020.

Book Chapters

REFERENCES

1. Manish Mandloi, Arijit Datta, and Vimal Bhatia. “Index Modulation Techniques for 5G and Beyond Wireless Systems.” 5G and Beyond Wireless Systems, Springer, 2020.
2. Arijit Datta, Manish Mandloi, and Vimal Bhatia. “Mutation-Based Bee Colony Optimization Algorithm for Near-ML Detection in GSM-MIMO.” Advances in Signal Processing and Communication. Springer, Singapore, 2019. 125-135.